

Biochips for the Detection of Biological Cell Potentials

Dissertation

zur

Erlangung des akademischen Grades

doctor rerum naturalium (Dr. rer. nat.)

der Mathematisch-Naturwissenschaftlichen Fakultät

der Universität Rostock

vorgelegt von

Philipp Julian Köster

geboren am 27.09.1976 in Düsseldorf

aus Rostock

Tag der Verteidigung: 29.03.2010

Gutachter: Prof. Dr. rer. nat. habil. Jan Gimsa

Universität Rostock, MNF / Institut Biowissenschaften

Herr Prof. Dr. -Ing. habil. Helmut Beikirch

Universität Rostock, IEF / Institut für Gerätesysteme und Schaltungstechnik

*Three, it's a magic number
Yes it is, it's a magic number
Because two times three is six
And three times six is eighteen
And the eighteenth letter in the alphabet is R
We've got 3Rs we're going to talk about today...*

*Jack Johnson, The 3Rs, 2006
(Original Soundtrack "Curious George")*

The following work is dedicated to my wife Monique and my family. I thank my parents for their confidence and financial support during the undergraduate studies. I thank Monique especially, for her help has motivated me from the first day on.

Acknowledgements

I want to thank Prof. Dr. habil. Jan Gimsa and Dr. Werner Baumann for their kind supervision during the last years and for giving me the chance to work with the innovative and extraordinarily interesting biochip technology at the Chair of Biophysics. Special thanks go to cand. Dr.-Ing. Carsten Tautorat for his superior electro-technical work and electronic contributions to the PoreGenic®, the Neurosensorix® and the modular glass chip systems. Cands. Dr. rer. nat. Sebastian Bühler, Marco Stubbe and Tom Reimer are thanked for their helping hands regarding the experiments with the glass neurochip. The colleagues at the Chair of Biophysics are thanked for fruitful discussions and friendly company.

Additionally, I want to express gratitude to Dr. Jochen Held, Dr. Andreas Trautmann, Dr. João Gaspar, Dr. Patrick Ruther and Prof. Oliver Paul (Department of Microsystems Engineering, IMTEK, University of Freiburg) for manufacturing the microneedle chips and discussions; cand. Dr.-Ing. Sönke Petersen (Ernst-Berl-Institute for Technical and Macromolecular Chemistry, University of Darmstadt) for the deposition of polymers on the microneedle chips as an alternative to another project partner. I am grateful to Peter Kumm (Department of Chemistry, University of Rostock) for his excellent mechanical work and to Wolfgang Labs (Electron Microscopy Center, Medical Faculty, University of Rostock) for sample preparation and SEM images. The author acknowledges BMBF and BFS funding of the projects mentioned in this thesis.

I am grateful to Dr. Gerd Friedrich (Forschungsgemeinschaft Funk e.V.) for providing a generic UMTS-signal generator that was developed by the group of Prof. Dr. Volker Hansen (University of Wuppertal). Thanks also to Dr. Jan Sakowski (Faculty of Mechanical Engineering and Ship Technology, University of Rostock) for programming MatLab® routines and for data analysis concerning the UMTS and heat experiments. Dipl.-Biophys. Derk Wachner is acknowledged for programming the DEP-software.

I thank Gründerflair MV e.V. and PVA-MV for their initiation of the science contest of the state Mecklenburg-Western Pomerania (venturesail 2007). I also wish to thank the founding office (Gründerbüro) of the University of Rostock for initializing the scientific idea contest (Ideenwettbewerb 2009). I am grateful to Jessica Lattif, Food and Environment at the Tufts University Friedman School of Nutrition, Science and Policy for proofreading the thesis manuscript.

Table of contents

ACKNOWLEDGEMENTS.....	IV
TABLE OF CONTENTS.....	V
ZUSAMMENFASSUNG	VII
SUMMARY.....	VIII
1. INTRODUCTION	1
1.1 BIOCHIP SYSTEMS	1
1.2 APPLICATION SPECTRUM OF BIOCHIPS.....	2
1.2.1 REACH.....	2
1.2.2 Pharmacovigilance	3
1.2.3 The 3Rs (reduce, refine, replace)	4
1.2.4 Biochips as in vitro diagnostic tools.....	4
1.3 EXTRACELLULAR POTENTIAL DETECTION.....	5
1.3.1 Neuronal information signals	5
1.3.2 Cardiac information signals.....	6
1.4 INTRACELLULAR POTENTIAL DETECTION	8
1.5 DIELECTROPHORETIC CELL ALLOCATION	11
1.6 POSSIBLE ADVERSE EFFECTS OF ELECTROMAGNETIC FIELDS (EMF)	12
1.7 THE APPENDED MANUSCRIPTS.....	13
2. MATERIAL AND METHODS.....	14
2.1 BIOCHIPS	14
2.1.1 The neuro-measuring adapter (NMA) and the silicon neurochip (SNC).....	14
2.1.2 Modular glass chip system and the glass neurochip (GNC).....	15
2.1.3 PoreGenic® system and the microneedle chip (MNC).....	16
2.2 CHIP PREPARATION AND CELL CULTURE	20
2.2.1 Sterilization methods.....	20
2.2.2 Biochip preparation	21
2.2.3 CO ₂ -aeration during cell culture and experiments.....	21
2.2.4 Preparation of primary neuronal cells (PNCs)	21
2.2.5 Preparation of primary cardiac muscle cells (PCMs)	24
2.2.6 L929 mouse tumor and normal human skin fibroblasts (NHDF)	24
2.3 EXPERIMENTS	25
2.3.1 Cell positioning with positive dielectrophoresis (pDEP).....	25
2.3.2 EMF experiments with the SNC.....	27
3. RESULTS AND DISCUSSION.....	32
3.1 OVERVIEW OF EXPERIMENTS.....	32
3.2 STATISTICS ON AUTOCLAVING AND NEW STERILIZATION METHODS	33
3.2.1 Autoclaving and other methods	33
3.2.2 Peracetic acid (PAA).....	33
3.2.3 knick'n'clean Flora sticks.....	35
3.3 BIOCHIPS	37
3.3.1 SNC	37
3.3.1.1 Electrode transmission test.....	37
3.3.1.2 Neuronal growth performance	38
3.3.1.3 Neuronal signal pattern controls	39
3.3.1.4 Spatial resolution of neuronal activity on-chip	42
3.3.1.5 pDEP with PNCs.....	43
3.3.1.6 SU-8 structures.....	48
3.3.1.7 Influence of UMTS-EMF on neuronal activity on SNCs	50
3.3.2 GNC.....	56
3.3.2.1 Examination of electrode noise	56
3.3.2.2 Neuronal action potential detection.....	56
3.3.2.3 Influence of sodium valproate (VPA) on neuronal firing frequency.....	58

3.3.2.4	Cardiac action potential detection.....	60
3.3.3	<i>MNC</i>	63
3.3.3.1	pDEP with PNCs using kidney-shaped electrodes	63
3.3.3.2	Polymer patterning of MNC surface	65
3.3.3.3	Electroporation of adherent cells using LOMINE	66
3.3.3.4	Fluorescence microscopy	68
3.3.3.5	Intracellular potential detection	70
3.3.3.6	FIB-SEM examinations.....	74
3.3.3.7	Extracellular action potential detection.....	75
4.	CONCLUSIONS AND OUTLOOK	81
4.1	SNC	81
4.2	GNC.....	83
4.3	MNC.....	83
4.4	RECOMMENDATIONS FOR THE APPLICATION OF BIOCHIPS	89
5.	REFERENCES	91
6.	APPENDIX A - PUBLICATIONS	103
6.1	MANUSCRIPT 1 – UMTS EMF SETUP WITH THE SNC	103
6.2	MANUSCRIPT 2 – MODULAR GLASS CHIP SYSTEM	104
6.3	MANUSCRIPT 3 – INTRODUCTION TO THE INTRACELLULAR POTENTIAL MEASUREMENTS WITH THE MNC AND THE POREGENIC® SYSTEM.....	105
6.4	MANUSCRIPT 4 – FIRST INTRACELLULAR RECORDINGS WITH 3D MICROELECTRODE ARRAYS AFTER LOCAL ELECTROPORATION .	106
6.5	MANUSCRIPT 5 – DIELECTROPHORESIS WITH THE SNC	107
6.6	MANUSCRIPT 6 – DIELECTROPHORESIS WITH THE MNC	108
7.	APPENDIX B - AUTHOR’S SCIENTIFIC ACTIVITY.....	109
7.1	ORAL PRESENTATIONS	109
7.2	PUBLICATIONS	111
7.3	CONFERENCE CONTRIBUTIONS.....	112
7.4	BOOK CONTRIBUTIONS	117
7.5	DIGITALLY PUBLISHED POSTERS.....	118
8.	APPENDIX C.....	119
8.1	SUMMARY OF THE AUTHOR’S ORIGINAL WORK	119
9.	APPENDIX D - TABLES	121
9.1	LIST OF FIGURES.....	121
9.2	LIST OF TABLES.....	122
9.3	LIST OF INTERNET LINKS	123
9.4	LIST OF ABBREVIATIONS	124

Zusammenfassung

Neue Testsysteme für den Nachweis von schädlichen Auswirkungen von z. B. Chemikalien, Arzneimitteln und Kosmetika müssen entwickelt werden, um Versuche am lebenden Tier entsprechend des 3R-Prinzips (*replace, refine, reduce*; Russel et. al., 1959) zu reduzieren. Diese *in vitro*-Testsysteme sollten vorzugsweise regenerierende Gewebe oder Zellkulturen als biologische Modelle nutzen. Die Dissertation beleuchtet mit biochemischen und biophysikalischen Versuchen die Anwendbarkeit dreier Prototypen von Biochipsystemen zur Detektion von Membranpotentialen einzelner Zellen mit integrierten Mikroelektroden, die in Zusammenarbeit mit verschiedenen Partnern am Lehrstuhl für Biophysik (Universität Rostock) entwickelt wurden. In der Dissertation werden verschiedene Möglichkeiten zur Sterilisation dieser Biochips vorgestellt, um sie auf sanfte Weise zu entkeimen und gleichzeitig deren empfindliche Strukturen zu erhalten. Darüber hinaus konnte der Autor die Biosignalausbeute muriner primärer Nervenzellen von Mäuseembryonen mittels positiver Dielektrophorese an den Mikroelektroden des Siliziumneurochip (SNC, NeuroSensorix®-System) bzw. speziellen nierenförmigen Elektroden des Mikronadelchips (MNC) erhöhen. Mehrere Versuchsanordnungen wurden exemplarisch untersucht sowie z. B. die Auswirkungen verschiedener biochemisch aktiver Wirkstoffe (Valproinsäure, Bicucullin) auf die elektrische Aktivität in Form von Aktionspotentialen (APs) von Nervenzellen tiefergehend in den Manuskripten im Anhang der Dissertation diskutiert. APs dieser Zellen wurden mit dem SNC sowie dem Glasneurochip (GNC) des neuartigen modularen Glaschip-Systems detektiert. APs von Herzmuskelzellen wurden auch mit dem MNC des neuartigen Prototyps des PoreGenic®-Patch-Clamp-Systems erfasst. Mit dem MNC wurden zusätzlich Transmembranpotentiale von L929-Tumor-Zellen und menschlichen Hautfibroblasten im Ganzzellmodus (whole-cell) untersucht sowie definierte Polymermuster verwendet, um deren Zellwachstum auf dem MNC zu steuern. Um die Interaktion dieser Zellen mit den Mikronadeln darzustellen wurden Fluoreszenz-Mikroskopie, fokussierte Ionenstrahlschnitte (FIB-Technik) und rasterelektronenmikroskopische Aufnahmen verwendet. In biophysikalischen Experimenten wurden AP-Muster von Nervenzellnetzwerken auf dem SNC bei gleichzeitiger Befeldung mit UMTS-Hochfrequenzfeldern aufgezeichnet und ausgewertet, um thermale und athermale Effekte auf die neuroelektrische Aktivität zu untersuchen.

Summary

New test systems must be developed for the detection of harmful effects of chemicals, pharmaceutical compounds and cosmetics in order to abolish animal experiments according to the 3R-Principle (replace, reduce, refine; Russel et al., 1959). Preferably, such *in vitro* tests should be based on regenerating tissue or cell cultures. My thesis highlights the biological applicability and high economic potential of three types of biochips containing integrated microelectrodes for the detection of single cell membrane potentials. The biochip systems were developed with different partners at the Chair of Biophysics (University of Rostock). Different methods for sterilizing the chips in a gentle way were examined in order to keep their detecting structures intact. Furthermore, by using positive dielectrophoresis the author positioned murine primary embryonic neurons at the detecting microelectrodes of the silicon neurochip (SNC, NeuroSensorix®-system) or at special kidney-shaped electrodes of the microneedle chip (MNC). A number of experimental setups were investigated and effects of different biochemically active compounds (sodium valproate, bicuculline) on the electric activity (action potentials, APs) of neurons are described in more detail in the appended manuscripts. APs of these cell types were detected with the SNCs and a novel glass neurochip (GNC) for a new modular glass chip system. Cardiac APs were also recorded with the MNC using the prototype of the PoreGenic® patch clamp system. Transmembrane potentials of L929 mouse tumor fibroblasts and human skin fibroblasts were detected in the whole-cell mode, with the same chip type and defined polymer patterns were deposited to guide cell growth on the MNC. Furthermore, fluorescence microscopy, focused ion beam (FIB) cut technique and scanning electron microscopy were used to show the interaction of the cells and the microneedles. In biophysical experiments, the neuronal cells were exposed to high-frequency electro-magnetic UMTS fields and neuronal AP patterns were recorded. The aim was to clarify whether such exposure might induce athermal cellular effects.

1. Introduction

1.1 Biochip systems

The development of microelectronics for the measurement of extracellular biosignals goes back to the 1970s and originated from chemistry research followed by the application in biochemistry and medicine (Reyes et al., 2002). Extracellular biosignals like action potentials (APs) are detected from the external medium surrounding the cell. In the early years, only square-cut glass blanks were coated with electrodes. Microelectrode arrays (MEAs) were deposited on glass wafers and the cell culture medium trough was provided by a simple rubber gasket. The G. W. Gross and J. Pine groups were all-important for the breakthrough of the MEA technology (Gross et al., 1977; Gross, 1979; Pine, 1980; Gross et al., 1982). This method found its application in pharmacological surveys. In Rostock, the Neuroproof GmbH uses this system (Gramowski et al., 2006). The reaction of error-tolerant and spontaneously active primary nerve cell networks is generally substance- and concentration-dependent (Ziegler, 2000). Approaches identifying substances by their neuronal fingerprint, i.e. the specific neuronal signal reaction on a chemical compound, are under way (Gramowski et al., 2004). However, such systems do not allow for the additional detection of physiological parameters (Baumann et al., 2002; Baumann et al., 2004). Glass MEA systems with integrated sensors for oxygen, pH and temperature were developed (Ilchmann et al., 2006) but are commercially not available. The Multi Channel Systems GmbH in Reutlingen (MCS GmbH) improved the simple MEA principle by miniaturization (Stett et al., 2003b) as well as by the introduction of different MEA types (e.g. flexible substrates and different electrode diameters). The MCS GmbH is the reference market leader for electrophysiological MEA measurements. Some other companies that commercially produce MEAs are Ayanda Biosystems SA, ELume Inc. and ALA Scientific Instruments. However, these systems do not allow for the measurement of additional parameters.

Several approaches to developing integrated field effect transistor- (ISFET) based systems to record neuronal activity exist (Fromherz et al., 1991; Fromherz and Stett, 1995). Nevertheless, the MEA technology is well-established and reliable. It found its niche in several commercial applications (Egert and Haemmerle, 2002). Different research projects at the University of Rostock led to cell monitoring systems (CMS®) (Baumann et al., 2002; Baumann et al., 2004; Baumann et al., 2005). Nowadays, the CMS® include the

measurement of different parameters like respiration and acidification by detecting oxygen and hydrogen (H_3O^+), respectively (Lehmann et al., 2001; Baumann et al., 2004). These methods can also be expanded and are suitable for the complex demands of high-content screening (HCS) surveys. Along with the extracellular measurement of cellular AP by neuronal cells, the presented silicon neurochip (SNC) and the glass neurochip (GNC) allow for the combined measurement of temperature and acidification as well as temperature and cell adhesion, respectively. With small technical modifications, respiration measurements are also possible with the SNC. Cell potential field effect transistors (CPFET) can be used for the measurement of long-wave cardiomyocyte APs on the SNC (Schrott, 2009).

The detection of intracellular biosignals, such as the classical patch clamp approach, is more complex. However, as with MEAs, the most important invention was published in the late 1970s, though the concept of voltage clamp measurements was already presented in the late 1930s by Kenneth S. Cole. The voltage clamp allowed for the detection of electrical biosignals with insertion-electrodes (Cole and Curtis, 1939). In 1976, Neher and Sakmann published their results on the patch clamp method (Neher and Sakmann, 1976) and became Nobel laureates for physiology or medicine in 1991. The patch clamp was a breakthrough in biophysics because it allows for the voltage clamp of single membrane channels of biological cells (Nicholls et al., 1995). A report on the refinement of this method with adherent single cells, e.g. nerve cells, was published later (Hamill et al., 1981). In this thesis, the author presents the microneedle chip (MNC) and the PoreGenic® system for patch clamp experiments on adherent cells.

1.2 Application spectrum of biochips

1.2.1 REACH

The new REACH-guideline regulates the registration, evaluation, authorization and restriction of chemicals (European Parliament and Council, 2006). REACH affects the production and use of chemical substances and their potential impacts on both, human health and the environment. The testing and evaluation of more than 30.000 substances and all newly developed chemicals will be at laboratory animals' expense. Nevertheless, this guideline opens new markets for developers and producers of alternative biotechnological assay methods. REACH has been effective since June 2007. Further, European and US-American test guidelines require investigations on the effects of neurotoxic and

developmental-neurotoxic substances. However, these tests are still based on animal experiments, contradicting the 3R-principle (*replace, reduce, refine*) and society claims to abolish animal experiments (Russel and Burch, 1959).

1.2.2 Pharmacovigilance

Drug development imposes a high economic risk on pharmaceutical R&D companies. The time span for testing all candidate-compounds for a single new drug has risen from 11.6 years in the 1970s to 14.9 years in 2001 (Birch, 2002). Globally, R&D costs increased to approximately \$ 2.3 billion per new active substance in 2004. This is an increase of 43 % compared to 2003 costs (Acharya, 2005). Only approximately 1% of tested compounds end up being used commercially. Therefore, blockbuster-compounds must generate maximum profits, especially within the effective patent-duration of 20 years. After this period, generic manufacturers, e.g. Ratiopharm GmbH, Ulm, and Cipla Ltd., Mumbai, India, exploit the results of researching pharmaceutical companies. Additionally, studies show that the cost of the clinical phases I to III rises exponentially (**Figure 1**). Due to this trend of costs and the high competition pressure, new candidates for the clinical phases must be examined particularly in an early phase of development, fast and primarily automatized for their diverse effects.

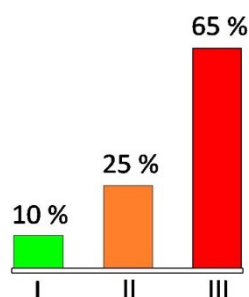


Figure 1: Distribution of clinical development cost. Redrawn after Deloitte Recap Inc., 2004.

The FDA (Food & Drug Administration) regulates that all new active substances must be tested for their hERG (human *Ether-à-go-go* Related Gene KCNH2) channel activity to identify the risk of life-threatening *Torsade de Pointes*-arrhythmias (Food and Drug Administration, 2005). The regulation was introduced after the commercial anti-allergic blockbuster drug terfenadine (Seldane) was identified as a blocker of the hERG- I_{Kr} (rectifier K^+ channel) (Food and Drug Administration, 2005). After that, several drugs such as cisapride (Propulsid), grepafloxacin (Raxar) and terodiline were withdrawn from the market for the same reason (Brown, 2004).

1.2.3 The 3Rs (reduce, refine, replace)

New test systems must be developed for the detection of harmful effects of chemicals, pharmaceutical compounds and cosmetics in order to abolish animal experiments. Since 2000, the number of animal experiments has risen by approximately 1-2 % annually due to legal standard tests. In 2005, more than 520.000 mice, rats and rabbits were "sacrificed" in Germany. The testing of cosmetics on animals is already banned in the Netherlands, Belgium, and the United Kingdom. Only in 2002, after 13 years of discussion, did the European Union (EU) agree to phase in a near-total ban on the sale of animal-tested cosmetics throughout the EU beginning in 2009, and to ban all cosmetics-related animal testing (Osborn and Gentleman, 2003). The use of animals is ethically, scientifically and economically doubtful; small, reusable and inexpensive alternatives like cell-based biochips following the 3R-Pinciple (Russel and Burch, 1959) and featuring comparable and reproducible results based on cell lines, primary tissue, 3D-cell cultures (e.g. artificial skin) or even single cells are state-of-the-art (Reyes et al., 2002).

1.2.4 Biochips as *in vitro* diagnostic tools

In general, biochips provide non-invasive medicine techniques such as high-throughput screening (HTS) and HCS (Lehmann et al., 2001; Baumann et al., 2008). Besides portable sensor systems, approaches to parallelize microelectrode screening exist for the pharmaceutical industry (Stenger et al., 2001). HTS and HCS can be valuable tools for REACH, pharmacovigilance and for the implementation of the 3R's (Buehler et al., 2007; Koester et al., 2007a). The biochips presented in this thesis can be used for neuronal/cardiac (GNC and SNC) and intracellular/cardiac (MNC) studies. Our biochips may become versatile tools for pharmaceutical companies, pharmacovigilance studies, HCS and the bioanalysis of substances. The integration of additional sensors allows for an improved versatility in future experiments.

1.3 Extracellular potential detection

1.3.1 Neuronal information signals

Primary neuronal and glial cells (PNCs) build networks when cultured on a biochip surface. Nevertheless, neuronal adherence requires a special treatment of the silicon surface (Parak et al., 2001). The PNCs exhibit APs generated by electrochemical exchange mechanisms at the neuronal membrane. These APs transport a code to other neurons via synapses. The waveform of a neuronal transmembrane AP consists of three different sections: (i) depolarization (rising phase), (ii) repolarization (falling phase) and (iii) hyperpolarization (undershoot) (**Figure 2a**). The signal length is approximately 1-2 ms, depending on the neuronal cell type. The neuronal communication can be recorded outside the cell with high-sensitive electrodes like those used in SNC and GNC.

The Na^+/K^+ - pump and other ion transporters carry the sodium (Na^+), potassium (K^+) and other ions, e.g. calcium (Ca^{2+}) to the outside or inside of the axon, respectively. It is energetically driven by the reduction of adenosine triphosphate (ATP) to adenosine diphosphate (ADP). The AP sections (i)-(iii) are determined by temporal permeability alterations, yet negligible concentration changes of Na^+ and K^+ inside and outside the axon. These alterations are guided by channels embedded in the cell membrane. Hence, the requirements for the further described processes are ATP-dependent ion gradients. The initiation of a new AP depends on the crossing of a threshold voltage by approximately 15 mV induced by an incoming AP. If the voltage exceeds this critical threshold beyond the resting potential, the Na^+ ion channels are activated (**Figure 2a**).

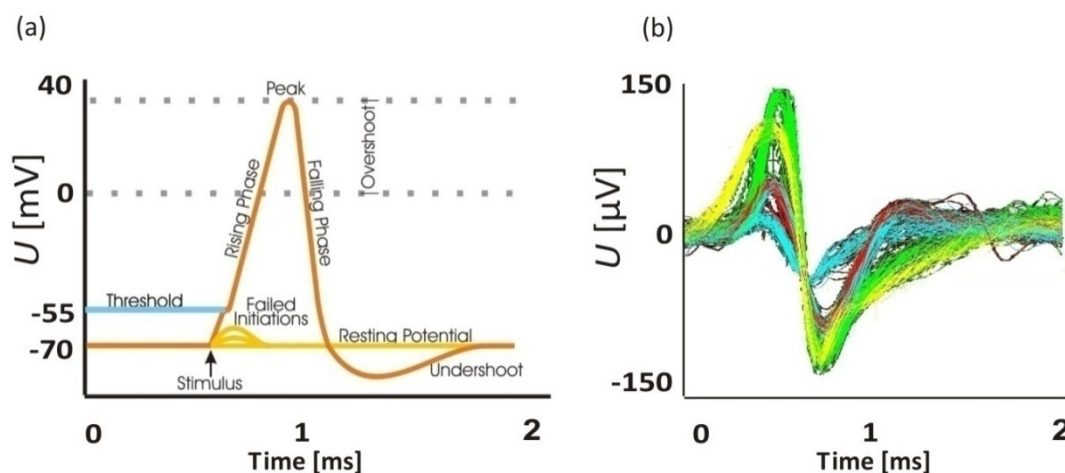


Figure 2: Neuronal information signals. (a) Schematic neuronal transmembrane action potential (Wikipedia, 2009); (b) superimposed waveforms of four different neuronal signal sources. Electrical activity was recorded out of the cell with the SNC.

The Na^+ channels open and allow for the entry of Na^+ ions into the neuron. This simple event may be followed by an activation cascade of other Na^+ channels and result in an AP. The inward flow of Na^+ ions increases the concentration of cations in the cell (depolarization). Now, the potential of the cell is higher than the resting potential. The Na^+ channels close at the climax of the AP, while K^+ channels begin to open resulting in an efflux of K^+ from the cell (repolarization). The membrane potential decreases and the resting potential is soon undershot (hyperpolarization). The channel opening probabilities can be influenced by a great variety of pharmacologically active substances, e.g. by tetraethylammonium (TEA) which blocks the I_K channel on the axoplasmatic side of the membrane (Taglialetela et al., 1991). The AP is picked up outside the cell by the electrodes of the MEA (**Figure 2b**). A low-impedance counter-electrode is located on-chip or formed by a separate Ag/AgCl-wire in the cell culture trough. Electrically, the potential of this reference can be assumed to be at ground potential. Therefore, the detected signals cannot simply be compared with a transmembrane detection of an AP. Additionally, due to the capacitive properties of the electrode, the varying distance and the geometric orientation between the axon and the electrode, the registered AP amplitudes are of different waveform and of a much lower amplitude than the transmembrane AP (**Figure 2a**).

1.3.2 Cardiac information signals

Surface electrocardiograms can only provide information about the length of the QT-phase (**Figure 3a**). The QT-phase is used as a parameter to predict life-threatening *Torsade de Pointes*-Arrhythmias and is a parameter for compound profiling (Netzer et al., 2001). The QT-phase is most important during the first preclinical phases of drug and substance testing.

The benefit of primary cardiomyocytes (PCMs) is immense. *In vitro* studies of extracellular APs of PCMs on MEAs have a long history (Jongsam and Schoonlingen, 1970; Thomas Jr. et al., 1972). Intracellular cardiac AP measurements can be accomplished *in vivo* with microelectrodes (Gintant et al., 2001). PCMs extracted from primary heart tissue, e.g. from mice or rats, exhibit long-wave cardiac APs with a period length of approximately 300 ms. PCMs show transmembrane cardiac AP amplitudes of approximately 120 mV (Ahmed et al., 2000). Like PNCs, the PCMs also build networks when seeded on the chip surface. They begin to pace synchronically approximately 5 h after seeding. **Figure 3b** shows the cardiac AP detected with the patch clamp approach (cell-attached mode).

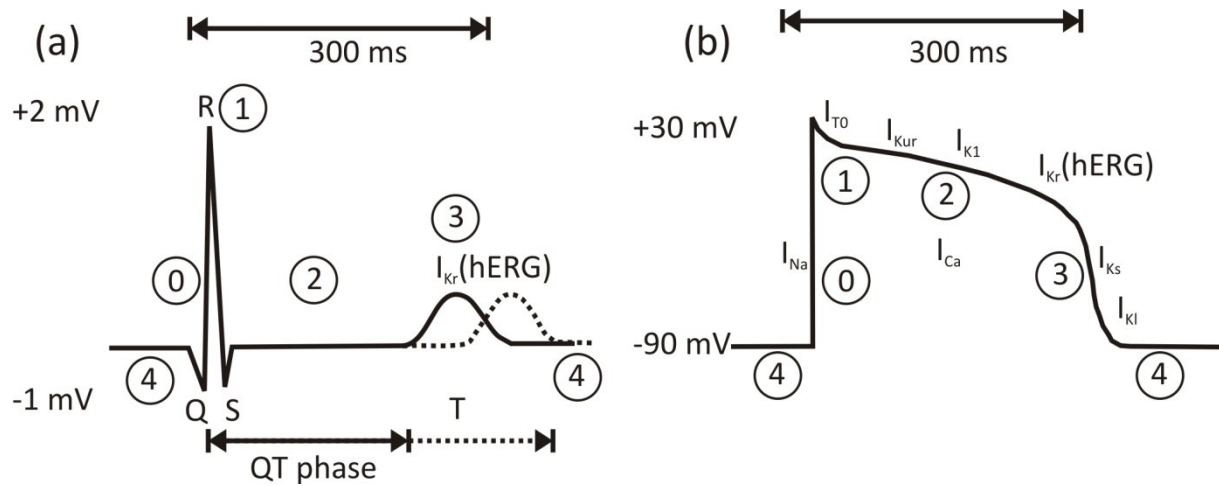


Figure 3: Comparison of the cardiac AP and the surface electrocardiogram. (a) Classical surface electrocardiogram; (b) intracellular cardiac AP recorded with a patch clamp setup, membrane channels activities e.g. I_{Kr} (hERG) contributing to the cardiac APs and the AP phases 0 – 4 are displayed (redrawn after Brown, 2004).

The potential is defined by the sum of all membrane channel activities embedded in the membrane. The intracellular detection of APs is especially useful in biochemical trials of membrane channel effects. As with PNCs, the waveform of a cardiac transmembrane AP consists of different sections: (i) depolarization, (ii) plateau phase, and (iii) repolarization. In the following, the AP progress is described in detail. A given ventricular PCM of the heart has a negative membrane potential, like neurons, when at rest. *Phase 4* is the resting membrane potential (**Figure 3b**). Phase 4 is followed by an electrical stimulation of an adjoining PCM of this functional syncytium. This phase corresponds to the contraction of the ventricles.

The rapid depolarization is exhibited in *Phase 0*. The depolarization is caused by an opening of the rapid Na^+ channels (I_{Na}), which results in a fast inflow of Na^+ ions to the PCM. During the cell excitation, the membrane potential allows the PCM to open the fast Na^+ channels during depolarization. The fast Na^+ channels close if the membrane potential is about -90 mV (baseline). The excitation will open these channels, which results in a large influx of Na^+ ions.

The inactivation of the fast Na^+ channels appears in *Phase 1* of the AP. The temporary net current out of the PCM membrane, causing the small downward deflection of the AP, induces the movement of Cl^- and K^+ ions. This movement is achieved by the I_{T0} currents and corresponds to phase Q-S in the electrocardiogram of **Figure 3a**.

The so-called plateau phase of the cardiac AP occurs in *Phase 2*. It is kept up by the inward flux of Ca^{2+} ions through T-type calcium channels (I_{Ca}) and outward movement of K^+ .

The ions move through the delayed rectifier potassium channels (I_{Ks}). During phase 2, the sodium-calcium exchanger current ($I_{Na,Ca}$; not shown) as well as the currents ($I_{Na,K}$; not shown) of the Na^+/K^+ pump play minor roles.

The rapid repolarization phase of the AP is exhibited in *Phase 3*. While the slow delayed rectifier (I_{Ks}) K^+ channels are still open, the L-type Ca^{2+} channels are closing ensuring a net outward current. This corresponds to a negative change in the membrane potential and allows more K^+ channels to open. Principally, the rapid delayed rectifier K^+ channels (I_{Kr}) and the inwardly rectifying K^+ current (I_{K1}) represent such channels. The I_{Kr} channel is expressed by the hERG (KCNH2) gene and corresponds to the T-wave of **Figure 3a**. This net outward, positive current (equal to loss of positive charge from the cell) causes the cell to repolarize. When the membrane potential is restored to about -80 to -90 mV, I_{Ks} and I_{Kr} close. I_{K1} contributes to set the resting membrane potential by remaining conductive throughout phase 4 (Silbernagel and Despopoulos, 2003).

1.4 Intracellular potential detection

The biological cell represents the smallest living unit. The basic structure of the cell membrane is the phospholipid bilayer in which a variety of functional proteins, e.g. membrane channels, are embedded (Singer et al., 1972). The interplay of active and passive ion channels and transporters as well as leak fluxes through the membrane generate a diffusion potential across the membrane between the extra- and intracellular space. The measurement of the physiological transmembrane potential V_m is a complex problem, even with penetrating electrodes. For univalent ions, V_m is described by the Goldman-equation (Goldman, 1943):

$$V_m = \frac{RT}{F} \ln \frac{\sum P_C c_C^e + \sum P_A c_A^i}{\sum P_C c_C^i + \sum P_A c_A^e} \quad (1)$$

R = gas constant, T = absolute temperature,
 F = Faraday constant, P = ion permeability,
 c = ion concentration, e = extracellular, i = intracellular,
 C = cations, A = anions

In living cells, typical V_m values vary around -65 mV, strongly depending on organism and cell type. Voltage changes in adherent single cells were examined using inserted microelectrodes (Hodgkin and Huxley, 1936; Hodgkin and Katz, 1949). In 1976, *Erwin Neher* and *Bert Sakmann* published their work on the refinement of the voltage clamp technique. Their revolutionary patch clamp setup allowed for measuring intracellular potentials and membrane channel currents on single adherent cells, e.g. neuronal and cardiac cells.

Figure 4 illustrates the method schematically and microscopically. The studies made the

measurement of membrane potentials (whole-cell) and ion channel currents (cell-attached) of biological cells possible (Numberger and Draguhn, 1996). For adherent cells, today's patch clamp setups still work like they did nearly three decades ago (Hamill et al., 1981). The latest developments have focused on the improvement of distinct technological features, e.g. signal amplifiers, pipette pullers and physiological buffers. Still, for the scientists this increases time and work expenditure in order to 'patch' an individual cell of a cellular network. Additionally, long and frustrating training periods prevent gathering results quickly.

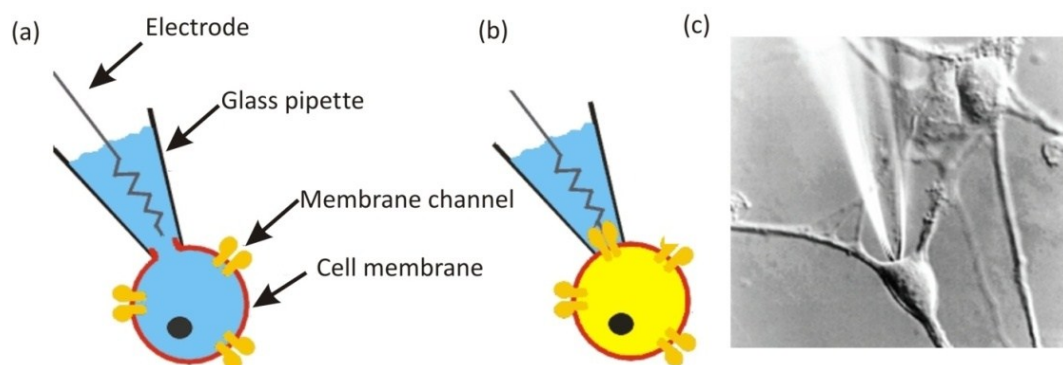


Figure 4: Schematic exemplary patch clamp configurations. (a) Whole-cell; (b) cell-attached; (c) a patch clamp pipette is attached to a neuron growing in a cellular network (Neher and Sakmann, 1992).

Later developments allowed for the automated detection with single cells in suspension (Stett et al., 2003a; van Stiphout et al., 2005). The high need for hERG-tests was one of the mainsprings for the development of the automated planar ion channel analysis of cells in suspension. A recent review summarizes the actual development, problems and limits in automated patch clamp technology with non-adhered cells in suspension, e.g. blood cells (Wang and Li, 2003). In contrast to the little number of cell types naturally living in a suspended state, most cells of the human body grow in networks. Adherence is the native state for most cells, e.g. neurons, liver, lung epithelia or cardiomyocytes. One should keep in mind that approximately 95 % of the 220 human cell types live in adherent cellular networks. Adherent cells cannot be analyzed with present commercial patch-on-chip systems. These cells can only be examined with automated patch-on-chip methods after they are torn out of the cellular networks. In addition, for the detachment of cells, for example with the protein-digesting enzyme trypsin, all receptors of the cell membrane, integrines and ligands are destroyed. Natural cell reactions are therefore unlikely. An intracellular examination of trypsinated and therefore detached cells does not reflect the physiological condition in the cell network. Therefore, in principle the work of *Neher and Sakman* still represents the state-of-the-art for adherent cells.

Modern therapeutic anti-bodies (New Biological Entities) to fight cancer cells, e.g. Avastin®, block the vascular endothelia growth factor (VEGF) leading to apoptosis. Adherent endothelial cells of the blood circulation, for example those that connect malignant tumors with the blood vessels, must therefore be examined in their adherent state, in order to reflect their natural characteristics.

In this thesis, I present a new method for the measurement of V_m with microstructured needle electrodes (MNE) after local electroporation pulses (LEPs) of single cells growing on MNCs. The aim of the local microinvasive needle electroporation (LOMINE) system is to detect alterations of V_m induced by pharmacological test substances or drugs. The patented LOMINE method (Baumann et al., 1998a; Baumann et al., 1998b) combines LEP with a patch-on-chip system and is the base of the PoreGenic® system. During LOMINE, the very high local electrical field at the tip of the MNE alters the lipid structure of the membrane; the binding forces i.e. (dipole-dipole and hydrophobic interactions, *Van der Waals* forces, etc.) are overcome allowing for a reassembling of the phospholipids. Strong external electrical fields may induce membrane pores, i.e. electroporation (Maswiwat, 2008). Extracellular compounds may cross the membrane via these pores and affect the cell metabolism. As in the classical electroporation (Olofsson et al., 2003), the pore size depends on the applied potential at the MNE, molecular membrane composition, pulse characteristics (length, rate and shape), medium properties, etc. Pores can reseal or enlarge until the membrane is torn apart and the cell dies (Rols and Teissié, 1998). Electroporation is observed when the transmembrane potential ($\Delta\phi$) induced by the external field reaches a “critical voltage” of approximately 1 V (Sale and Hamilton, 1968; Kinosita and Tsong, 1977; Zimmermann, 1996; Maswiwat, 2008). The author assumes that such voltage amplitude should lead to LEPs of cells growing over MNEs, because the cell stretches over the MNE in the very small distance of a few nanometers (see 3.3.3.5, p. 70).

In contrast, the classical setup for the electroporation of cells in suspension leads to the formation of many membrane pores due to increased transmembrane voltages (Weaver, 1993). A good overview is given by *Neumann* (Neumann et al., 1989).

1.5 Dielectrophoretic cell allocation

Defined networks with small numbers of neurons are a prerequisite for reproducible signal acquisitions and the observation of specific information exchange. This is difficult and complex in non-defined cultures. Additional methods have to be applied for culturing single cells, cell aggregates or networks in a predetermined way. Photolithographical techniques (Shu et al., 2004) and dielectrophoresis (DEP) can be applied to allocate cells to a specific adhesive site or to electrically conducting chip structures (Heida et al., 2001; Prasad et al., 2003). For cells, DEP was first described in the 1950s (Pohl, 1951). Uncharged particles or cells can be moved by DEP induced in a non-uniform AC field of a given frequency when their effective polarizability exceeds that of the suspension medium (Gimsa, 1991; Gimsa, 2001). The field-induced dipole moment leads to a net movement of the whole cell into (positive DEP; pDEP) or away from (negative DEP, nDEP) regions of higher field strength (Gimsa et al., 1996). The choice of buffer is important for successful pDEP at frequencies in the MHz-range; the external conductivity must be lower than that of the cytoplasm for pDEP, and higher for nDEP, respectively. Choosing the right buffer conditions, the scientist must balance between high-nutrition buffer with high conductivity and good pDEP performance in low conductive buffer. High-nutritive medium will result in nDEP (cell repulsion). Low conductive buffer will lead to cell damage, weak cell adhesion, poor neuronal sprouting, cell starvation and finally cell death during pDEP. Higher voltages must be applied for larger electrodes and/or electrode distances. However, higher voltages and/or lower frequencies (nDEP) may cause cell damages. The movement depends on factors like cell shape, cell parameters, and medium conductivity (Gimsa, 1991; Jones, 1995). The dielectrophoretic force (F_{DEP}) (Gimsa, 1991) of a spherical cell is given by:

$$F_{DEP} = \frac{2}{3} \pi \cdot \epsilon_0 \cdot \epsilon_e \cdot r^3 \cdot \text{Re}(K) \cdot \nabla E^2 \quad (2)$$

here ϵ_0 , ϵ_e , and r stand for the dielectric constant of the vacuum, the relative dielectric constant of the surrounding medium and the radius of the cell, respectively. $\text{Re}(K)$ and E stand for the real part of the Clausius-Mossotti-Factor, i.e. the frequency-dependent part of the induced dipole moment and the electric field (Gimsa, 2001).

Practically, DEP is easily applicable because the same electrodes can be simultaneously used for cell allocation and electric detection. In my thesis, pDEP was applied to SNCs and MNCs to allocate PNCs at the electrodes to improve the signal yield and quality.

1.6 Possible adverse effects of electromagnetic fields (EMF)

The possible effects of EMFs on biological systems are a subject of public concern and scientific discussion. EMF like in a microwave oven (2.455 GHz) cause heating of aqueous matter due to the imperfect re-orientation of water molecules at microwave frequencies, as these frequencies are close to the dispersion frequency of water (approximately 18 GHz). Additionally, due to classical structural and Debye dispersions, bound water structures are heated by the absorbed EMF at lower frequencies (Pottel et al., 1984; Simeonova and Gimsa, 2006). In principle, these processes appear during the use of Universal Mobile Telecommunications System (UMTS) telephones. Fortunately, mobile phone radiation is limited in power. Nevertheless, to a small extend, this radiation will also cause a heating effect, which is time, distance, power and frequency dependent. Warming an organism leads to higher metabolic rates and faster cellular respiration. The parameter describing this effect is the specific absorption rate (SAR) of the mobile phone. Locally, the EMF of a cell phone antenna interacts with the water content of skin, skull, veins, and blood and only to a smaller extend with the brain tissue because of the attenuation of the EMF during the passage through the skull. Finite-difference time domain-based computations showed temperature elevations well below 0.1°C inside the inner ear structures, when considering typical SAR values of handheld devices (Schmid et al., 2007).

Studies on EMFs mainly center on animal experiments (Waldegrave, 1986). Those can focus on brain reaction time (Bawin et al., 1975), cognitive functions, brain morphology (Beall et al., 1996), behavioral science (Adair and Adams, 1980), embryonic development (Thalau, 2002) and breast cancer (Baum et al., 1995) and also on dosimetry studies with human volunteers (Graham et al., 1994). In 2000, the auction of UMTS licenses in Germany carried a yield of 50.8 b€. Approximately 17 m€ were spent for the German mobile communications research program (Deutsches Mobilfunkprogramm) to examine possible effects of UMTS on biological matter. The program started in 2002. Until 2007, about 50 research projects (biology, dosimetry, epidemiology and risk communication) were conducted. The 2006 WHO Research Agenda For Radio Frequency Fields demands further studies at the cellular level (World Health Organization, 2006). One of these cellular systems are nerve cells, e.g. in the hippocampal brain slices (Gluckman et al., 1996; Ghai et al., 2000; Tattersall et al., 2001). The membranes of nerve cells, e.g. in the central nervous system, are in focus of the search for possible targets of EMF. In the framework of one of the projects of

the German mobile communications research program, these circumstances led to the idea to use PNCs for biophysical exposure experiments and to record the neuronal AP patterns and additionally the temperature during exposure. In this thesis, PNCs were cultured on SNCs for exposure experiments. The technique was developed as an alternative to the common patch clamp approach. The aim was to clarify whether SNCs can be used under EMF exposure and whether possible athermal effects on neuronal network can be detected. The PNCs were exposed to different EMF power levels and AP patterns were detected. In parallel experiments, neurons were heated stepwise and patterns were recorded. The setup is partly presented in **Manuscript 1, p. 103ff**.

1.7 The appended manuscripts

The biochips allow the acquisition of electrophysiological signals of PNCs as described in **Manuscript 1 – UMTS EMF setup with the SNC, p. 103ff** (Koester et al., 2007b) and in **Manuscript 2 – Modular glass chip system, p. 104ff** (Koester et al., 2010a). **Manuscript 3 – Introduction to the intracellular potential measurements with the MNC and the PoreGenic® system, p. 105ff** (Koester et al., 2008a) and **Manuscript 4 – First intracellular recordings with 3D microelectrode arrays after local electroporation, p. Fehler! Textmarke nicht definiert.ff** (Koester et al., 2010b) introduce the principles of the measurement as well as first results of transmembrane potential detection. A study presenting APs of cultivated PCMs is presented in. pDEP experiments are introductorily described in **Manuscript 5 – Dielectrophoresis with the SNC, p. 107ff** (Koester et al., 2008c) as well as in **Manuscript 6 – Dielectrophoresis with the MNC, p. 108ff** (Koester et al., 2008b).

This thesis presents different tests with prototypes of completely new biochip systems. Due to the limited time available and the high experimental demands, the results must be regarded as basic proofs of concepts.

2. Material and Methods

2.1 Biochips

2.1.1 The neuro-measuring adapter (NMA) and the silicon neurochip (SNC)

The SNCs used were a combination of a passive MEA of 58 microelectrodes for acquiring APs with ISFETs for pH measurement as well as a temperature diode using state-of-the-art silicon CMOS technology (Baumann et al., 2004; Koester et al., 2007b). The temperature diode and the pH sensors are located underneath the cell layer and allow for real-time temperature and pH detection. The pH could not be measured, because most of the SNCs' pH sensors did not withstand the conditions during four weeks of culture. Hence, the pH-sensors were not used in the studies. The SNC layout was developed at the Chair of Biophysics (Baumann et al., 2004). Silicon chips were bonded on ceramic carriers (Kyocera Fineceramics GmbH, Esslingen) and were provided by Micronas GmbH, Freiburg.

The assembly of the SNCs ($1.7 \times 1.7 \text{ cm}^2$) was done at the Chair of Biophysics. Two separate gluing steps are necessary for a successful interconnection of the silicon chip and the ceramic carrier with the encapsulation component. For this, the PNC culture-tested adhesive Med-1511 (NuSil, Carpinteria, CA, USA) was used. It consists of two silicone components mixed at a ratio of 1:10. The first gluing step ensured the secure sealing of the chip interior. For the second filling step, Sylgard 184 adhesive (Dow Corning GmbH, Wiesbaden) was used. For the gluing and filling steps, approximately 0.05 g and 0.23 g of adhesive were required, respectively. Gluing and filling were carried out manually with a modified syringe. The gluing and filling components were cured at room temperature for two days each to ensure tight cross-linking of the silicone compounds.

For data registration, the SNCs were inserted into standard ceramic leadless chip carrier (CLCC) sockets (**Manuscript 1, p. 103ff**). A sophisticated neuro-measuring adapter (NMA) system was integrated closely beneath the CLCC socket for filtering and amplification of AP signals from the cultivated PNCs. Neuronal signal acquisition quality depends on the electrode transmission. Therefore, each cell-free SNC must be controlled and characterized with a special signal generated by a function generator (Model 33120A; Agilent Technologies Inc., Santa Clara, CA, USA). The signal simulates the amplitude ($U = 1 \text{ mV}$) and frequency ($f = 1 \text{ kHz}$) of neuronal APs using a sinusoidal waveform. The detection of the neuroelectric activity is described in detail in **Manuscript 1, p. 103ff**.

2.1.2 Modular glass chip system and the glass neurochip (GNC)

The Chair of Biophysics (Prof. Gimsa) aimed to develop a new glass chip for detecting the electric activity of neurons. The author was involved in the design of this new chip prototype combining a MEA with different on-chip sensors. The goals were to fabricate a very robust, autoclavable (121 °C) neuronal signal detection platform that would be microscopically observable and reusable up to 100 times. This new GNC combines three functions: (i) electrical recording of neuronal and cardiac APs from 52 microelectrodes, (ii) analysis of alterations in the cell adhesion from an interdigitated electrode structure (IDES) impedance, and (iii) an on-chip control of the chip temperature. The GNC was designed for HCS requiring a very small space (length of only 16 mm, height of 6 mm) and is produced by GeSiM mbH, Großkrummannsdorf. At present, the headstage is the size of a 3.5" hard disk. Details of the chip structures are described in **Manuscript 2, p. 104ff**. The following advantages highlight the innovations of this system:

- smaller design than competing products, e.g. MCS GmbH or chips of the Gross group (University of Texas, USA)
- efficient, high-precision manufacturing due to the glass wafer technology,
- very good microscopic observability,
- reproducibility of experiments,
- small substance doses can be used due to the small culture volume, and
- improved image and reputation among customers due to the reduction of animal experiments.

2.1.3 PoreGenic® system and the microneedle chip (MNC)

As the basis for the detection of intracellular potentials, the technical aspects had to be realized first. The starting point for this technical development was to get a suitable equivalent circuit reflecting the substantial relations between cell, bioanalytical MNC and electronic circuitry (**Figure 5**). Our preliminary test version allows for the parallel individual control of 15 MNEs. One MNE is disconnected, in order to observe the deterioration of this MNE. The electronic periphery of each electrode contains circuits for cell manipulation, the measurement of the needle potential is further described in **Manuscript 3, p. 105ff**. Two different circuit types could be used for intracellular or extracellular potential measurements.

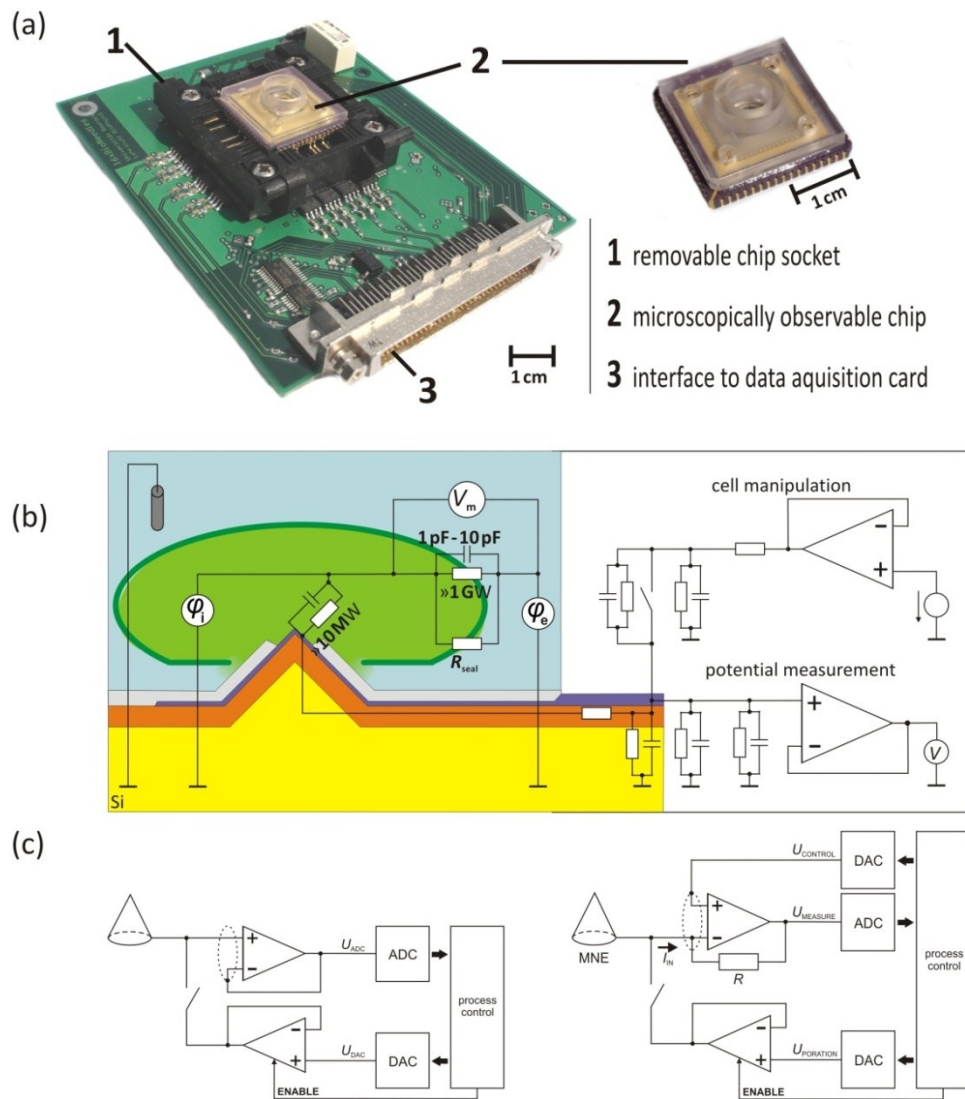


Figure 5: Schematic layout of the PoreGenic® system (C. Tautorat). (a) The sensor measuring board with the MNC; (b) equivalent circuit for modeling the interrelations of the cell, the MNE and the electronic circuitry. Colored structures sketch an electroporated cell (green) with a penetrating MNE on the silicon substrate (yellow); (c) the current-voltage converters (left) and the scheme for cell manipulation (right).

While twelve voltage-followers will be limited to measuring voltage, the four current-voltage converters will allow for intracellular membrane potential measurements as well as current measurements in the voltage clamp mode (**Figure 5c left**). Therefore, a defined control voltage can be applied if necessary. In addition to the intracellular potential measurement for the conditions $I_{IN} = 0$, this system also allows for an examination of the electrical characteristics of the electroporated cell, e.g. testing of the gigaseal¹ quality R_{seal} (**Figure 5b**). The signals measured by all eleven voltage followers are sampled at 15 kHz with a resolution of 0.1 mV. **Figure 5c (right)** presents additional electronic features of the LOMINE method used for cell manipulation. The complete electronic setup is mounted in an aluminum-housing (**Figure 6**). The test application used administers rectangular pulses (bi- or unipolar) with a minimum single pulse interval time of 5 μ s. Amplitude, duration, and polarity of the pulses can be defined by the user. Special reed relays and tri-state circuitry are used to minimize stress effects to the cell caused by leak currents etc. The convenient software allows for the selection of a single MNE or an arbitrary group of electrodes for LEPs. The control headstage and the software of the complete system were developed at the University of Rostock by C. Tautorat. The headstage allows for data acquisition (DC voltages and currents) and electroporation (local microinvasive membrane rupture, stimulation) for the cells, which overgrew the MNEs.

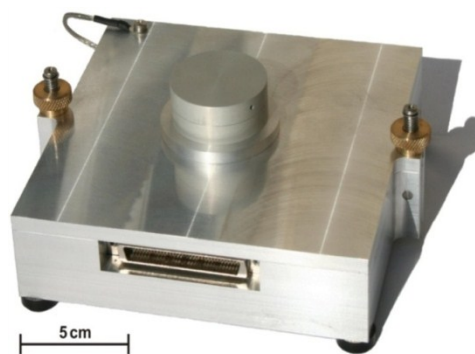


Figure 6: Robust and washable aluminum-housing for the *PoreGenic*® setup. The MNC is inserted into CLCC socket and the aluminum-cover is screwed on the heating block. The cylindrical aluminum-cap allows for application of substances and aeration e.g. with artificial air.

The MNC comprises 64 MNEs arranged in an 8x8-MEA mounted on a 68-Pin-CLCC. The MNC layout and production (Trautmann et al., 2004) were adapted to the requirements of the LEPs. The silicon chip was glued onto the ceramic carrier by Dr. J. Held at the Department of Microsystems Engineering (IMTEK) of the University of Freiburg. The MNCs were assembled

¹ gigaseal = tight connection between MNE and biological cell with a typical resistance > 1 gigaohm.

by the author with a cell culture trough according to the procedure demonstrated with the SNC. It was designed for water immersion objectives (up to 100x) and allows for long-term culturing of adherent cells, simultaneous LEPs of independently selectable single MNEs, and the measurement of intracellular potentials of biological cells. Additionally, the MNC allows for the detection of APs of adherent PCMs on independently selectable single MNEs. In summary, three different types of electrodes were processed.

The chip layout was processed in different versions - those of the MNE shape, the MNE material, and pinning at the IMTEK (Held et al., 2007; Held et al., 2008a; Held et al., 2008b; Held et al., 2009). The complex processing steps of the MNE are shown in **Figure 7**.

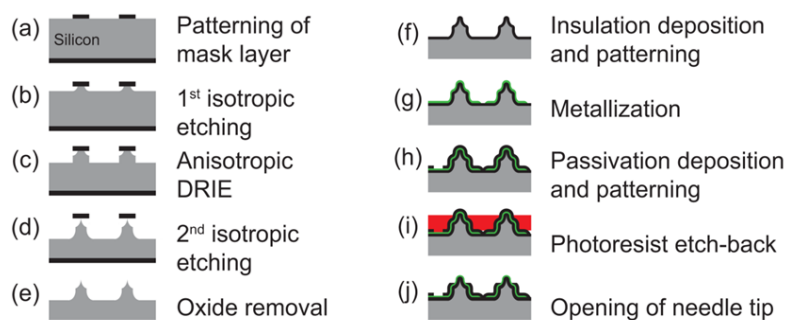


Figure 7: Schematics of MNC fabrication processes. The stepwise *isotropic* - *anisotropic (DRIE)* - *isotropic* process of MNE arrays for cardiac AP and intracellular transmembrane potential recording applications (Dr. J. Held, IMTEK).

Further deep reactive ion etching (DRIE) processing steps are described in Dr. J. Held's thesis (Held, 2009). The MNE's three-dimensional design required three consecutive DRIE steps: one isotropic, followed by an anisotropic DRIE and another isotropic silicon-etching step.

The pDEP electrodes were integrated to increase the likelihood that cells would overgrow the MNEs. One-hundred twenty-eight kidney-shaped pDEP electrodes were integrated into the MNC containing 64 MNEs, each framed by two pDEP electrodes that were 30 μm apart. **Figure 8** shows microscopic images of the MNC MEA, the pDEP electrodes and the MNEs. First, however, the biocompatibility of the completed chips was checked. The chips were cleaned and inoculated in the cell culture laboratories with several cell types (human, murine) at the Chair of Biophysics. Cell positioning and cell adhesion was subsequently examined by scanning electron microscopy (SEM). The successful electroporation was demonstrated by means of the FIB technology in combination with the SEM (Fraunhofer Institute for Mechanics of Materials, Fh-IWM). The FIB-SEM technique allows for the cutting of all materials used. The MNC surface and cells presented in this thesis were cut by

A. Cismak (Fh-IWM). By this technique the penetration of cells by the MNEs could be demonstrated (Heilmann et al., 2007). The electroporation process itself was followed microscopically by fluorescence methods. For cardiac AP detection, three types of chips were tested. The fabrication steps are described in detail by Dr. J. Held (Held, 2009) and are experimentally tested in a later chapter.

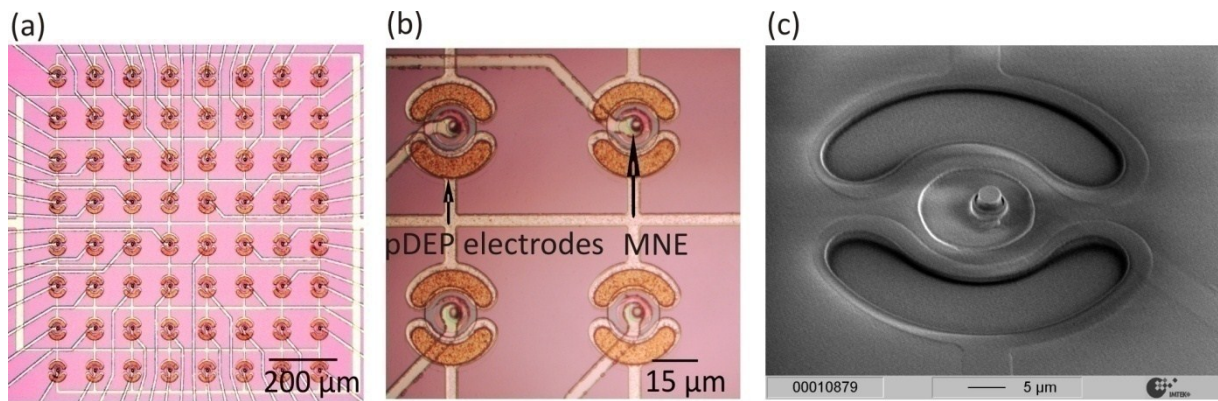


Figure 8: Kidney-shaped pDEP-electrodes. a) MNE and pDEP array; (b) magnification of left image; (c) SEM of pDEP-electrodes framing a MNE.

2.2 Chip preparation and cell culture

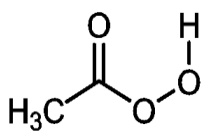
2.2.1 Sterilization methods

Three new sterilization methods (formaldehyde, peracetic acid and chlorine dioxide) were tested as alternatives to the standard autoclaving of biochips. In any case, the chips were enzymatically cleaned before sterilization with trypsin (Biochrom AG, Berlin) in order to remove protein contaminations. The detergent Terg-A-Zyme® (Alconox Inc., White Plains, USA) was used for chip cleaning to dissolve fatty acids and lipids from the culture trough. After cleaning, the chips were rinsed several times with deionized water ($< 1\mu\text{S}/\text{cm}$).

For autoclaving, SNCs were sterilized with a desk autoclave (Model 2540EL; Systec GmbH, Wettenberg) using a standard protocol (20 minutes, $121\text{ }^{\circ}\text{C}$).

Formaldehyde (methanal, CH_2O ; Carl Roth GmbH, Karlsruhe) was the first agent to be tested for its disinfecting characteristics. For that process, chips were submersed in a solution of 5 % formaldehyde in water.

A second agent was peracetic acid (PAA, $\text{C}_2\text{H}_4\text{O}_3$, 0.2 Vol.-%). Chips were entirely submerged in PAA (Applichem GmbH, Darmstadt) for one hour. Its aqueous solution was a mixture of acetic acid (CH_3COOH) and hydrogen peroxide (H_2O_2).



PAA is colorless with a pungent odor and a low pH (2.8). PAA is produced by a reaction between acetic acid and hydrogen peroxide. When PAA is dissolved in water, it disintegrates to acetic acid and hydrogen peroxide, which further reacts to water, oxygen, and carbon dioxide. The PAA degradation products are non-toxic and can easily dissolve in water.

The third agent was chlorine dioxide. Commercially available chlorine dioxide releasing sticks (knick'n'clean *Flora*, courtesy of Dipl.-Ing. H. Bobke, Hannover) were combined with cleaned chips in a depressurized vessel (Volume approximately 1 l). The SNCs, the GNCs and one stick were let together for 48 h. The concentrations of ClO_2 were measured during the sterilization step with a hand pump and single-use gas probes (No. 8La, GasTec Gasgerätetechnik GmbH, Neuenhagen).

2.2.2 Biochip preparation

In general, the biochips were coated with the cell-adhesives PDL and laminin. The sterilization with PAA allowed for an easier adhering of the cell adhesive molecules on the Si_3N_4 -surface. The central MEA (approximately 1 mm^2) and the culture surface of the chip (approximately 38 mm^2) were coated with PDL in water and a laminin/DMEM mixture. The adhesion fluid incubated on the chip overnight at room temperature (24°C). The coating procedure and the properties of these molecules are described in detail in the Manuscripts.

2.2.3 CO_2 -aeration during cell culture and experiments

The following cultures were maintained at 37°C in artificial air with 10 % CO_2 (Westfalen AG, Münster) for 30 to 60 days *in vitro* (DIV) to keep the pH at 7.2-7.4 in the culture medium. A higher concentration of CO_2 ($> 10\%$) in air will result in an acidification of the medium ($\text{pH} < 7.3$). Both pH states result in the slow decline of neuronal and cardiac activity and finally to death of all type of cells (PNCs, PCMs and fibroblasts). Therefore, all experiments described were conducted under local CO_2 -aeration.

In order to terminate neuroelectric signals at the end of the experiment and to prove that the recorded signals were of biological origin, the detergent Triton®-X 100 (Carl Roth GmbH, Karlsruhe) was added to the medium. This detergent dissolves the phospholipid bilayers and kills the cells.

2.2.4 Preparation of primary neuronal cells (PNCs)

PNCs were isolated from the frontal cortex of embryonic NMRI mice (E15-E17, **Figure 9**) and postnatal Wistar rats (P1-3, not shown) provided by the core facility “animal house” (Medical Faculty, University of Rostock). The postnatal animals were prepared in the first days after birth because PNC quality and the ability to sprout begin decreasing immediately after birth. The following procedures were carried out in accordance with Directive 86/609/EEC for animal experiments (Waldegrave, 1986) under sterile conditions using a stereo microscope (Stemi 2000-C, Carl Zeiss AG, Jena) in a horizontal laminar flow cabinet (ESCO® AHC-3A1, SLEE GmbH, Mainz). The mother animals (mice) or the rat pups were narcotized with CO_2 . After sedation, the mouse embryos were extracted and decapitated or the rat pups were decapitated; their heads were rinsed in alcohol (70 %) for disinfection and transferred into D1SGH-buffer (Garrido et al., 2001).

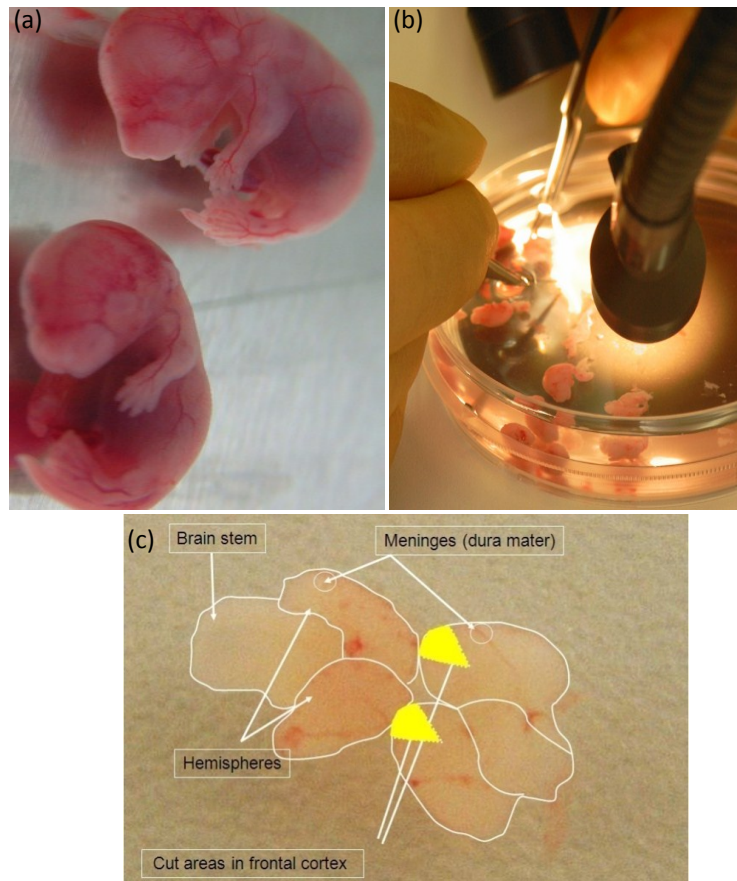


Figure 9: The preparation of the mouse brain. (a) Explanted mouse embryos (E15); (b) dissection of embryo heads; (c) bordered silhouettes of two brains and explanted frontal cortex areas (yellow).

The foreheads were opened medially and the brains were removed with a pair of honed forceps (Fine Science Tools GmbH, Heidelberg). The meninges were peeled off and removed to avoid autoimmune reactions and contamination with alien cells in the culture vessels. The frontal cortex was extracted. The following steps were conducted using a vertical flow safety cabinet (Microflow, NUNC GmbH, Wiesbaden). The supernatant D1SGH buffer was discarded. The tissue fragments were chopped and 3 ml papaine solution (10 units/ml; Roche Diagnostics GmbH, Mannheim) enriched with 50 μ l of dissolved desoxy-ribonuclease I solution (8000 units/ml; Roche) was added. The enzyme-containing solution and the tissue were incubated for 20 minutes at 37°C and were then triturated. No enzymes were used to segregate the rat pup PNCs. The obtained homogenate was then triturated in D10/10 (DMEM; Biochrom AG, Berlin, enriched with 10 % fetal calf serum (FCS) and 10 % horse serum (HS) (both PAA Laboratories GmbH, Cölbe), and 1 % l-glutamine, 200 mM (Biochrom AG, Berlin) and centrifuged for 4 min at 1000 RPM. The supernatant was discarded and the cell number adjusted to 1.28×10^6 cells/ml D10/10. High quality FCS and

HS were prerequisites for the successful culture of PNCs. Many serum batches were checked under culture conditions to select the one most suitable for neuronal growth.

Biochips were cultured in an incubator (Model CB-150, Binder GmbH, Tuttlingen). To dispose of metabolic waste, half of the medium of each chip culture was replaced by fresh, pre-warmed DMEM containing 10 % equine serum (D10) three times a week. No additional FCS was added to reduce glial growth. To inhibit proliferation of the glial cell population, 100 μ l of a DMEM solution enriched with fluorodesoxyuridine (50 μ M) and uridine (126 μ M; both Sigma-Aldrich GmbH, Taufkirchen) was added to the on-chip cultures depending on cell concentration. Uncontrolled glia overgrowth led to neuronal death. After about one week, the cultures started to exhibit neuroelectric activity in the form of spontaneous APs. Generally, the full activity with neuronal bursting was observed after about four weeks and the networks were considered mature and suitable for experiments.

Another very important parameter is the cell number in the cell suspension. For long-term cultures (up to several weeks or months), the cell number has to be perfectly adjusted to the given culture surface, medium type and volume and the cell type. In addition, the ratio of glia to neurons is highly important. The cell number was determined with a *Neubauer* counting chamber. Neurons and glial cells have diameter of approximately 10 μ m. Cell types cannot be distinguished after papaine-digestion. The optimal empirically obtained cell number for the SNC was 1.28×10^6 cells/ml. At this concentration, the PNCs showed robust neuronal growth and a balanced glia-to-neuron ratio for many weeks. For experiments requiring short-term observations (up to days), the cell number is of lower priority since neurons can survive for a short time under suboptimal conditions. On SNCs, cell numbers that were too low ($< 0.8 \times 10^6$ cells/ml) led to cell-cohorts and 'lonely' cells. Subsequently, cells died because of the excessive distances between the cells. Plausible reasons for this are that no tightly adhered networks could be established and the PNCs were unable to condition the trough-medium. In comparison, PNCs growing in a cell culture flask or on GNCs showed good growth at low cell numbers (0.5×10^6 PNCs/ml) possibly due to the more electronegative surface of polystyrene or the GNC surface. In addition, high cell numbers ($> 2.0 \times 10^6$ cells/ml) led to cell-death due to a peel-off phenomenon starting at the outer gluing seam near the medium trough. This observation may be explained by a local oxygen depletion of glial layers underneath the neuronal cell layers. Biochemical experiments are described in **Manuscript 2, p. 104ff.**

2.2.5 Preparation of primary cardiac muscle cells (PCMs)

The hearts of murine embryos (E15-E17, not shown) from mice as well as rats (**Figure 10**) were dissected. The procedure was carried out in conformity with Directive 86/609/EEC for animal experiments and is based on the preparation of PNCs.

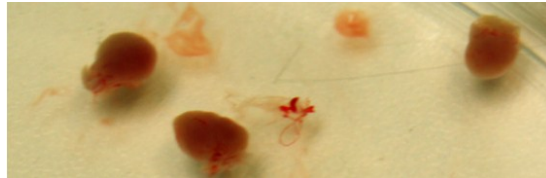


Figure 10: Three explanted hearts of postnatal rats (P3). Hearts have diameters of approximately 3 mm. The hearts still contain little amounts of blood, which must be squeezed out to prevent immunological reactions during the PCM culture. The heart-enclosing pericardium must be removed to avoid fibroblast outgrowth.

The cell number was adjusted to 0.5×10^6 PCMs/ml D10 for the culture on the GNC and the MNC. Tissue preparation was conducted under sterile conditions as described above. To dispose of metabolic waste, the medium of each cultured chip was replaced by fresh, pre-warmed D10 every day. Cultures were ready for experiments 2 DIV after confluence was reached and the PCMs showed constant muscular contractions on the MEA. Preliminary experiments with PCMs prepared by the author were also done by Dr. R. Schrott at the Chair of Biophysics (Schrott et al., 2006; Schrott et al., 2007; Schrott, 2009).

2.2.6 L929 mouse tumor and normal human skin fibroblasts (NHDF)

L929 mouse tumor and NHDF were detached and plated every second DIV using trypsin in phosphate-buffered saline (PBS, without CaCl_2 and MgCl_2). The culture medium was DMEM with 10% FCS, 1% l-glutamine, 1% penicillin, and 1% streptomycin.

2.3 Experiments

2.3.1 Cell positioning with positive dielectrophoresis (pDEP)

The idea was to increase the neuroelectric yield of PNCs by building neuronal networks on the MEA. **Figure 11** gives a schematic overview. This procedure was accomplished in an incubator (Model B-15, Thermo Electron LED GmbH, Langenselbold) at 37 °C.

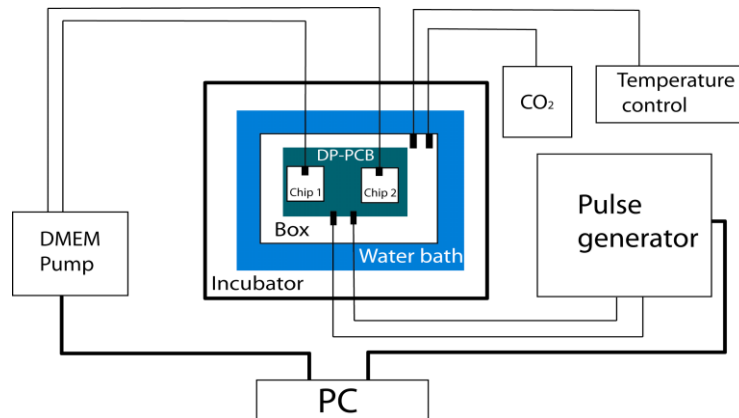


Figure 11: Setup scheme for pDEP cell allocation. Two SNCs containing pDEP buffer and suspended neuronal cells can be worked on simultaneously in the chip socket. The socket was installed in a plastic box. This setup was located in an incubator (37°C) featuring a water bath. The chip socket was connected to the pulse generator that provided the AC signals. The SNCs were connected with a peristaltic pump that gently injected D10/10 into the SNC through a medical syringes after completed pDEP.

An optimal buffer for pDEP was empirically designed. The best option was D10/10 diluted with water (ROTIPURAN® p.a., ACS, conductivity < 1 $\mu\text{S}/\text{cm}$; Carl Roth GmbH, Karlsruhe) at a relation of 1:6 (DMEM/water). The author chose DMEM without NaHCO_3 (Invitrogen GmbH, Karlsruhe) in order to maintain the pH. Several buffer compositions were tested. For energy supply, the diluted buffer was enriched with 4.5 g glucose/l (Sigma-Aldrich GmbH, Taufkirchen). Osmolarity was adjusted with sucrose (approximately 90 g/l; Sigma-Aldrich GmbH) to 345 mOsmol using an osmometer (Osmomat 030; Gonotec GmbH, Berlin). The pH (7.37) and the resulting conductivity (1.8 mS/cm) were checked with a pH meter (Cyberscan 500; Eutech Instruments Europe B.V., Nijkerk, NL) and a conductometer (Model LF539; WTW GmbH, Weilheim), respectively. For viability control, PNCs were let for 6 h in pDEP-buffer before plating in a cell culture flask. Long-term viability was checked after 24 h by adding trypan blue (Biochrom AG, Berlin; data not shown). Only few dead cells were observed with this diluted enriched DMEM (pDEP-buffer) that was used for pDEP experiments. The number of dead cells was comparable to control flasks with high-conductive DMEM. Experiments with purely inorganic buffers and very low conductivities

like Na_2CO_3 - NaHCO_3 -sucrose-buffer (e.g. pH 7, 203 $\mu\text{S}/\text{cm}$, 298 mOsmol) led to weak cell adhesion and were therefore aborted.

A complex setup was developed for pDEP positioning of neuronal cells on the MEAs of SNCs. First, the dried cell-adhesive laminin/DMEM solution was washed away with 50 μl pDEP-buffer in order to remove salts, medium compounds, etc. and to maintain the correct conductivity. The SNC medium trough was filled with only 50 μl of the cell/pDEP-buffer solution. The voltage was immediately applied to prevent cell adhesion at undesired locations beyond the MEA. The volume used corresponds to approximately 2×10^3 neuronal cells on the MEA. A USB-camera (Model SMX-M73; Sumix Corp., Oceanside, USA) was installed on a reflected light microscope (Model BX-51WI; Olympus Corp., Japan) and connected to a PC to record the pDEP procedure visually. A 300 MHz pulse generator (Model 8130A; Hewlett-Packard, Wilmington, USA) was connected to the CLCC socket containing two SNCs. The generator was controlled by homemade software. MEA electrodes were supplied with phase shifted AC signals (**Figure 12**).

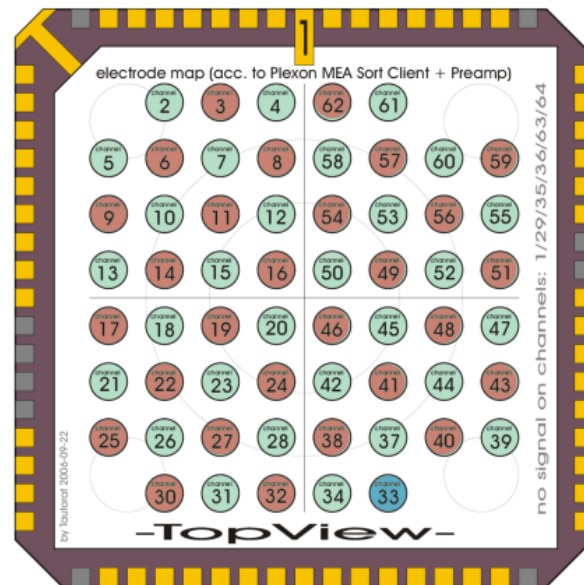


Figure 12: Electrode mapping for pDEP cell allocation. Green/red: electrodes driven with 0° and 180° shifted AC voltages. Blue: disconnected electrode.

For the positioning of PNCs, a 10 MHz signal was used at a voltage of 2 V_{pp} for 60 minutes in order to attract the cells to the influence radius of the AC field. This time span is sufficient to allocate all cells in the 50 μl suspension. After cell allocation, the generator power was reduced to 1 V_{pp} to keep the cells adhered to the SNC surface for 60 min. The pulse generator was turned off after positioning and adhesion when the electrodes were covered

by bell-shaped cell aggregates. For filling the trough with nourishing D10/10, a sterile and honed hypodermic needle (true short bevel, inner \varnothing 0.2 mm, Sterican®, B. Braun-Melsungen AG, Melsungen) was fixed to the ends of autoclaved latex tubes (inner \varnothing 0.9 mm) and inserted into the medium troughs directly onto the chip surface. The tubes were connected with a peristaltic pump (Model IPC-N-8; Ismatec GmbH, Wertheim-Mondfeld). The pump was controlled by a LabVIEW® program (National Instruments, Austin, TX, USA). Enriched DMEM was pumped into the trough of the SNC from a 50 ml reservoir located in the incubator. The pump flow was adjusted to 1.38 μ l/min for 180 min (total 250 μ l) to dilute the buffer in the chip's culture trough very carefully with enriched DMEM. The pump cycle was divided into stop (3 s) and pump (2 s) phases. This procedure ensures a gradient-like adjustment from the low-nutrient condition to physiological conditions avoiding osmotic cell and shear stress for the cells. The evaporation of approximately 15% of the water content from the fluids was observed. In order to maintain a constant osmolarity of approximately 345 mOsmol/l, the DMEM was initially diluted with 15 % water. At the end of the experiments, the osmolarity reached 350 mOsmol/l. The temperature was checked with a WLPI glass fiber thermo sensor (GFT, PicoSens; Opsens Inc., Quebec, Canada). The GFT digital readout signal shows an accuracy of ± 0.1 °C. This GFT was also used during the UMTS EMF experiments. The whole procedure ensures cell friendly pDEP at low conductive conditions and a subsequent adherence of the cells with high conductive enriched DMEM without mechanical stress.

As an alternative to the pDEP approach, SU-8 structures were processed on the SNC surface by Dr. J. Held (IMTEK) to guide neuronal growth and to minimize shear stress due to medium exchange. SU-8 is a commonly used epoxy-based negative photoresist. The idea was to guide the seeded cells onto the electrodes and connecting channels in between the electrodes to induce the growth of defined neuronal networks. The transparent structures have a length of 50 μ m and a height of 50 μ m.

2.3.2 EMF experiments with the SNC

In this thesis, the author used a standardized UMTS signal with repeating signal modes provided by a special UMTS-Generator (Model GUS 6960 S; courtesy of the University of Wuppertal) (Ndoumbé Mbonjo Mbonjo et al., 2004; Koester et al., 2007b). A signal in the frequency division duplex (FDD) mode was used. **Figure 13** shows the power adjustments of

the UMTS generator. **Table 1** describes the different frequency fractions of the UMTS signal. In the FDD mode, uplink and downlink of cell phone signals is simultaneously realized in different frequency bands. The test signal was developed according to the technical specifications of UMTS to mirror a real signal. Focus was placed on the differences between second generation (2G, e.g. GSM and DECT) and 3G (UMTS) mobile phone systems.

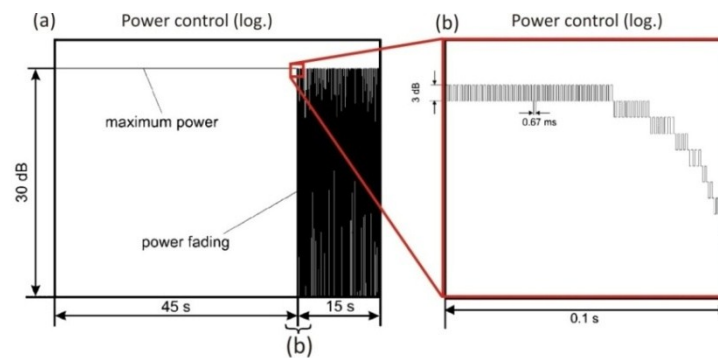


Figure 13: Power adjustments of the UMTS generator. (a) Signal over one minute, the generator is driven at full power for 45 s and switched into the fast power adjustment for 15 s; (b) magnified insert of (a), fast power adjustment during 100 ms (redrawn after Hansen et al., 1998).

Table 1: Frequency fractions of the UMTS signal.

range	range description
16.7 mHz	Slow switching sequence in a minute cycle: 45 s of maximum power output and 15 s in the fading mode
10 Hz	Power adjustment during the fading mode
740 Hz	Fast power adjustment which permanently overlays the generic UMTS EMF.

Varying power and fading phases were combined to simulate a worst-case scenario. For biological exposure experiments, the signal refresh rate must be clearly lower than the modulation frequency of UMTS as well as frequencies of biological events. A schematic representation of the experimental procedures and the setup is given in **Figure 14**. A wave-guide was designed by the group of Prof. V. Hansen, University of Wuppertal (Hansen and Streckert, 1998) and provided as a courtesy. The inner dimensions (12 x 3 x 50 cm) were calculated for the frequency band of GSM. Dr. H.-W. Glock (Faculty of Computer Science and Electric Engineering, Chair of Theoretical Electrotechnics, University of Rostock) adapted the internal antennas for UMTS experiments. This design and parts of the actual experiment setup are described in detail in **Manuscript 1, p. 103ff**. However, experiments showed that the SNC-integrated temperature diode mentioned in the manuscript is not suitable for thermo-sensing during exposure due to an antenna-effect of the sensor: the EMF power was clearly reproduced by the sensor; the temperature information was overwritten by the applied EMF power. Alternatives for temperature measurement and experimental

improvements are described below. Only the chip surface, the culture trough, and the PNC network rise into the wave-guide. The wave-guide is located in an incubator with side-openings (Model BD-105, Binder GmbH, Tuttlingen).

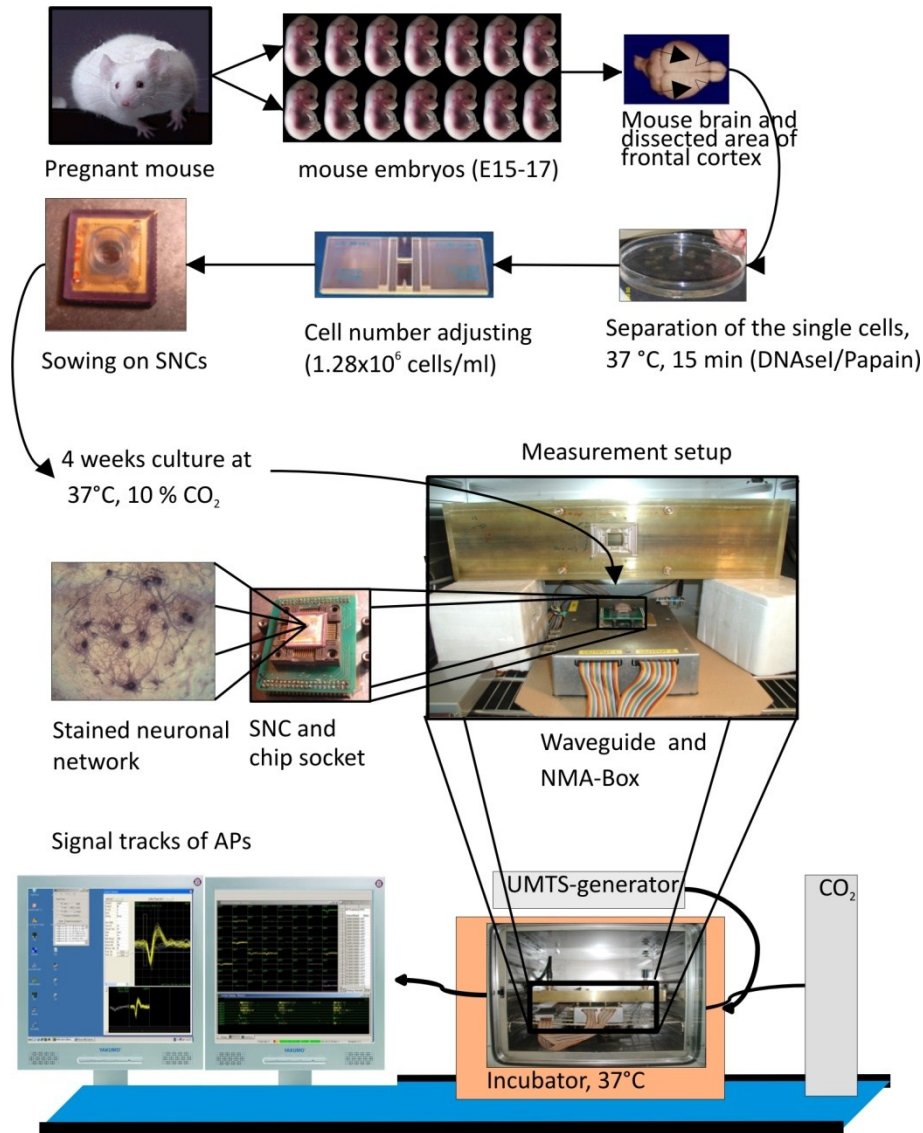


Figure 14: Setup scheme of EMF exposure.

As the wave-guide is located in the incubator, the SNC preamplifier (NMA-box) had to be located in the incubator also. Since the NMA-box has a power consumption of approximately 5 W, it produces heat itself; hence, the incubator temperature was adjusted to 34.5 °C to compensate for this additional heat input. The temperature established in the incubator was 37 °C. A 12 V-ventilator was connected to the amplifier and located in the incubator for secure ventilation. The recordings were not disturbed by the fan. Before exposure started, cultured SNCs were checked in a test recording setup at room temperature to count firing

PNCs as well as signal quality of the SNC. A SNC was of good quality and usable when at least five firing neurons were observed.

A cap was plugged onto the SNC during exposure to avoid evaporation of the culture medium. Therefore, a simple semi-permeable polythene film (polyethylene, PET, permeable for CO_2 , non-permeable for H_2O) was affixed with silicone lubricant on this special homemade acrylic glass cap produced by Dr. Baumann. **Figure 15** shows the acrylic cap with the mounted PET foil and the inserted GFT. In addition, a Petri dish with water was put into the incubator in order to humidify the air inside.

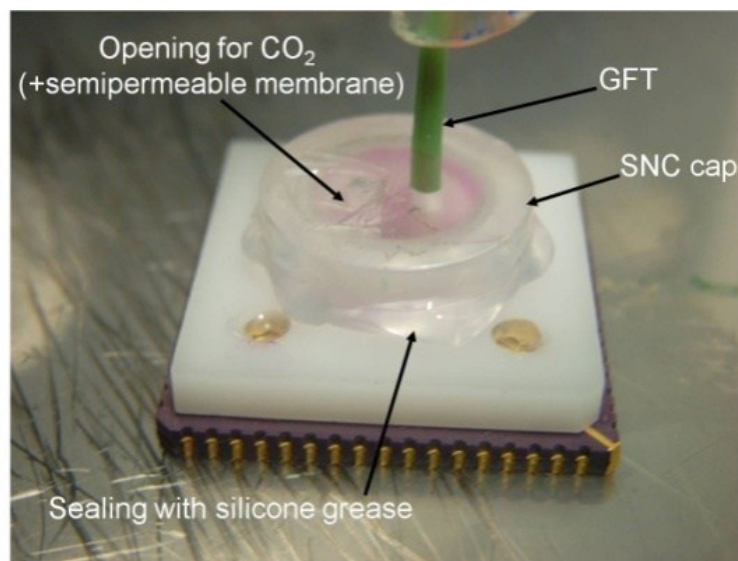


Figure 15: Acrylic cap for PNC protection during EMF exposure. It minimizes evaporation and allows for the insertion of the GFT and the uptake of CO_2 .

Two holes were drilled into the cap, one for CO_2 -aeration of the medium and another for the insertion of the GFT that did not contact the chip area. No cells were irritated by the sensor. The GFT is metal-free and does not hinder or demodulate the EMF exposure. The GFT-reader was connected to a PC that recorded the temperature over time in 5-second intervals. Values were exported into a Matlab® template developed by Dr. J. Sakowski. Cell reactions to UMTS exposure may be due to thermal effects, for example increasing metabolic rates with increasing SNC temperature. To avoid pseudo-correlations, chip heating experiments were performed. For this, the pre-amplifier-integrated heating system was adjusted manually in different temperature intervals and the neuroelectric activity was recorded. In this way, temperature was adjusted to mirror UMTS exposure heating. The temperature rise was $0.3\text{ }^\circ\text{C}$ and was repeated a minimum of five times for each experiment. The temperature rise in the SNC was recorded with the GFT. The conductivity of the culture medium, $\sigma = 1.8\text{ S/m}$

(37 °C), was checked with the conductometer. The electrical connections for the NMA-box, the fan, the GFT and CO₂-aeration were made through the incubator side-opening.

Neuronal signals can be visually detected due to the unique waveform types and by the well-known burst-behavior of neurons. Noise is clearly distinguishable from neuronal signals and shows no classifiable patterns. Stepwise UMTS exposure patterns were performed. The idea behind the stepwise exposure patterns was to form a sinusoid-shaped pattern and to find possible activity alterations due to the pattern style. The power output was adjusted to the sensitivity of the electrodes. Outputs greater than 1 W irreversibly destroyed the electrodes (**Manuscript 1, p. 103ff**); therefore, the highest output chosen was 0.5 W. Destroyed electrodes show permanent noise, however, they could not be identified optically. For data analysis, the fast Fourier transformation (FFT) was used to obtain power spectral density (PSD) plots and to check for a possible reflection of frequency portions of the UMTS EMF in the neuronal activity. The PSD computation elegantly analyzes the time signals, describing the energy of the signals as a function of their frequency.

All procedures for biochemical experiments are described in detail in the appended manuscripts (appendix A) noted in the specific chapters.

3. Results and Discussion

3.1 Overview of experiments

The author presents applications to demonstrate the versatility of three types of different biochips. All of them were developed at the Chair of Biophysics of the University of Rostock.

Table 2 summarizes the experiments with the specific chip types.

Table 2: Experiments with different biochip types.

Measurement	Chip type	Cell type			Sterilizing tests	Biochemical experiments	Biophysical experiments	
		PNCs	PCMs	Fibroblasts	(Autoclaving, Alcohol, Formaldehyde, PAA, knick'n'clean)	Substances	pDEP	HF-EMF
Extracellular	SNC	x			x	Bicuculline	x	x
Extracellular	GNC	x	x		x	VPA		
Extra- and intracellular	MNC	x	x	x	x	---	x	
Thesis/ manuscripts	Both	Both	Both	Both	Only in Thesis	In detail in Manuscript, parts in Thesis	Both	Both

3.2 Statistics on autoclaving and new sterilization methods

3.2.1 Autoclaving and other methods

Autoclaving is the standard method for the sterilization of laboratory goods. It is also used for standard glass MEA chips (Gramowski et al., 2006). **Figure 16** demonstrates that after autoclaving only a few SNCs can be used for electrophysiological experiments.

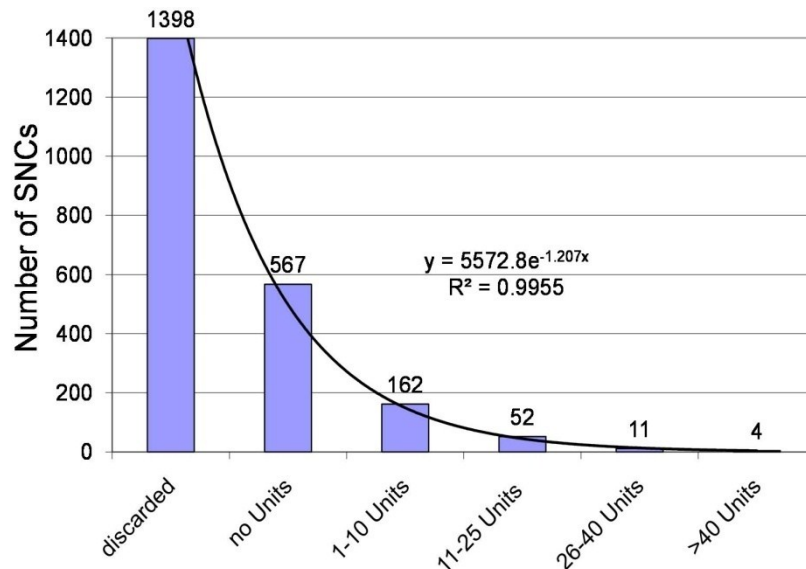


Figure 16: The effect of autoclaving on the SNC quality. The number of SNCs cultured with PNCs sorted after their number of detectable units is shown. Due to chip defects, the signal yield was strongly decreasing. In total, 2194 SNCs were cultured during approximately 2 years.

Only four SNCs with more than 40 electrical active neurons (units) were found. Additionally, autoclaving regularly led to leaky medium troughs.

Therefore, a new sterilizing method had to be found. Different approaches to increase the signal yield were tried with little success. Only when SNCs were disinfected with alcohol (70 % in water) was the yield higher (data not shown). However, alcohol disinfection fails to eliminate yeast spores and several bacteria species. Soon, cultures were contaminated with yeast colonies (data not shown). Back-diffusion of sterilizing formaldehyde out of the medium trough into the culture medium hindered cell growth on the biochips.

3.2.2 Peracetic acid (PAA)

Here, sterilizing tests with PAA were more successful. **Figure 17** demonstrates that the autoclaving procedure led to degradation of the electrode sensitivity; the signal yield decreased with the number of autoclaving cycles. The measured test signal decreased to approximately 0.2 mV after the fourth autoclaving cycle (red circle). However, after the administration of PAA, the detected test signal was approximately 0.55 or 0.8 mV after 2 h

or 2 days of PAA influence. It seemed that the electrodes quality could be re-established by PAA. The PAA procedure can be used to avoid autoclaving, which causes mechanical stress due to high temperature and pressure. The long-term aseptic properties of the chip were very good -, no infections were observed. After administration of PAA, the contact angle of wetting on the chip's active area decreased from nearly 90° to very low angles, demonstrating the strong positive hydrophilizing effect of PAA on the silicon nitride (Si_3N_4).

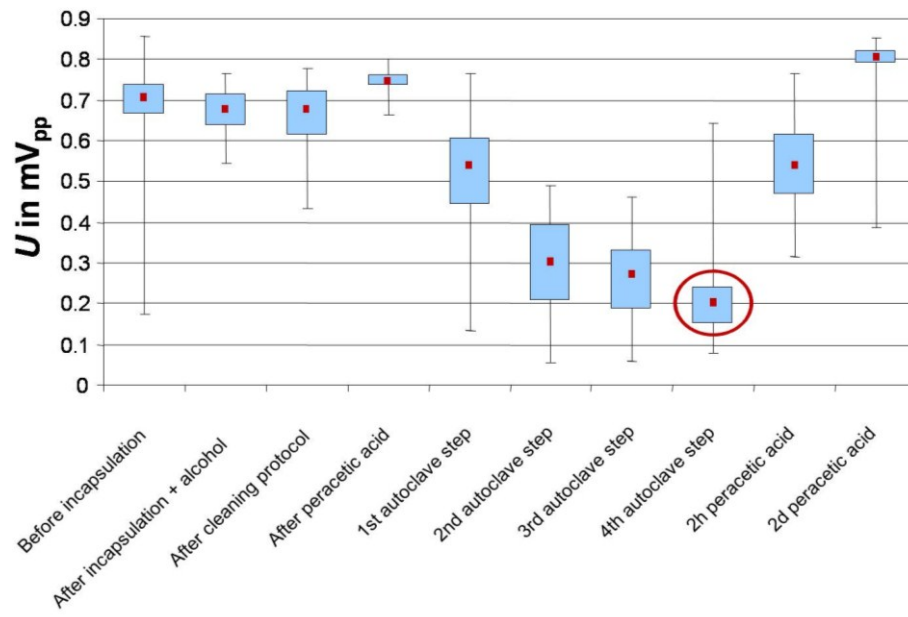


Figure 17: Averaged fidelity of 58 electrodes of a SNC is decreasing due to destructive processes in the autoclaving cycles. The measured test signal decreased to approximately 0.2 mV after the fourth autoclaving cycle (red circle). The following positive effect of PAA is residence-time-dependent.

The hydrophobic surface characteristic of Si_3N_4 can be avoided by means of this easy method. The culture trough was rinsed three times with deionized water (Rotipuran® p.a., Carl Roth GmbH, Karlsruhe) in order to remove the PAA. Additionally, good signal acquisitions were observed. However, the positive influence of PAA on the chips does have a negative side effect. The acid parts of PAA were able to creep into the SNC and the MNC (data not shown) through the ceramic chip carrier from outside the culture trough. Inside the chip carrier, redox reactions evolve and the copper (Cu^{2+}) fraction of the gold bond contacts reacts to form copper acetate ($\text{Cu}_2(\text{CH}_3\text{COO})_4$, a greenish copper salt). This observed effect appears after about 60 DIV and destroys the chips irreversibly. Nevertheless, PAA has more advantages than disadvantages. From the first step on, autoclaving is more destructive than the PAA method. For the GNC, the destructive effect of the autoclaving could not be observed, which means that the GNC is autoclavable.

3.2.3 knick'n'clean *Flora* sticks

The knick'n'clean *Flora* sticks were used for biochip sterilization. The gas concentration increased over the course of two days of incubation. The measured gas concentrations were within the range of the disinfecting concentration specified by the producer (1-2 ppm). The successful detection of electric activity is demonstrated for two cell preparations in **Figure 18**. Culture tests with seeding medium showed no contaminations with foreign organisms after more than four weeks. No adverse effects on the cells could be observed in SNCs and GNCs. For SNCs, knick'n'clean *Flora* sticks were used. In the conclusion, the knick'n'clean® sticks are a fine alternative for sterilizing our biochips. As the standard method for GNC sterilization, the author used PAA (data not shown). **Figure 19** gives a comparison of the electrical activities of autoclaved SNC versus pDEP-SNCs sterilized using knick'n'clean *Flora* sticks. It shows that most autoclaved SNCs demonstrated little neuroelectric activity. The two pDEP-SNCs show much higher activities. **Table 3** gives a short overview of the sterilization experiments conducted and summarizes the sterilizing recommendations regarding the three biochips.

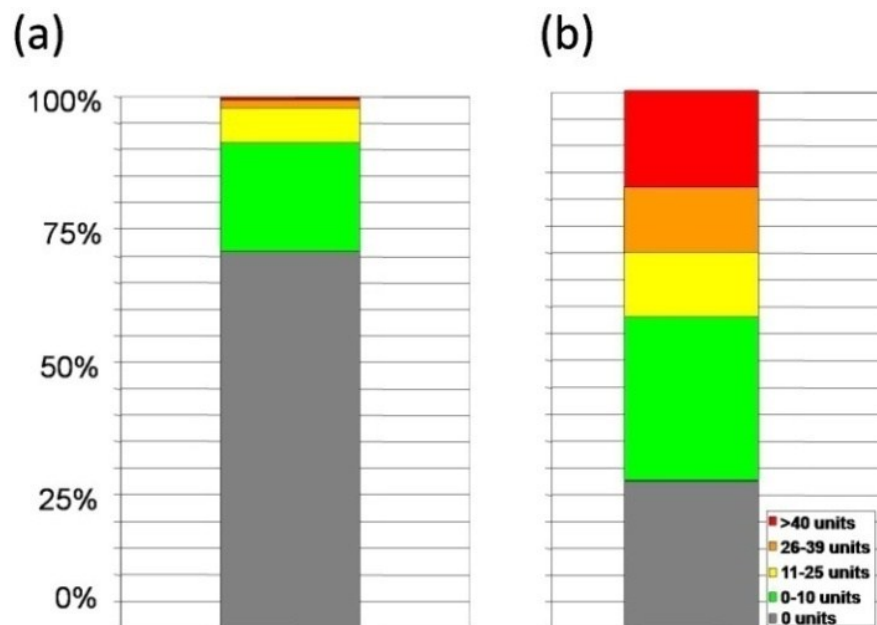


Figure 18: Comparison of autoclaving and knick'n'clean *Flora* sticks on the signal yield. (a) Total percentage yield of the preparations of Figure 19. (b) Total neuroelectric activity yield of SNCs that were sterilized with knick'n'clean *Flora* sticks and cultured with PNCs on the December 8th and 16th 2007. Recordings were done one month later.

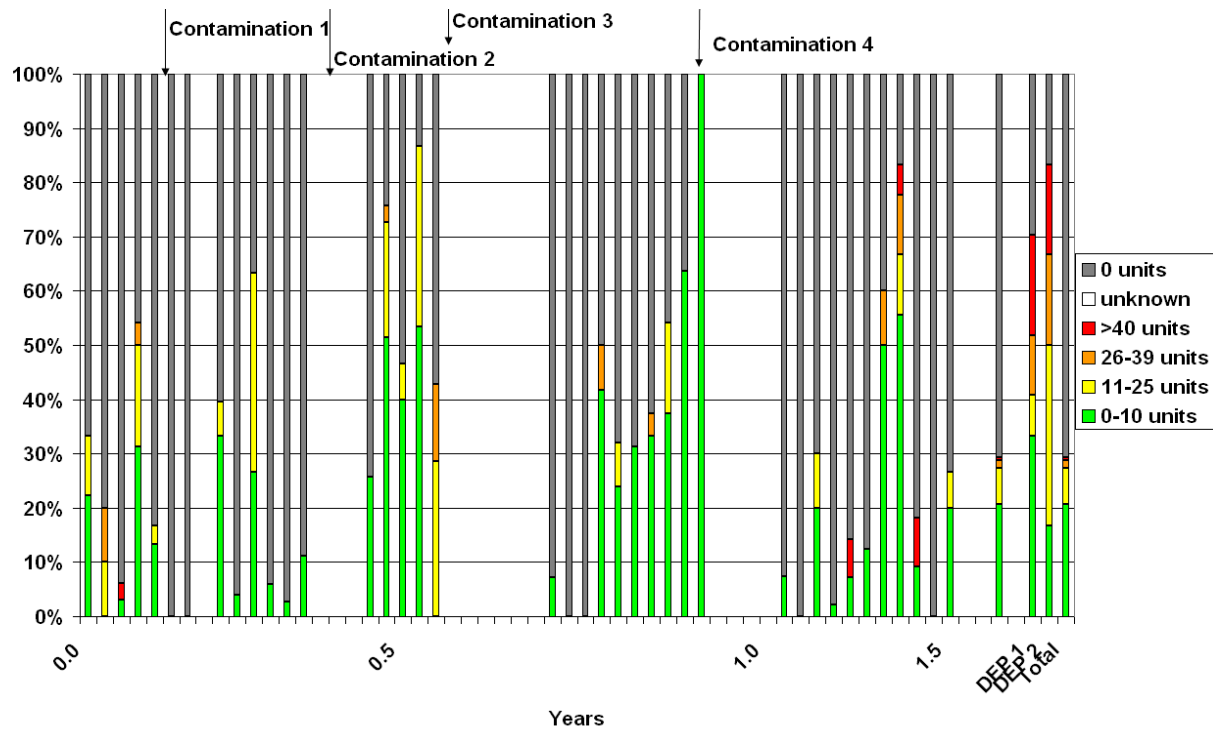


Figure 19: Neuronal activity yield over approximately 2 years. SNCs were autoclaved over a period of 1.5 years SNCs. Contamination appeared in the incubator due to the high SNCs used with the experiments DEP 1 and 2 show higher signal yield and were sterilized with knick'n'clean.

Table 3: Overview of the sterilization experiments.

Chip type	Autoclaving	Alcohol	Formaldehyde	PAA	Knick'n'clean
SNC	x	x	x	x	x
GNC	x	x	x	x	x
MNC	x	x	x	x	x
Applicable alternative	Only for GNCs	Only disinfecting	Only for GNCs	GNCs or short-term experiments (SNCs, MNCs)	Recommended for all chips

3.3 Biochips

3.3.1 SNC

3.3.1.1 Electrode transmission test

The quality of neuronal signal acquisition depends on the electrode transmission. Therefore, each SNC was controlled with a special signal generated by a function generator (Model 33120A; Agilent Technologies Inc., Santa Clara, USA). The signal simulates amplitude $U_{in} = 1$ mVpp and frequency $f = 1$ kHz of native neuronal APs by sine waveforms. Due to the potential divider characteristics of the medium, the electrode and the electronics' characteristics, the signal was attenuated to approximately $U_{eff} = 0.8 U_{in}$ (Tautorat, 2005) (**Figure 20**). A conducting buffer (PBS with 10 % ethanol) and an $Ag^+/AgCl$ signal electrode were used to take measurements.

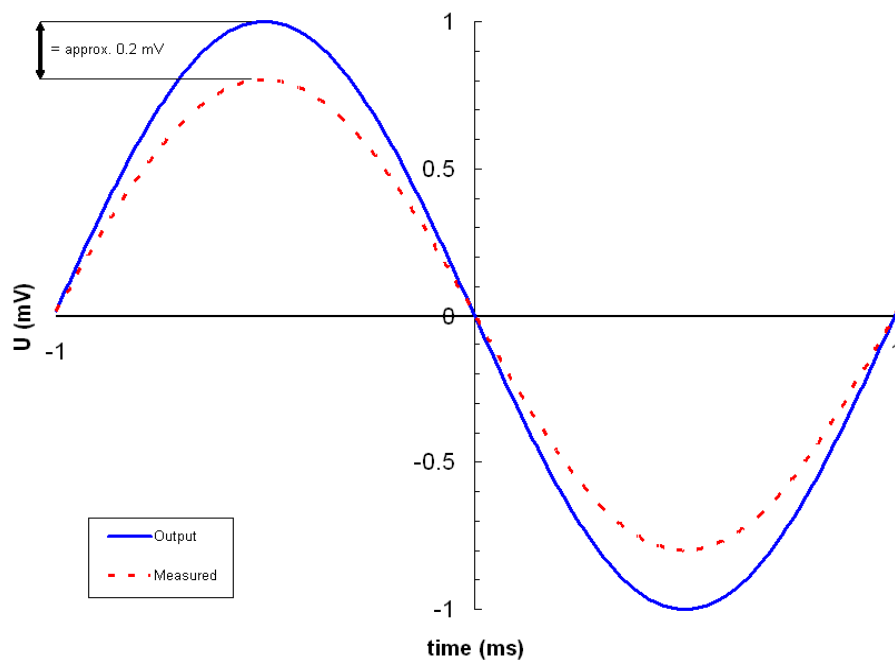


Figure 20: Modeled sinusoidal output signal and measured voltage at the electrode.

Figure 21 demonstrates the test signal measured with the MEA. Electrodes that registered about 80 % of the applied voltage were considered intact. However, sometimes a complete SNC lot was defective. In order to check the signal acquisition hardware, a test chip was developed by C. Tautorat (Chair of Biophysics, University of Rostock). This test chip emulated the SNC electrodes with high-impedance resistors to transmit the above-mentioned test signal to the pre-amplifier and filter box.

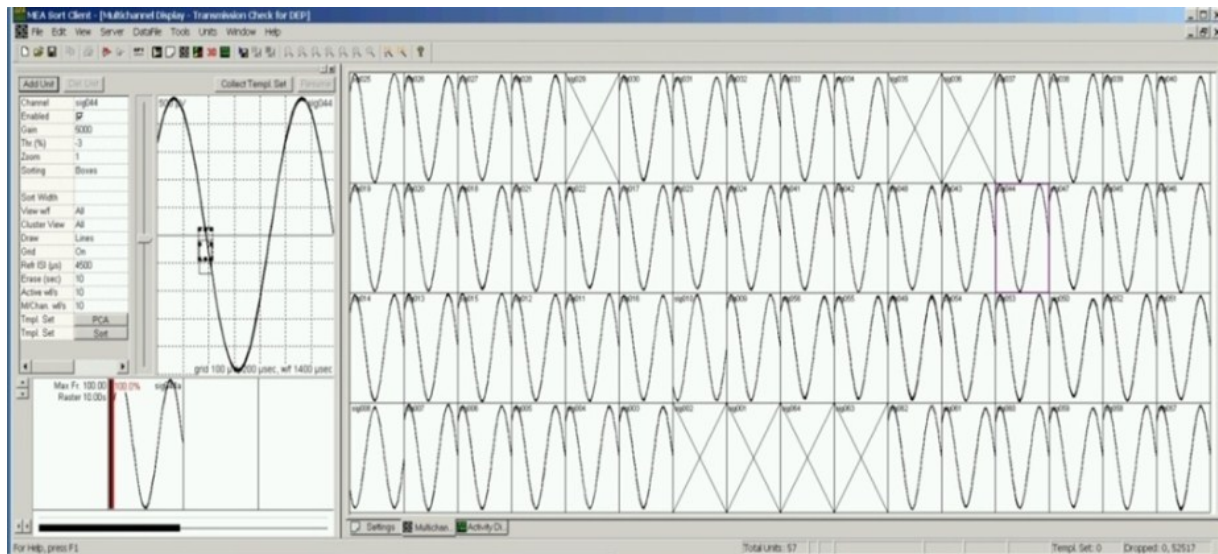


Figure 21: Signal transmission test. 58 electrodes show good sinusoidally shaped signal transmissions. Striked signal boxes: electrodes, not connected to chip electrode pads. These were used as counter-electrodes for the other sensors.

3.3.1.2 Neuronal growth performance

In general, cells showed good growth performance on the SNCs (**Figure 22**). **Figure 23** is a fluorescent image of a cultured network on a SNC. The sophisticated preparation procedure ensured the accurate and long-term adherence of the neurons and glial cells to the SNC or GNC surface over many weeks.

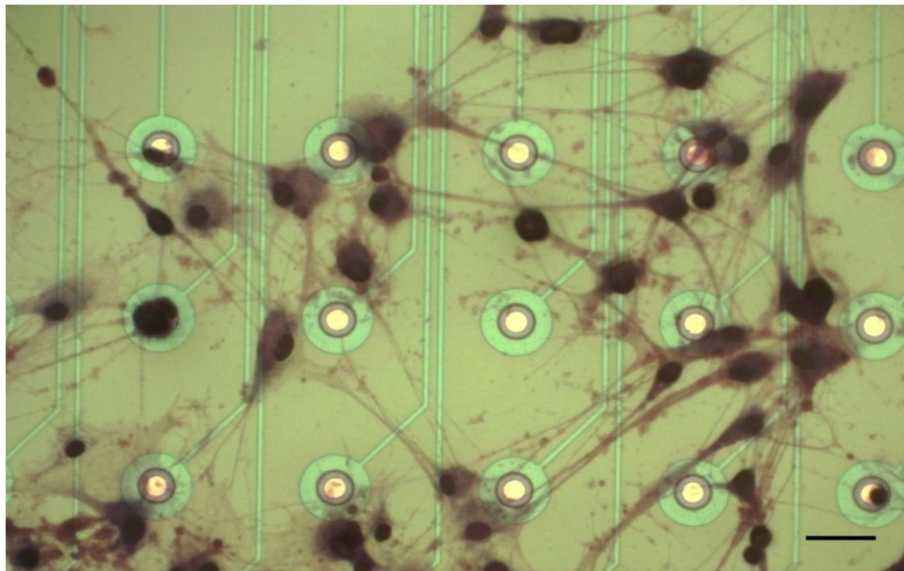


Figure 22: Neuronal network cultured on a SNC. Scale bar = 25 μ m.

The longest cultivation time observed on a SNC for a useful neuronal network for experiments was more than 3 months. Nevertheless, the growth rate decreases in culture

troughs made of poly-oxymethylen (POM) (data not shown). Therefore, methacrylat (Plexiglas®) was used as culture trough material.

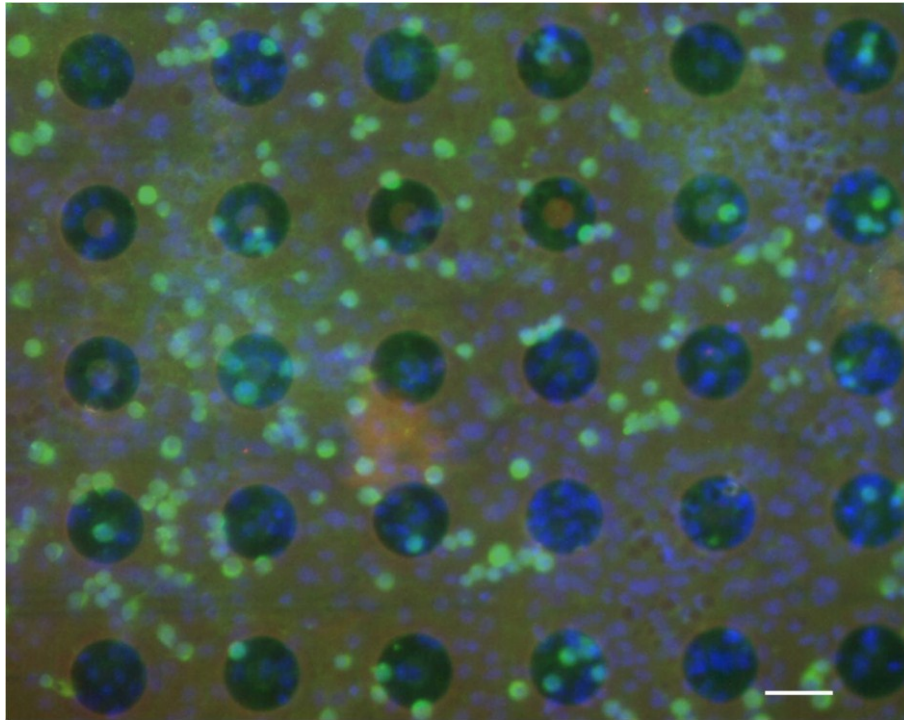


Figure 23: Fluorescent image of PNC network (green) growing on an SNC and cell nuclei (blue). For staining, anti-beta-tubulin-II and DAPI (4',6-Diamidin-2'-phenylindoldihydrochlorid) were used. Electrode diameter is 20 μm . Scale bar = 25 μm .

3.3.1.3 Neuronal signal pattern controls

No standardized method exists for a non-manual neuroelectric signal recognition and unit separation, though attempts have been made (Schrott, 2009). Despite the established supporting tools such as online data visualization, the use of so-called trigger boxes and the application of the principal component analysis (PCA), the detection and classification of neuroelectric signals are highly affected by the investigator's subjectivity. These methods require advanced laboratory experience in order to optimally evaluate signals under various conditions. However, two different users evaluating the same data record may obtain slightly different results. This fact might influence the interpretation of the described neuronal data. In some cases, noise signals were falsely detected as neuroelectric signals, because the noise basically resembles very weak APs. This is due to the algorithms used by the recording software. To reduce this source of error and to improve the researcher's neuron identification ability, a biochemical test system was established. Bicucculline was applied to the neuronal control cells of embryonic mouse. It is an antagonist of

γ -aminobutyric acid (GABA_a)-receptors and alters neuronal communication. Triton®-X 100 is added to the medium, stopping neuronal signals immediately. This test was applied to discriminate against biological signals (**Figure 24** to **Figure 26**). Here, no statistical contrast of data due to different researchers is shown.

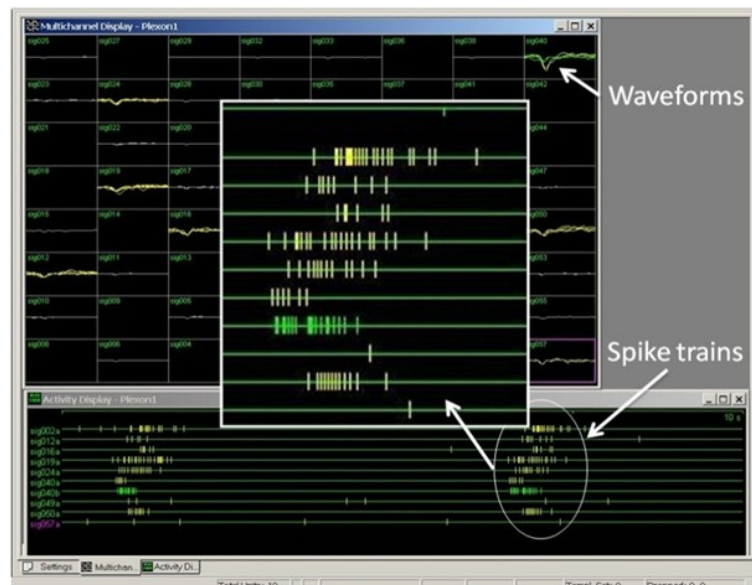


Figure 24: Electrical control recording of PNC activity. Ten active neurons were detected. The green signal track is one of two units recorded by the same electrode. No biochemical substances were added. Therefore, the natural pattern of pace-maker neurons can be observed (see insert). The fourth signal from top is the pace-making neuron.

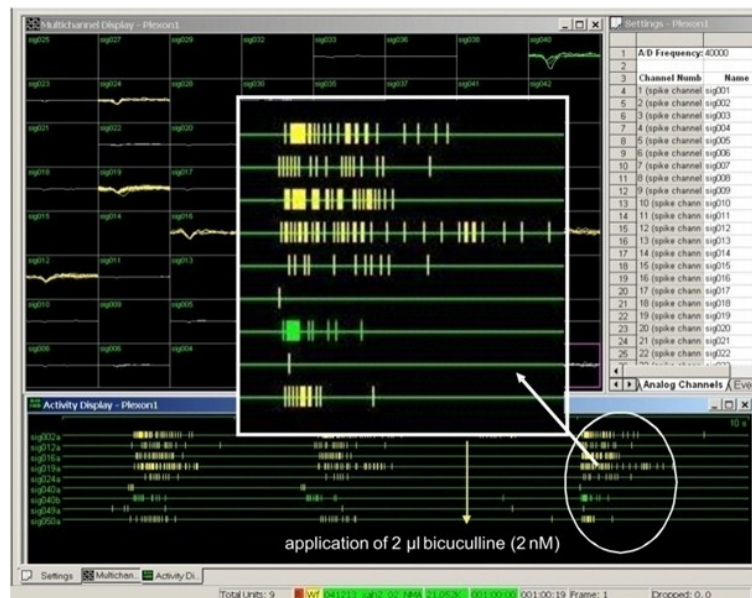


Figure 25: Recorded signals of the same SNC after application of 2 μ l bicuculline (2 mM). The pace-making neuroelectric signal cannot be identified. The time distances between the neuronal answer signals are very small compared to the situation without bicuculline.

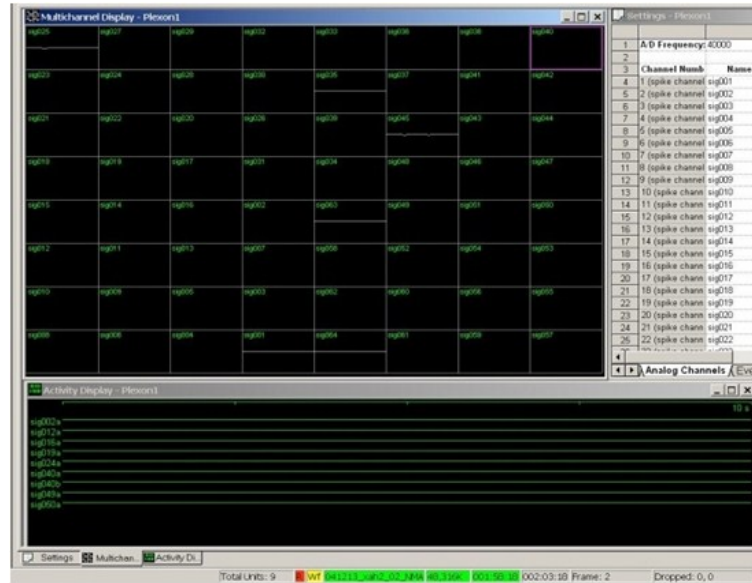


Figure 26: Recorded signals after application of Triton®-X 100. 20 μ l Triton®-X 100 (10 % in DMEM) applied to the chip of Figure 24 cause an immediate stop of the neuroelectric activity. No signals could be recorded.

Electric detection of postnatal rat neurons with another SNC is demonstrated in **Figure 27**. However, the number of units (e.g. $n = 93$) was extraordinarily high and did not present the average unit number of SNCs. No higher unit number was ever detected with the SNC or the GNC.

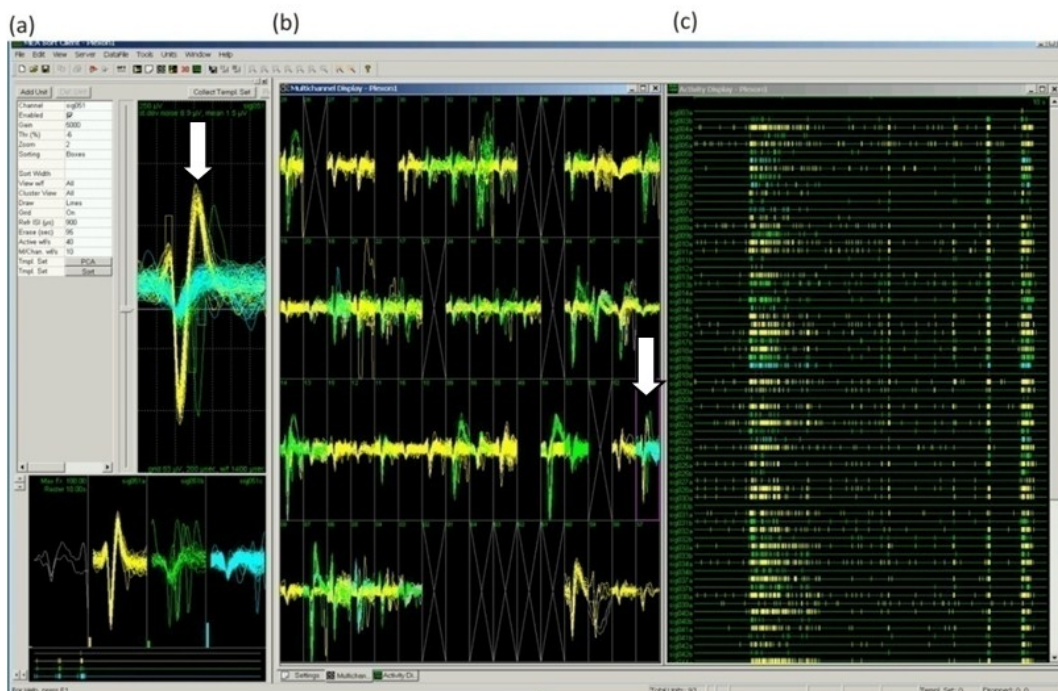


Figure 27: Electric detection of primary postnatal rat pup neurons. 93 units were detected. (a) Superimposed waveforms of electrode 51 (white arrows) reflecting three different units (yellow, green and light blue); (b) multichannel display with all detected unit waveforms; (c) signal tracks over time (10 s) showing the burst trains of the detected neurons. The significant volley-like behavior is clearly observable.

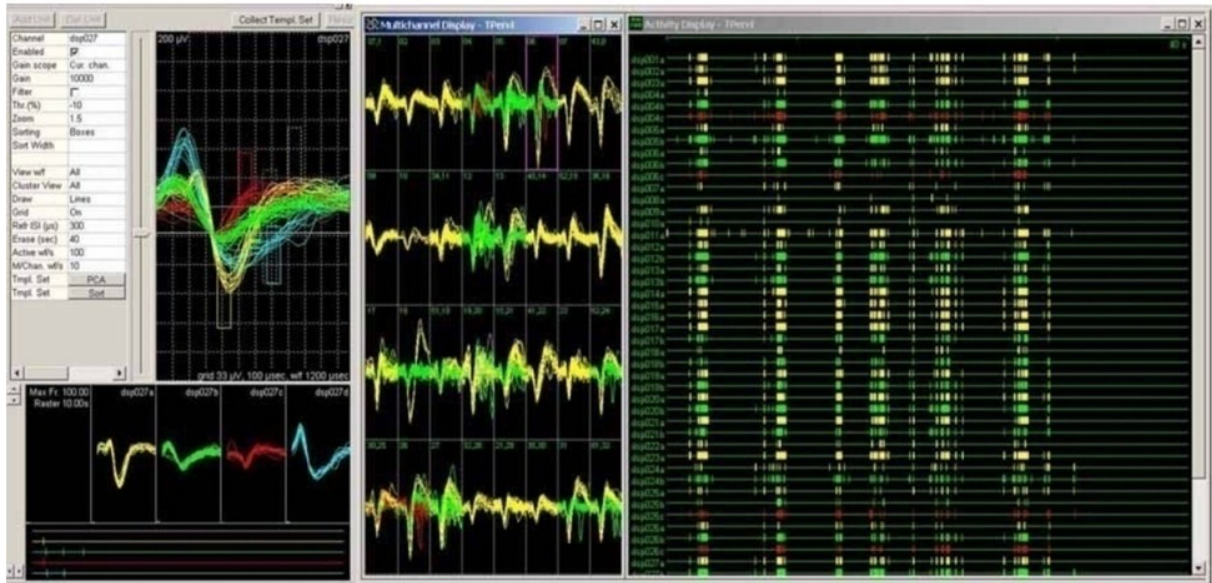


Figure 28: Data recording with a competing MEA type. Units recorded by Dr. L. Mehnert with the glass chip MEA developed by the group of G. W. Gross (Gross et al., 1982; Mehnert, 2005).

The control experiments show the system's equivalence to conventional systems (Mehnert, 2005) (**Figure 28**). Such conventional systems show amplitudes of up to $80\ \mu\text{V}$ with cryopreserved neurons (Otto et al., 2003). Maximum amplitudes of $300\ \mu\text{V}$ were measured in another study (Krause et al., 2006). However, these values vary over a broad range, and several groups have tried to improve amplitude detection with new electrode structures (Huys et al., 2008; Hai et al., 2009). Recently, micronail-structured electrodes were developed to improve the cell-electrode contact (Gimsa et al., 2007; Braeken et al., 2008; Huys et al., 2008).

Even though the SNC has limited microscopic observability, it allows for the registration of additional factors (pH, oxygen; data not shown).

3.3.1.4 Spatial resolution of neuronal activity on-chip

The recorded signals of another SNC can be traced back to its spatial position on the chip MEA surface. This observation can be considered as optical proof of electrically active regions on the SNC and is demonstrated in **Figure 29**. The detected signals from the electrodes are numbered and their locations on the SNC are marked with red circles (**Figure 29a**). At the same time, the clusters mirror the growth centers of the neuronal network and their neuroelectric activity (**Figure 29b**). This means that electrically active areas can be microscopically observed on the chip surface.

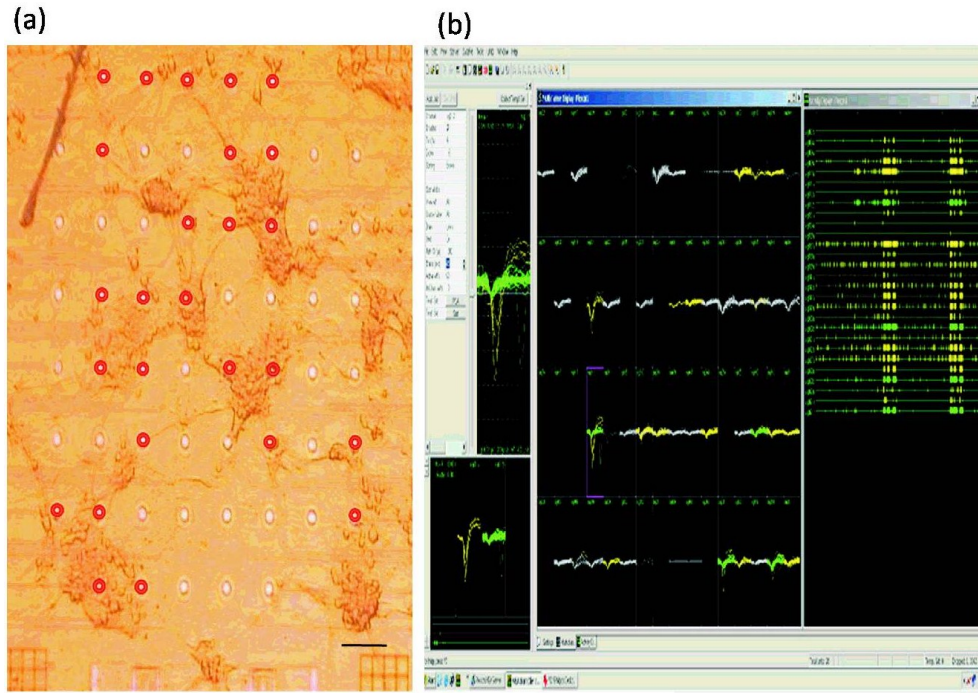


Figure 29: Correlation of neuronal growth on a SNC and the recorded neuroelectric signal patterns. (a) Red circles mark electrodes that exhibited high neuronal activity as displayed in (b). Boxes in (b) that do not show neuroelectric activity can be identified in (a), here, electrodes without red circles represent areas of reduced cell growth. Scale bar = 100 μm .

3.3.1.5 pDEP with PNCs

Results of positive dielectrophoretic cell positioning on SNCs (pDEP-SNCs) are shown in **Figure 30** to **Figure 32**. After adding the cell suspension in the prepared SNCs and application of the AC field, increasingly fast movement and a localization of the suspended cells to the attracting electrodes were observed (**Figure 30**).

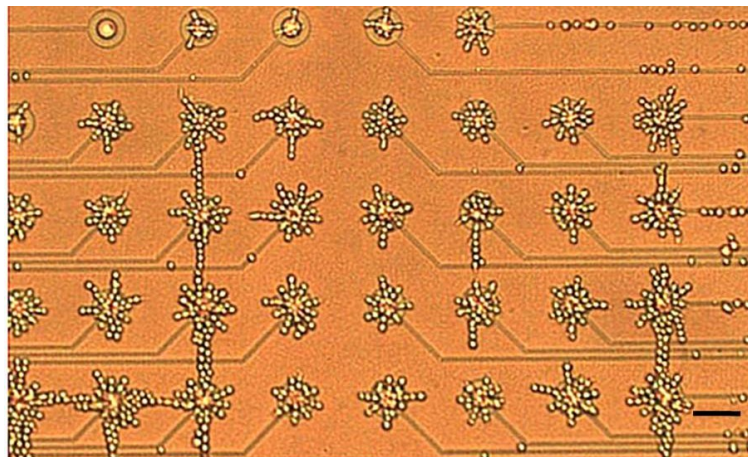


Figure 30: pDEP with PNCs on a SNC. pDEP was applied for 60 minutes with an alternating AC field of 3 V_{pp} at 10 MHz on the pDEP-SNC no. XKF730. PNCs were allocated on and around the electrodes. Cells begin to form cell soines. The peristaltic pump cycle was started directly after pDEP positioning in order to exchange the pDEP-buffer by medium to initialize cell adhesion and growth. The top left electrode no. 33 is disconnected. Scale bar = 25 μm .

Cells build star-like formations (pearl chain formation) around the electrodes (Pohl and Crane, 1971). The spaces between the electrodes were void of cells. The effect of pDEP is a translator motion of the particles due to the non-uniformity of the applied electric field. However, if the externally applied electric field was uniform, the formation of pearl chains resulted, due to the mutual pDEP or interaction among the particles (Zimmermann and Scheurich, 1981; Arun et al., 2004). **Figure 31** shows the same pDEP-SNC after 1 DIV. Cell migration is obvious; the star-like pearl chain formations are no longer apparent. An example of another chip is given in **Figure 32**. An image sequence shows the individual movement of cells within the first 2 DIV. The regular cell positioning is still visible in the cell networks. Cells were left to grow for several DIV and their positions on nine specific electrodes were observed. Within the first few hours, cells were adhering to the electrodes to which they were allocated.

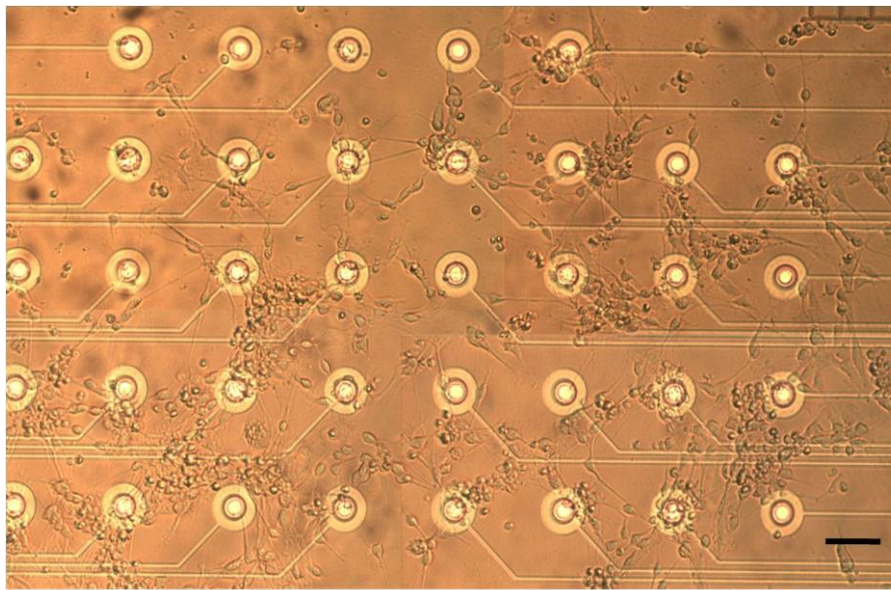


Figure 31: Cell growth after pDEP. Growth of survivor cells after 24 h in culture on pDEP-SNC no. XKF730. The image is a combination of four pictures of different areas of the SNC of the Figure 30. Scale bar = 30 μm .

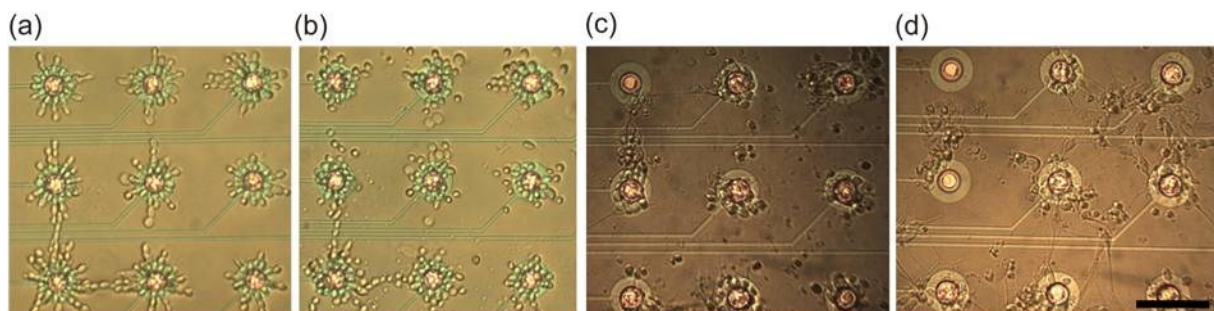


Figure 32: Cell growth after pDEP. pDEP was applied for 60 min with $3 V_{pp}$ at 10 MHz on pDEP-SNC no. XKF732. Cells were let to adhere before medium fill-up with a peristaltic pump (200 μl D10/10). (a) Allocated PNC around electrodes; (b) 1 h after pDEP; (c) 1 DIV after pDEP; (d) 2 DIV after pDEP. Scale bar = 50 μm .

However, as with the pDEP-SNC no. XKF730 (**Figure 30**), cells tended to migrate away from the electrodes after 1 DIV, leaving the area of signal detection. After 2 DIV, some electrodes were completely without cells.

There were many setbacks regarding the cell culture before recordings of pDEP-SNCs were successful. Because the experimental preparations for pDEP are very labor-intensive, the electrical activity could be usefully compared only among three SNCs. **Figure 33** presents one of the three pDEP-SNCs. The chip is compared with a control SNC with a cultured neuronal network.

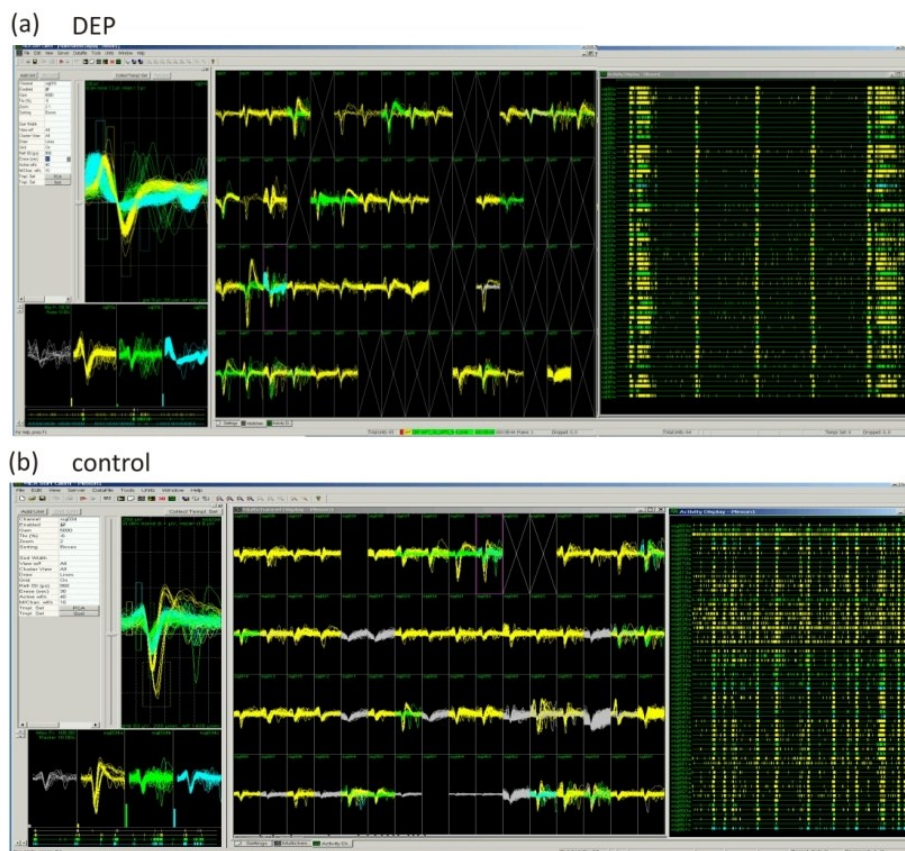


Figure 33: Comparison of a pDEP-SNC and a control SNC. (a) Altogether 64 units were detected from a pDEP-SNC; (b) with the control SNC altogether 65 units were registered.

SNCs with the highest unit yields were selected as controls. The pDEP-SNC showed 64 units, while the control SNC showed 65 units. The cell allocation was supposed to result in significantly higher signal yields than with non-allocated cells on the control SNC. One might argue that the first allocation on the electrodes was fully compensated by the high motility of the cells as shown in **Figure 32**. However, when the signal yield of the complete preparation is considered, an interesting fact appears. It reveals that only one of the control SNCs ($n = 6$) showed 65 units. The rest of the control SNC showed 49 units at maximum. On

average, the signal yield for the controls was 39 units. **Figure 34** summarizes this fact. In average, more units were recorded when pDEP was applied.

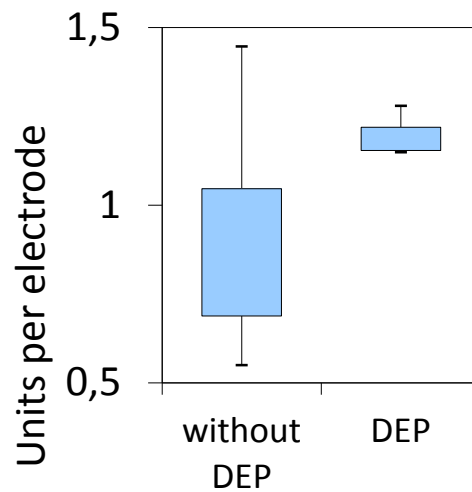


Figure 34: Comparison of control SNCs with pDEP- SNCs.

The three pDEP-SNCs showed constantly high unit yields. On average, pDEP-SNCs showed 56 units (+43 % compared to control SNCs). Even though only three SNC were treated with pDEP, this experiment shows that pDEP might become a valuable tool in SNC preparation in the future. However, this experiment did not show why the signal yield of pDEP-SNC was not significantly higher than with control SNCs. Possibly, the positions of the axons and dendrites found right after pDEP influence the signal yield more than the positions of the cell bodies themselves. One new idea that came up was to keep the cells from migrating away from the electrodes after pDEP. In addition, the axons and dendrites developing by the neurons after pDEP must be kept near the electrodes to guarantee a high signal yield. Briefly, a mixture of cell-adhesive PDL and laminin in water (4:1:100) was applied to the electrodes with a micropipette (**Figure 35**). The space between the electrodes was left uncoated and was therefore non-attractive for cells (**Figure 36**). Accordingly, the cells should have kept their positions near the electrodes after pDEP. Again, PNCs of mouse embryos were seeded on the SNC and pDEP was applied (**Figure 37a**). In the following experiments, fewer cells were applied to the chip, decreasing the cell number in order to observe whether cells kept their position on the spotted electrodes. **Figure 37b** demonstrates the growth of the cells after 1 DIV. The growth of axons and dendrites could be observed, but again, cells tended to migrate away from the electrodes. Unfortunately, no neuroelectric activity was recorded

from these chips. For this reason, and because of the immense time and effort required by these experiments, they were not continued.

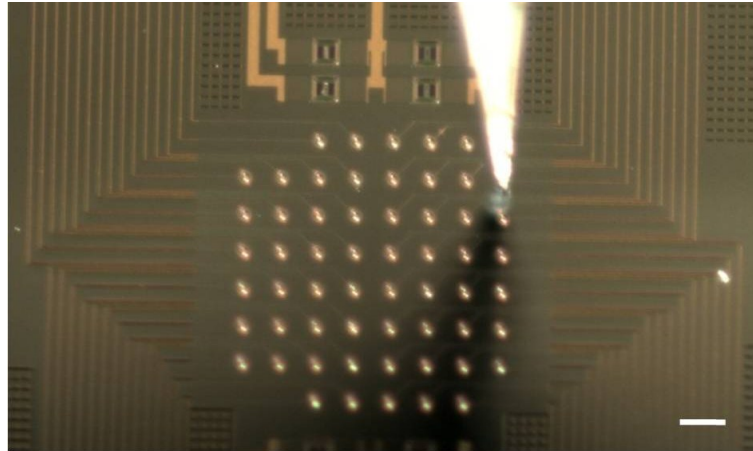


Figure 35: A single SNC electrode is coated with a glass micropipette. The pipette was pulled with a pipette puller and controlled with a micromanipulator (Model MS314, Märzhäuser Wetzlar GmbH & Co. KG, Wetzlar). The solution was filled into the pipettes with a medical syringe ($\varnothing = 450 \mu\text{m}$). The pipette opening was allocated to each electrode and a thin PDL/laminin solution film was applied using capillary forces. The pipette was let on each electrode for five minutes. This duration was sufficient for adhesion of PDL and laminin molecules to the electrode surfaces. A stereo microscope (Stemi 2000-C, Zeiss, Jena) was used for the observation of electrode coating and to control the micropipette movement. Scale bar = $100 \mu\text{m}$.

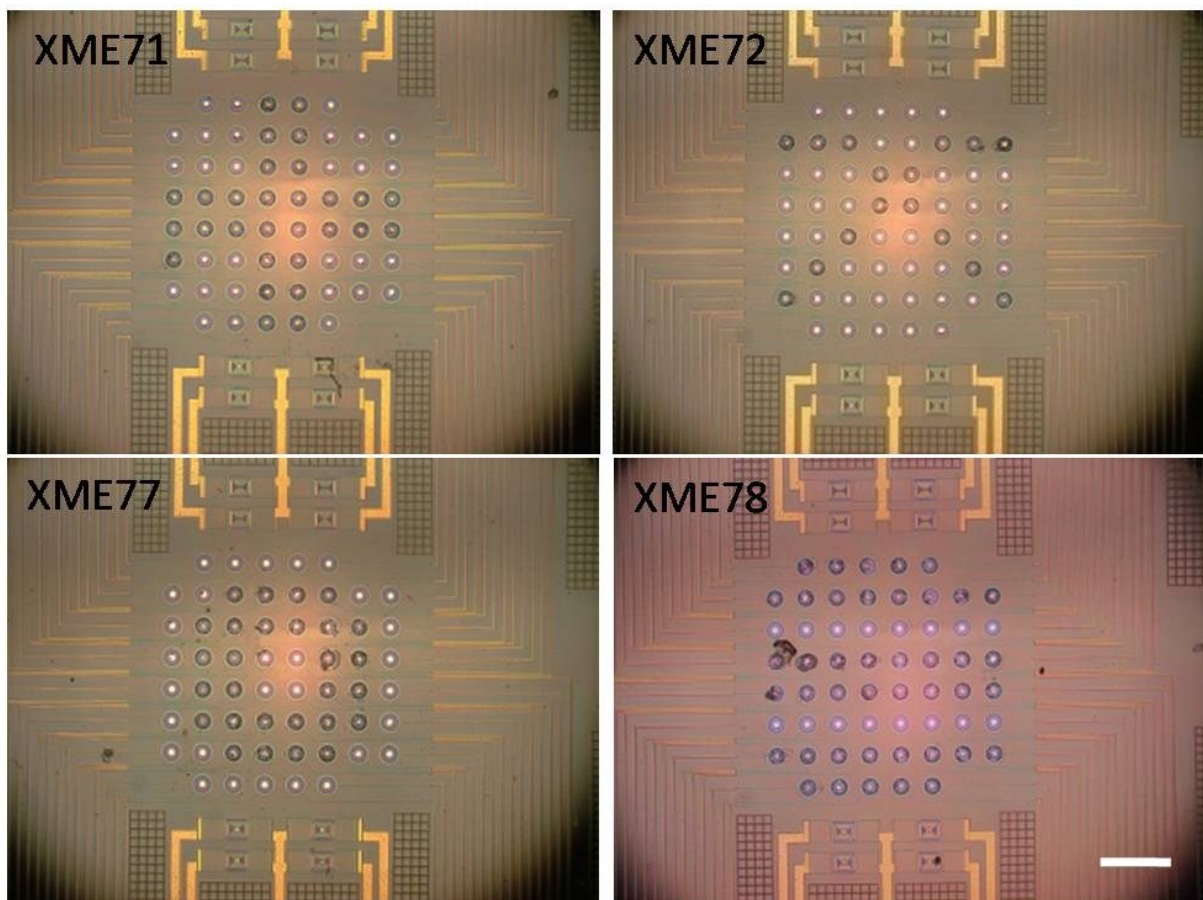


Figure 36: SNCs with spotting patterns on specific electrodes and uncoated areas. Four different patterns were developed with the PDL/laminin solution. Each chip was coated within four hours. Scale bar = $300 \mu\text{m}$.

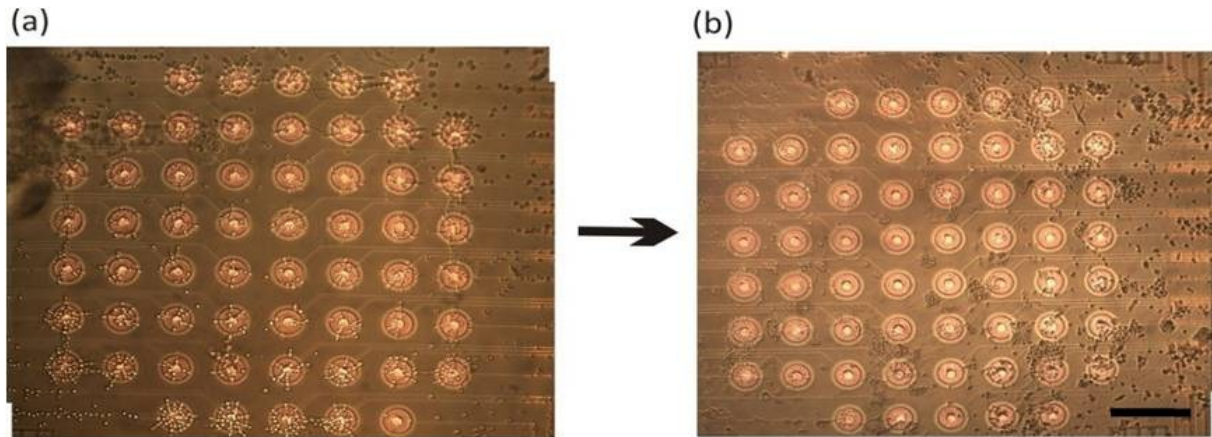


Figure 37: Comparison of neuronal motility after PDL/laminin-spotting of electrodes on chip XME71. (a) PNCs were seeded under the application of pDEP, star-like formations were observed; (b) after 1 DIV, cells had moved away from the adhesive electrode spots. Each images was combined from two pictures to show the complete area of the SNCs in high resolution. Scale bar = 100 μ m.

The pDEP-experiments were very time-consuming. It was not possible to observe the cells microscopically without hindering the cells' adherence. Therefore, the author could not observe the cell movement microscopically and cannot give an indication as to when the cells began to move away from the electrodes.

However, the author was able to detect neuroelectric activity after applying pDEP. Therefore, the author cannot understand why other studies were not able to present neuroelectric signals (Heida et al., 2001), or showed activity for hours or up to 1 DIV (Prasad et al., 2003). In another study (Zhe et al., 2004), cortical neurons with a density of 10×10^4 cells/ml were cultured for 14 DIV and showed little motility. Here, no neuroelectric activity was demonstrated either. Zhe et al. assume that cell density was too low to result in signal activity. Long-term cultivation of pDEP-allocated cells resulting in neuroelectric activity could not be found in the literature, possibly due to the high motility of neurons observed by other authors. Nevertheless, the author could detect neuroelectric activity from such pDEP-SNCs after four weeks of culture. On average, the unit yield was higher than with control SNCs.

The results with polymers on MNEs on MNCs described below show that cell migration could be impeded by properly applied cell-adhesive and cell-repellent polymers. Unfortunately, it is impossible to manually apply these polymers with a micropipette and micromanipulator to a chip.

3.3.1.6 SU-8 structures

As an alternative to the pDEP approach, PNCs were located at the electrodes and in the spaces between the electrodes to stimulate defined perpendicular neuronal networks. The

processed SU-8 structures are shown in **Figure 38**. Seeded neuronal cells were cultured on SNCs with these additional SU-8 structures.

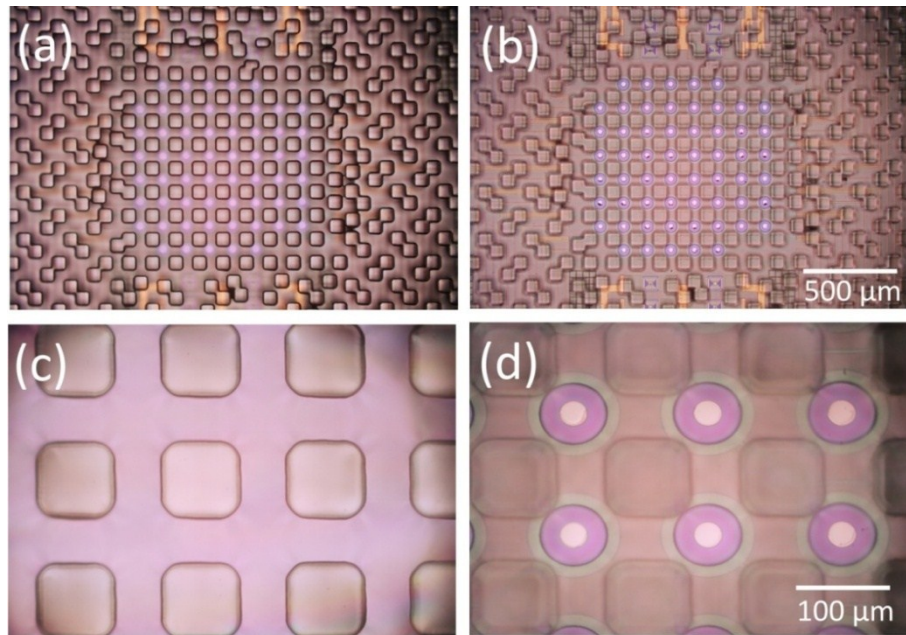


Figure 38: SU-8 structures on the SNC. (a) and (c) foci at the structured surfaces; (b) and (d) foci at MEAs.

Figure 39 shows the neuronal growth over one week. The network in **Figure 39a**, was built during 1 DIV. No cells were found on top of the SU-8 cubes. Surprisingly, the cells moved away from the SNC surfaces after 7 DIV (**Figure 39b**).

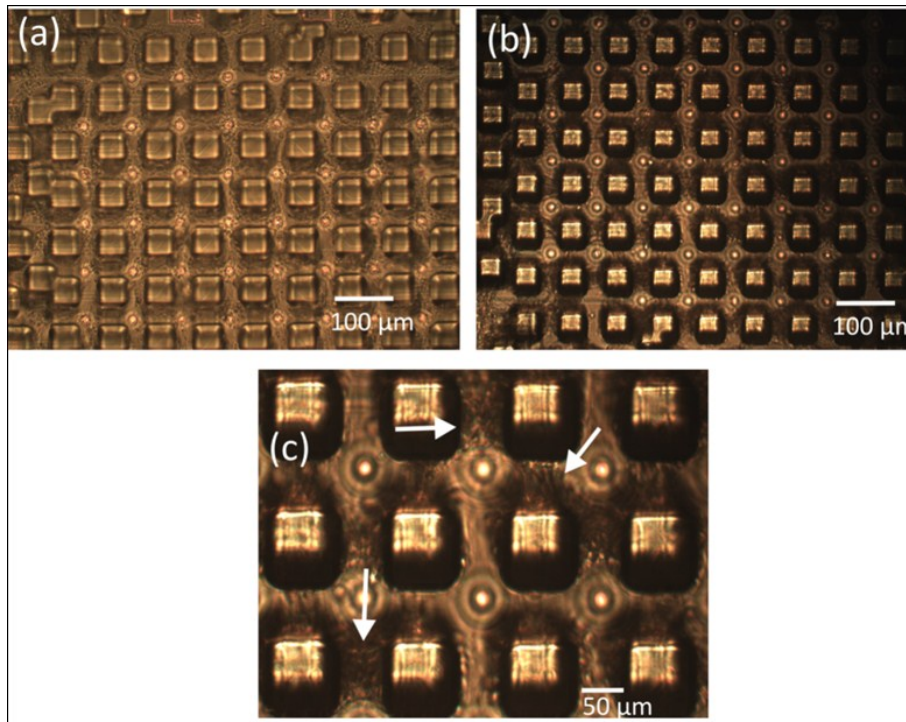


Figure 39: Neuronal growth between the SU-8 structures. (a) 1 DIV; (b) 7 DIV; (c) zoom of (b), cells leave the SNC surface and migrate to the cube sidewalls. No PNCs remained on the electrodes.

Here, the SNC surface shows no more cell growth. The reason was that the cells migrated to the sidewalls of the SU-8 cubes. The image in **Figure 39c** demonstrates this observation (white arrows). This cell movement might be explained by the high number of negative charges in the SU-8 photoresist, which seems to be more attractive than the cell adhesive molecules on the SNC surface. This phenomenon was observed with every SNC featuring the SU-8 structures. No neuroelectric activity could be observed from these SNCs though most electrodes were checked to be intact.

One could hypothesize that the PDL/laminin solution on the electrodes was dissolved by the pDEP-buffer and small portions adhered to the free silicon spaces between the electrodes. Another possibility is that neurons tended to shorten their axons, therefore spanning the uncoated areas as cell clusters. Further investigations are necessary to find methods for keeping the cells in place. The author suggests coating the SU-8 cubes with cell repellent polymers, e.g. poly(dimethylacrylamide) (PDMAA), to avoid cell migration to the cubes as a prerequisite for defined PNC networks.

3.3.1.7 Influence of UMTS-EMF on neuronal activity on SNCs

Exposure experiments have to be carried out very carefully in order to yield a high number of active neuronal networks. Programming of the signal analysis routine and signal sorting was conducted by Dr. J. Sakowski. The results presented here were obtained in the BFS project StSch 4316 A "Mechanisms at cells under exposition with highfrequency electromagnetic fields of the mobile phone technology" and are presented below if not otherwise stated. Preliminary stages of the experiments are described in detail in **Manuscript 1, p. 103ff.**

Assumed parameters

The relative permittivity ϵ_r of the medium was extrapolated to about 70 (Sudsiri et al., 2007). The electric field intensity distribution in then culture volume has been calculated for an incoming power of $P_{inc} = 1 \text{ W}$ using the software *CST Microwave Studio™*, Ver. 5.1. (CST GmbH, Darmstadt). The distribution in the sample volume for the propagating and standing wave modes were modeled in **Manuscript 1, p. 103ff.** The modes differ in the homogeneity of field distribution over the active SNC areas. For the propagating wave, a field strength gradient was obtained over the chip.

In the standing wave mode, the constructive interference of the UMTS waves leads to a largely homogeneous field in the chip trough. The neuronal signals are amplified and filtered before online visualization of their patterns by a special MEA setup (Plexon Inc., Dallas, TX, USA, further described in **Manuscript 1, p. 103ff**).

SNCs were exposed to a generic UMTS field in the rectangular waveguide in successive 1800 s-intervals with different effective field strengths. Seven SNCs with 50 neuroelectrically active units altogether were used. The aim was to examine possible power-dependent effects of the generic UMTS signal on the registered neuronal activity of the SNCs in the range of several mHz to 100 Hz, as well as at 740 Hz. As shown later, a comparison with the control neuronal activity following the exposition was not representative since the microelectrodes were damaged over time and with increasing gpower. An exposition power of 14 mW corresponds to a SAR value of 0.14 W/kg body weight (personal communication Dr. J. Sakowski). No temperature rise was measurable with the GFT at this power level.

Technical observations

The 740 Hz UMTS signal frequency is detected, which lowered the possible number of detectable neuronal signals. **Figure 40** clearly shows this situation. When the 740 Hz signals were detected, fewer neuronal signals could be registered. This can be explained by the sampling rate and the interconnected limited receptiveness of the Plexon PC card.

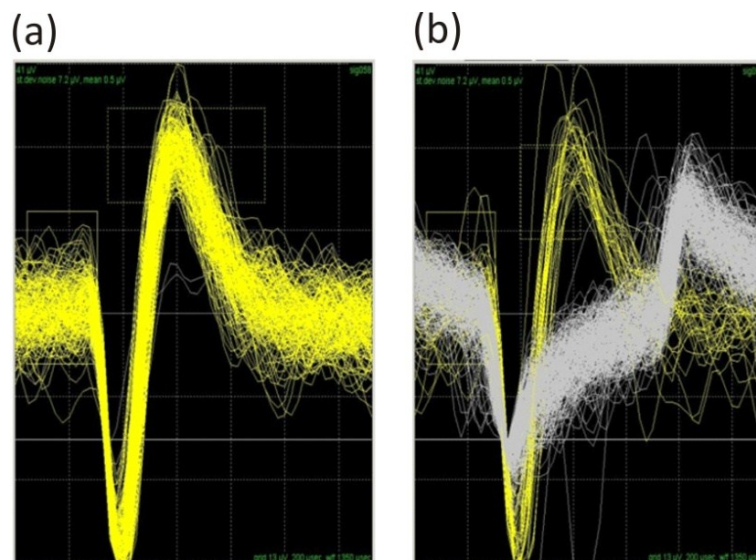


Figure 40: Signal waveform with the UMTS signal. (a) Superimposed neuronal APs over 5 s (yellow); (b) eigenfrequency of the high-frequency part of the amplitude spectrum of the generic UMTS signal over 5 s at a field power of 200 mW (grey); This portion of the UMTS signal correspond to $f_0 = 740$ Hz and is the only component that can be displayed by the electrical recording software used.

Data examination

The dependence of neuronal signals was observed to be a function of the effective field power during the exposure of SNCs to UMTS. PSDs of the spike rates were calculated as functions of time (exemplary **Figure 41**). The PSDs of the spike rates were compared with the UMTS spectrum for similarity in the neuronal frequency range.

In the heat experiments (**Figure 42**), the PSD of the temperature course was compared with the PSD of the spike rates (**Figure 43**). Exposure of SNCs with an effective power of 126 mW and 251 mW, with SAR values of 1.3 W/kg and 2.6 W/kg. This correspond to an temperature increase of approximately 0.12 °C and 0.24 °C and gave indications, but no clear proof of a correlation between the neuronal spike rate and the UMTS signal. Only for approximately 33% of the evaluated signals (intact electrodes) did the spike rate PSDs exhibit frequency maxima of about 170 mHz, as observed in the fundamental frequency envelope (16.7 mHz, data not shown).

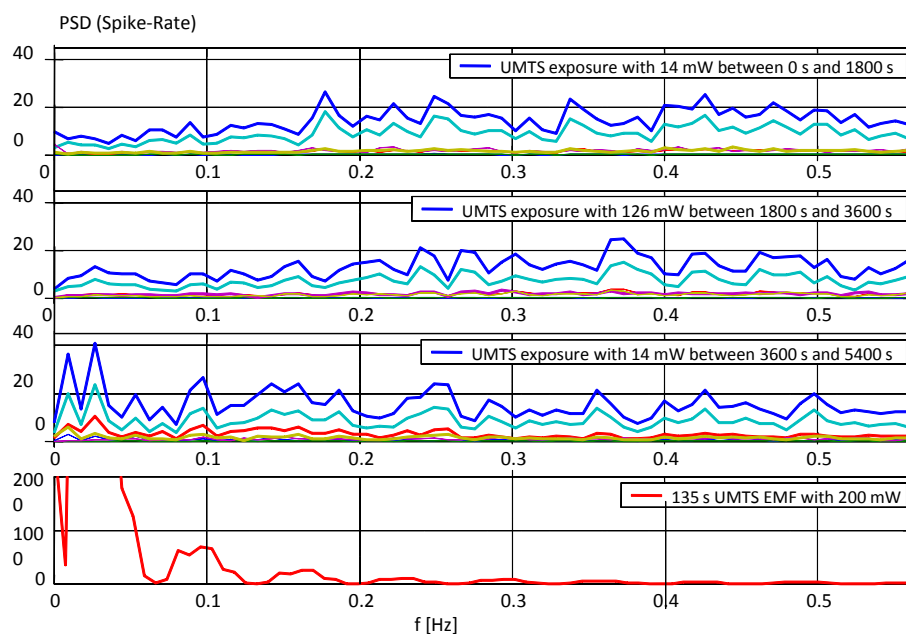


Figure 41: PSDs of the spike rates. Six units of the SNC XMA23 were examined. The sum of all units is given in blue.

Obviously, the slow power adjustment of the UMTS signal in 60 s loops causes a thermal effect (**Figure 43**). This means that neurons could be affected by EMF absorption at an effective field power of up to 126 mW, when the power/heating interval was longer than 10 s. Apart from the qualitative discussion of this effect, a systematic effect of the UMTS expositions could not be determined for the remaining neuronal signals. There were no signs

that the faster power adjustment of the UMTS signal at 740 Hz affected the neuronal activity.

However, during data evaluation it became evident that UMTS exposition caused unwanted electrode effects for approximately 67 % of all neuronal signals (7 SNCs with a total of 50 units). At higher effective field power and a longer exposure time, these effects could even result in the destruction of electrodes. Simultaneously, some unit amplitudes rose exponentially with time. These neuronal signals were excluded from the data evaluation. Independent measurements with a purely thermal stimulation of the SNCs over hours with temperature-changing intervals of approximately 40 minutes could not be evaluated (**Figure 42**), because the neuronal activity strongly decreased during the experiment (data not shown).

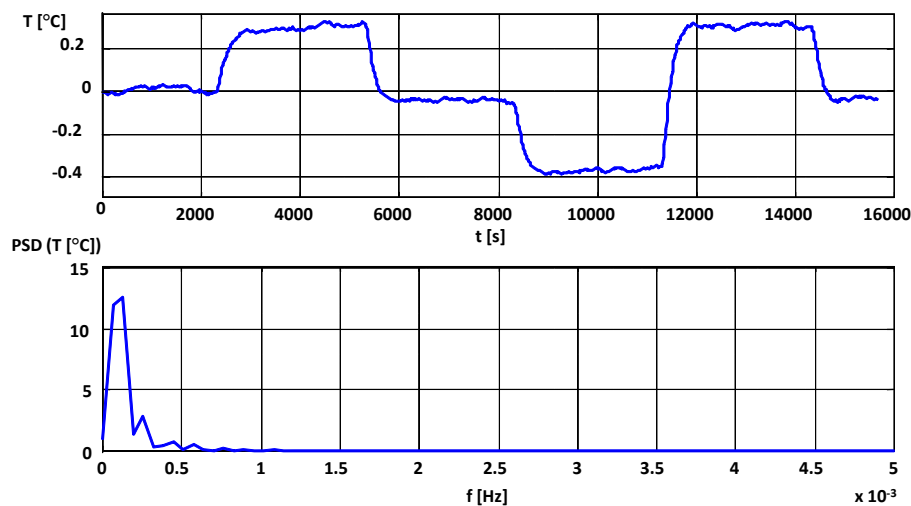


Figure 42: Temperature profile according to the PSD of the heating experiments.

The energy portion in the spike rate representing the decreasing neuronal activity (upper diagram in **Figure 43**, maximum at 70 μHz), covers the majority of the observed temperature effect. This effect is found in the satellite maximum of the PSD of the temperature gradient (lower diagram in **Figure 43**, local maximum at 250 μHz). Hence, possible temperature effects in the PSD from the spike rates remain hidden in the error margin.

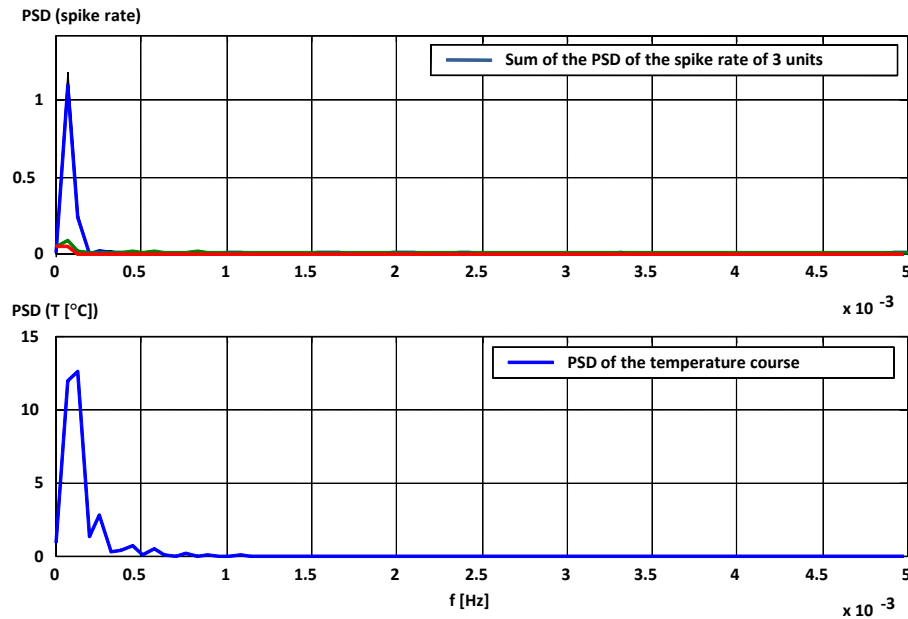


Figure 43: Comparison of the sum of the PSD of the spike rates with the PSD of the temperature profile.

To date, measurable EMF effects cannot be separated from thermal effects. The results are ambivalent. Thermal effects were always present when effects were detected at higher EMF exposure powers. Varying quality of SNCs, high power and time-dependent aging of the MEA, as well as local fluctuations of the cells' physiological parameters (adhesion, cross-linking and positioning of the neurons, neuron/glia relationship) complicate the systematic evaluation of the neural activity under EMF exposure.

Comparative heat experiments with interval lengths at a maximum of 10 minutes per temperature step are more informative than testing pure thermal stimulation of the SNC at one temperature, e.g. 37 °C. The stability of the neural activity over the time of the experiment is an experimental prerequisite. During the experiment, at least 5 cycles of the temperature change and the detected neural activity reacting to these temperature alterations should be observed. The author suggests performing follow-up experiments with more stable SNCs or with GNCs without metallization of the glass trough.

Other groups have also found ambivalent results. In the International Workshop on EMF Action-Mechanisms (Oberschleißheim, 2007) all results presented were ambivalent. For instance, Ammermüller and colleagues (University of Oldenburg) examined the effects of GSM-800, GSM-900 and UMTS signals on retinal ganglion cell activity in a wave-guide, but found no systematic dependencies. Simko and colleagues (University of Rostock) did not find an effect on free radical production with human primary monocytes and lymphocytes

isolated from human umbilical cord blood. However, GSM-DTX signals with a SAR of 2 W/kg induced a significant increase of free radicals compared to sham controls. Nevertheless, such SAR-values are not emitted by modern cell phones. Lerchl (University of Bremen) and colleagues investigated the melanin production of isolated pineal glands from Djungarian hamsters under GSM-1800 exposure. Their data did not support the "melatonin hypothesis" (Stevens, 1987) according to which non-thermal exposure suppresses melatonin synthesis (Sukhotina et al., 2006).

None of the above studies or my own results were able to provide evidence that would make necessary the revision of policies or the standards of mobile communication systems.

3.3.2 GNC

3.3.2.1 Examination of electrode noise

The background noise level was investigated for four different MEA-electrode diameters. Surprisingly, average values of 1.2 μV were obtained for all electrode diameters. The standard deviation of the average noise increased with the electrode diameter (**Table 4**). The detected noise without an inserted GNC was also approximately 1 μV . This means that the noise mainly stemmed from the electronic compounds of the headstage. T. Reimer registered neuronal signal amplitudes of up to 595 μV with MEA-electrodes of 35 μm diameter. This corresponds to a maximum signal-to-noise-ratio (SNR) of approximately 496.

Table 4: Electrode characteristics

Electrode diameter [μm]	15	20	25	35
Average noise [μV]	1.2	1.2	1.2	1.2
SD [μV]	6.4	5.2	4.4	3.7

3.3.2.2 Neuronal action potential detection

Parts of the following results were obtained during the “venturesail” (a competition for scientific innovation based in Mecklenburg-Pomerania) project grant no. UR07140 (*Mini glass chips with optical metabolite sensors for stem cell based neural networks*). A study with sodium valproate (VPA) was inspired by grant no. 31P4590² of the German Federal Ministry of Education and Research (BMBF) to J. Gimsa and W. Baumann. The experimental approach of this project was to examine a possible developmental-neurotoxicological effect of VPA on PNCs. Furthermore, PNCs were cultured on the GNCs, and networks microscopically observed. **Figure 44a** shows neuronal growth on a GNC and the recorded neuroelectric activity. The observability was improved compared to the SNCs due to feasible transmitted light (**Figure 44a**) and fluorescence microscopy (**Figure 44b**). Neurons, axons and dendrites were stained with the green-fluorescent neuronal antibody-3-tubulin marker when excited with blue light. The first neuroelectric control experiments with eight active units are shown (**Figure 44c and d**), which were recorded in the framework of the *venturesail* grant no. UR07140 to P. Köster.

² BMBF-Verbundprojekt „Entwicklung prädikativer *in vitro* Tests zur sicherheitstoxikologischen Prüfung auf Entwicklungsneurotoxizität“

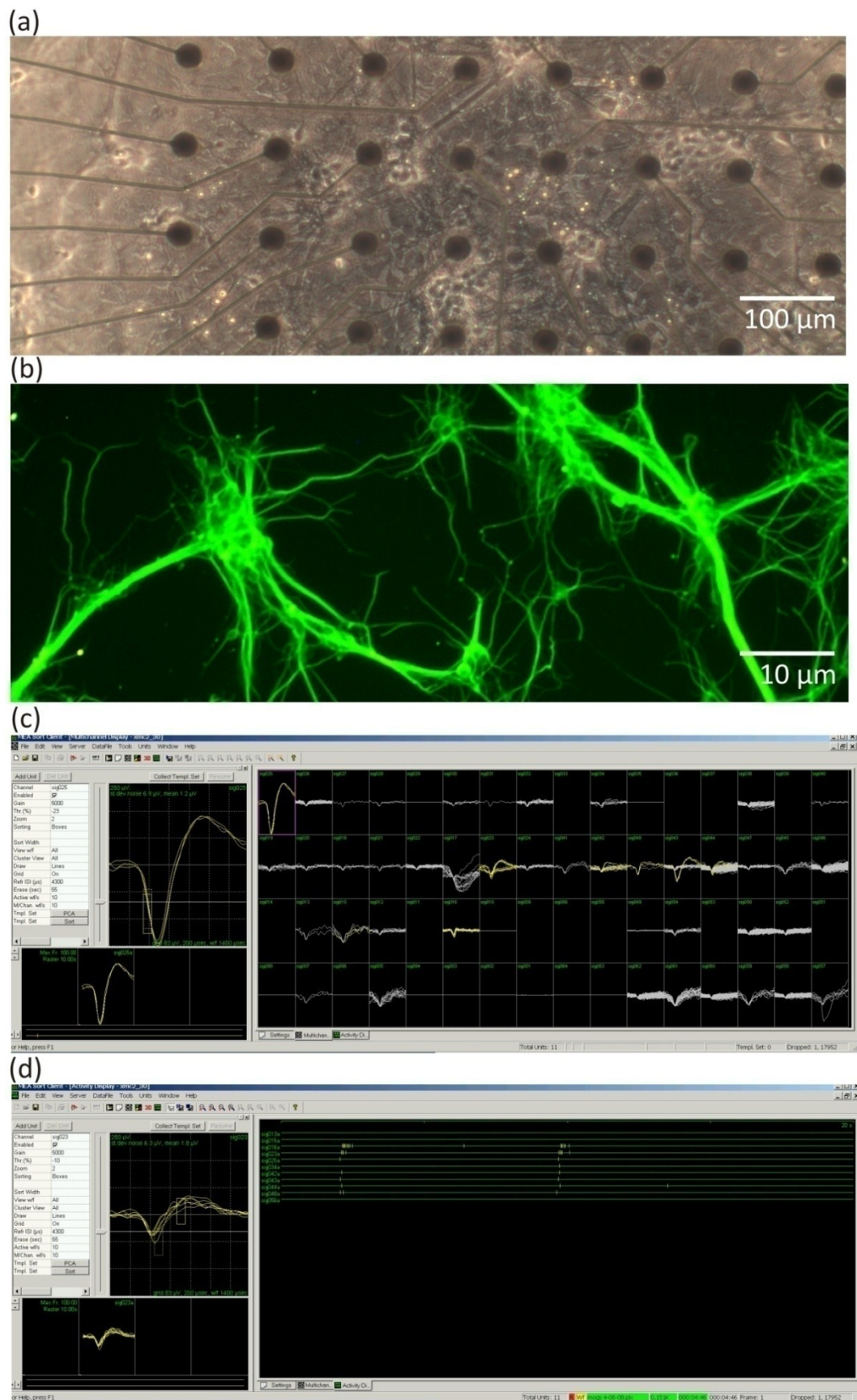


Figure 44: Neuronal growth and neuroelectric control registration on a GNC after 21 DIV. (a) Neuronal network on the GNC MEA; (b) fluorescently stained neuronal network; (c) waveforms; (d) signal trains. An Olympus BX-51 WI microscope was used.

3.3.2.3 Influence of sodium valproate (VPA) on neuronal firing frequency

Neuronal networks were cultured on the SNCs under the influence of VPA (0.27 mM and 0.81 mM) for 12 and 21 DIV. The following experiments were inspired by the grant no. 31P4590 and done in cooperation with S. Bühler, M. Stubbe and T. Reimer. In summary, three control chips and six chips with VPA were examined at 12 DIV (**Figure 45**) and 21 DIV (**Figure 46**). In both figures, the units were sorted according to their firing frequency, in order to consider the homogeneity of firing neuronal networks. The detected neuronal signals show that the mean frequency is strongly affected by VPA. The homogeneous firing frequency of the control chips ranged from 0.01-1.2 Hz. In contrast, the firing frequency of the chips with 0.27 and 0.81 mM VPA varies between 0.5-7.8 Hz and 0.1-12 Hz, respectively. VPA seems to induce a desynchronization of the neuronal activity in dependent on the administered concentration. The most obvious effect is that no electric activity could be detected with concentrations >0.81 mM VPA (**Figure 45**).

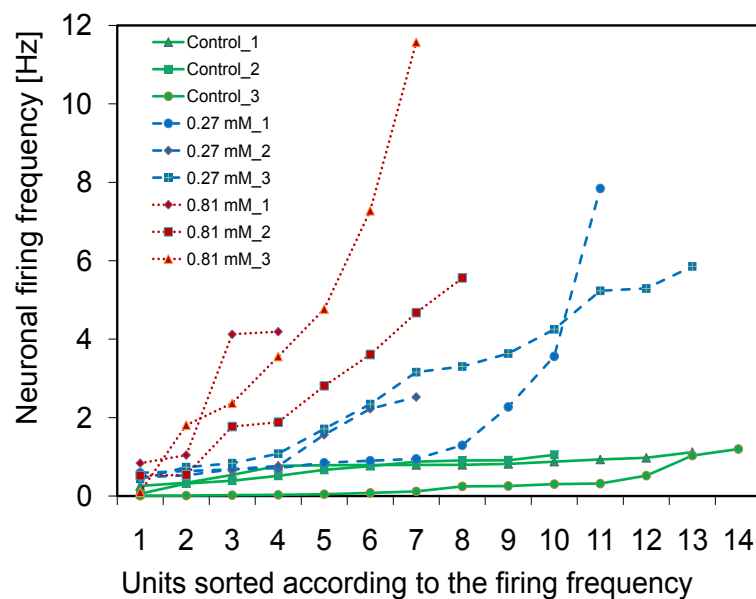


Figure 45: Effect of VPA on the uniformity of AP frequency at 12 DIV.

Experiments on 21 DIV show a different state of the neuronal networks (**Figure 46**). No electrically active units could be found for 0.81 mM VPA. The three control chips were compared with two test chips (0.27 mM VPA). Four other chips with 0.27 mM (1) and 0.81 mM (3) showed no neuronal activity. In contrast to 12 DIV, the control chips showed higher neuronal firing frequencies (0.1-7.2 Hz) while the chips with 0.27 mM VPA fired similarly to those after 12 DIV, with frequencies of 0.3-6.3. The obtained results are of great value for the project BMBF grant no. 31P4590. The figures were taken from the **Manuscript**

2 p. Fehler! Textmarke nicht definiert. ff. This manuscript also reports in detail on measurements with the GNC-integrated IDES, the temperature sensor, and a microfluidic head that was developed by the author.

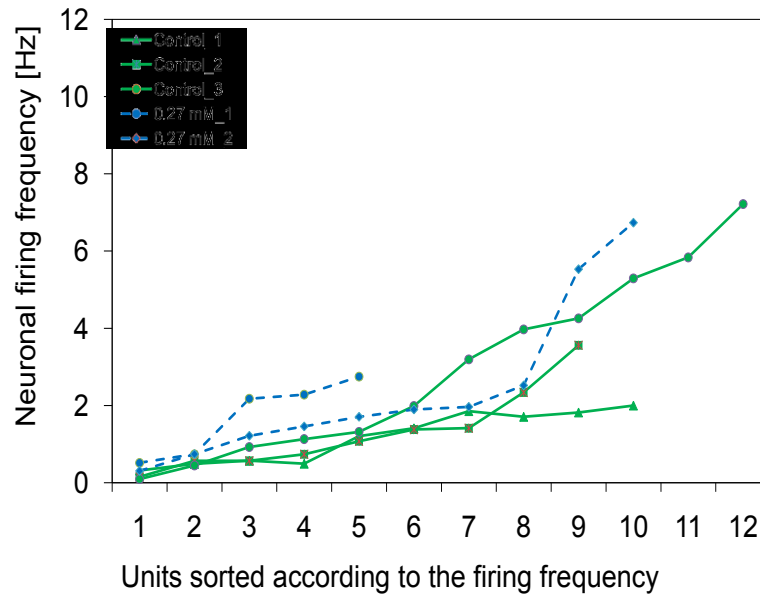


Figure 46: Effect of VPA on the uniformity of AP frequency at 21 DIV.

In utero injected doses (800 mg/kg) of VPA, can lead to severe developmental delays in newborn rodents and alterations in neurexin (NX) expressing neuroligin (NL) genes which are indispensable for neuronal cross-linking (Kolozsi et al., 2009). The NX expression by NL is hindered by VPA, which results in autism-like behavior of mice. Autism-like NL-mutations cause reduced spontaneous activity patterns in mice due to a decreased complexity of axonal architecture (Gutierrez et al., 2009). VPA was found to increase the GABA and glutamate decarboxylase (GDA) levels in synapses of mice (Gale and Iadarola, 1980; Löscher, 1981). GDA is an enzyme that catalyzes the decarboxylation of glutamate to GABA and CO₂. GABA has long been known to inhibit the neuronal activity of cortical neurons (Krnjevic and Schwartz, 1967).

Hence, the presented results are in accordance with the literature. In this study, long-term administration of increasing concentrations of VPA lead to desynchronized or absent electric activity. These results correspond to former findings on single unit activity of *substantia nigra pars reticulata* neurons in rats undergoing VPA administration (Löscher et al., 1995; Rohlf et al., 1996). This desynchronization could be a consequence of the decreased neuronal network complexity induced by VPA. The total absence of neuroelectric activity with higher concentrations (2.43-21.87 mM VPA) could be explained by the impact

of increased concentrations of GABA and GAD. Obviously time-dependent, the decreased network complexity could lead to a loss of axon/dendrite-electrode contact. These findings are confirmed by the presented IDES experiments described in **Manuscript 2 p. Fehler! Textmarke nicht definiert.**ff. Here, the cellular growth over 12, 14 and 16 DIV is severely hindered with VPA concentrations >0.81 mM VPA. However, neuronal activity was not detected with 0.81 mM VPA after 12 DIV suggesting a negative long-term effect of VPA on PNCs.

The neuronal networks showed the bursting behavior typical to conventional chips. The signal amplitudes were high (up to 595 μV) compared to the established system (Gross et al., 1977; Gross et al., 1982; Gross et al., 1995; Fromherz and Stett, 1995; Stett et al., 2003b). These conventional systems show amplitudes of up to 80 μV with cryopreserved neurons (Otto et al., 2003). A maximum amplitude of 300 μV was measured in another study using conventional glass MEAs (Krause et al., 2006). These values are comparable to the GNC with its planar electrodes.

3.3.2.4 *Cardiac action potential detection*

Electrical control measurements with PCMs and video recordings were made on 14 DIV (**Figure 47**). **Figure 47a and b** demonstrate that PCM attempted to build a contiguous muscle cell cluster. The electric detection of the rhythmic PCM APs is shown in **Figure 47c and d**. The waveforms are shown in **Figure 47c**. In shape, they resemble neuronal signals. The signal amplitudes shown in the left box are 66 μV , 100 μV and 132 μV . The PCMs fire with a frequency of approximately 2.4 Hz. The MEA Server program could not display the high amplitudes correctly. However, these fluctuations are small in amplitude and short in length compared to the extracellular detection with the MNC (see below). The signal form is characterized by the electrode properties; that is, slower components of the signal cannot be displayed by the platinum electrodes. These findings correspond to the results from tests using PCMs and platinum hollow needles with the MNC (see below). However, cardiac APs have signal lengths of approximately 300 ms. The displayed waveform amplitudes decrease much faster due to the changing properties of the platinum electrodes. Surprisingly, the signal amplitudes of the PCMs were very high.

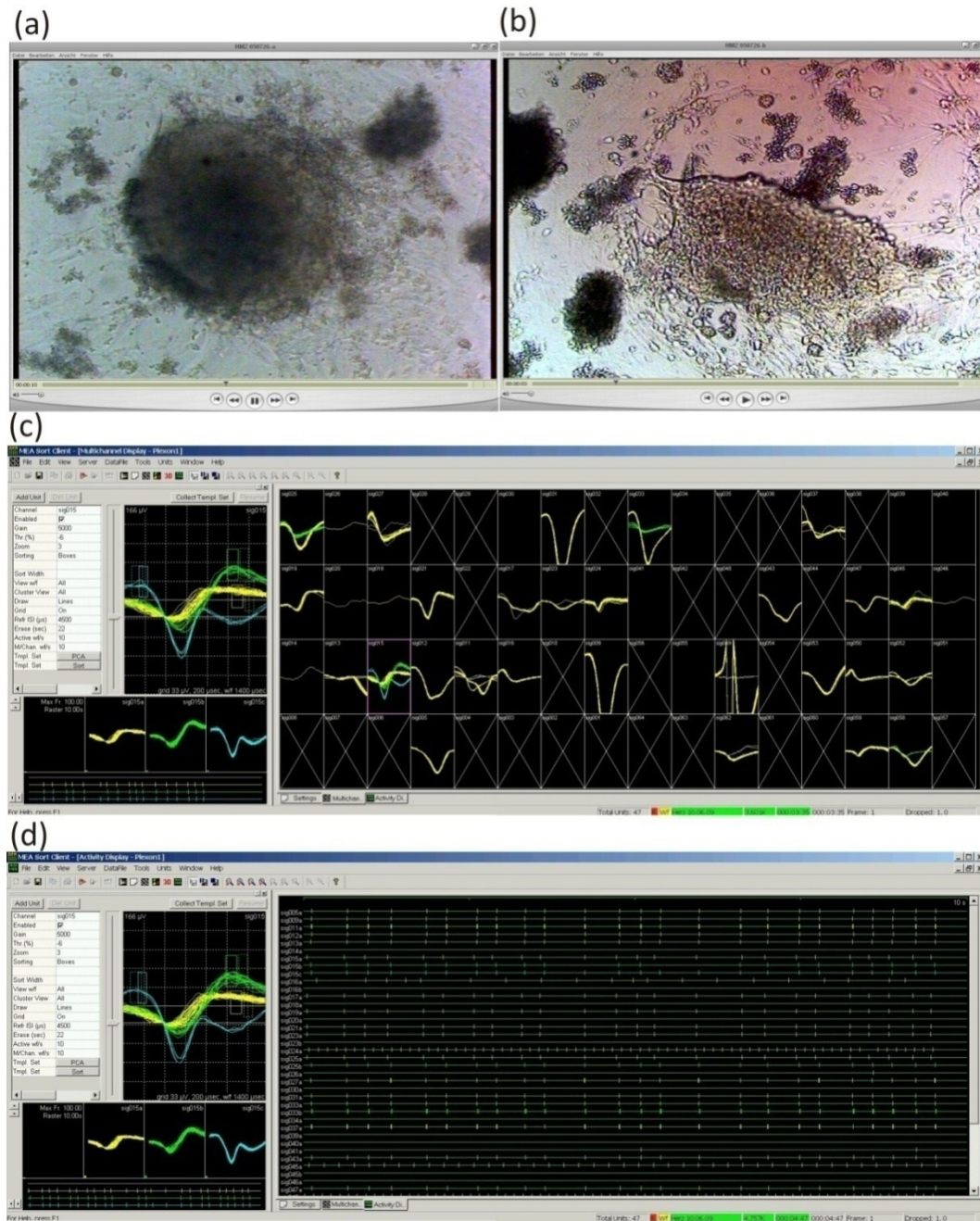


Figure 47: PCM growth and electric registration on the GNC after 14 DIV. (a) and (b) video screenshots of PCM networks growing on the GNC; (c) waveforms with several cardiac units on single electrodes; (d) rhythmic signal trains.

The GNC is a robust device for the detection of APs of PNCs. The detection of PCM APs has, to the knowledge of the author, not yet been attempted with commercial MEAs designed for neuronal cells. Surprisingly, signal amplitudes were up to approximately 1 mV (personal communication T. Reimer). The GNC allows for the administration of biochemically active substances and is of comparable quality to commercial MEA systems.

The GNC is economic, because it allows for the cultivation of 120-160 PNC or 220-320 PCM networks harvested from 15-22 embryos on GNCs. The small headstage will allow for the system's use in different laboratories without increasing effort. The detection of APs after dozens of autoclaving steps proved the system to be a reliable tool for extracellular electrophysiological experiments.

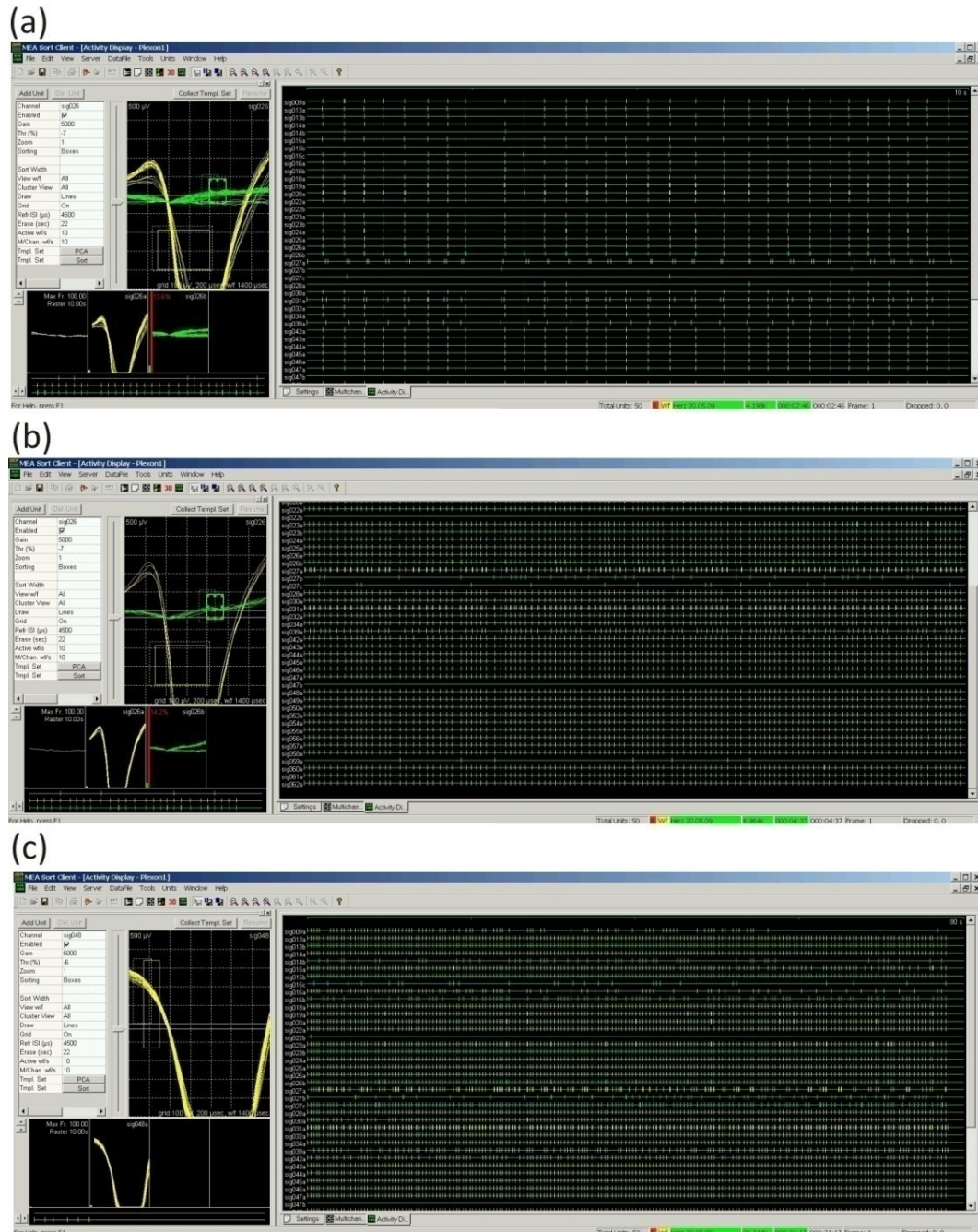


Figure 48: Cardiac AP detection with three different GNCs (a-c). Amplitudes were estimated to be approximately 1 mV. The signal amplitudes were too high to be correctly displayed by the waveform window of the MEA Server program (left). The activity window shows the cardiac AP events over 10 s (a and b) and 80 s (c). Screenshots courtesy of T. Reimer.

3.3.3 MNC

3.3.3.1 pDEP with PNCs using kidney-shaped electrodes

The following results were obtained within the framework of the BMBF grant no. 16SV2339 (*Microstructures and methods for the intracellular bioanalytics – MIBA*). The cell allocation could be helpful for the exact and reproducible LOMINE (Tautorat et al., 2008; Held et al., 2008a; Koester et al., 2008a), opening new ways for intracellular measurement and bioanalysis of pharmacologic or xenobiotic compounds with adherent cells in culture. The author suggested integrating kidney-shaped pDEP electrodes into the MNC. The MNC and the MNE and pDEP electrode array is shown in **Figure 49**.

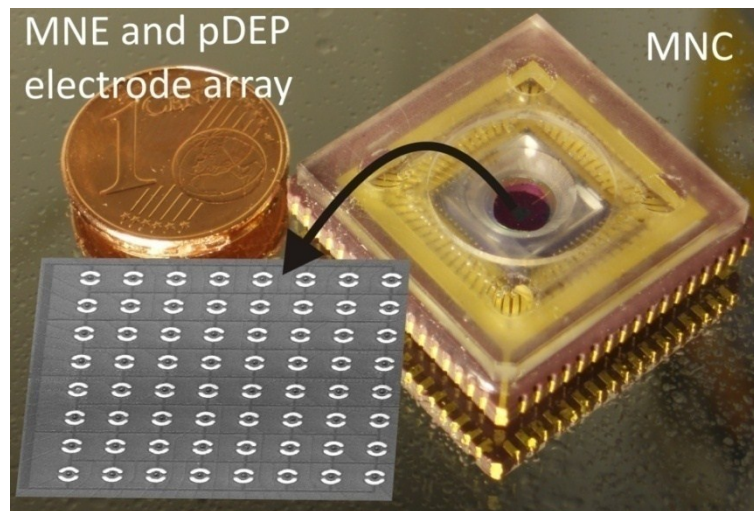


Figure 49: Dimensions of the MNC. The inserted SEM shows the MNE array ($A = 1 \text{ mm}^2$) with two pDEP electrodes framing each MNE.

Using pDEP with the MNEs alone resulted in strong fields at the tips of the MNEs and possible destruction of the cell membrane. Different pDEP electrode arrangements were tested (data not shown). The layout and a SEM photograph of the pDEP electrodes framing the MNE are shown in **Figure 50**. NHDF (data not shown), L929 tumor fibroblasts and PNCs were positioned in the proximity of the MNE and were able to adhere there as shown in the SEM image of **Figure 51**. However, without polymer sites, cells tend to migrate after some time (see **Figure 51b right** and compare to pDEP with SNCs). The method presented allows for direct allocation of different cell types by pDEP with kidney-shaped electrodes. Preventing cells from leaving the electrodes and increasing the probability of successful cell positioning is a task for the future. The author suggests patterning the MNC's silicon surface with polymer coating, which would provide additional guiding structures for the cell. The first results are presented below.

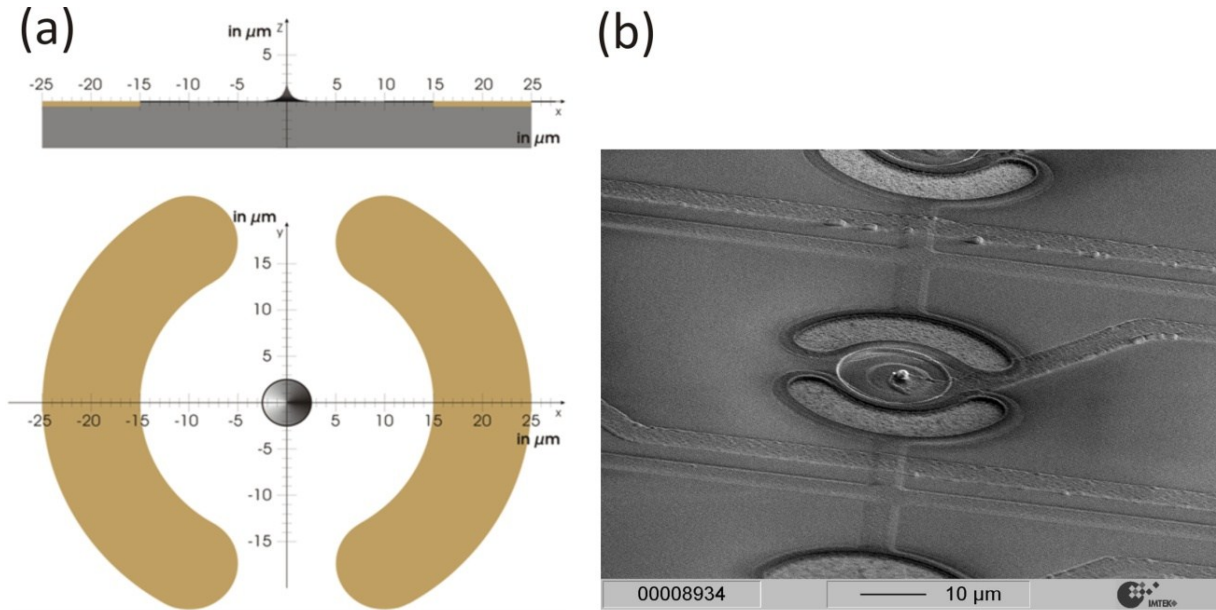


Figure 50: Dimensions of two pDEP electrode framing one MNE. (a) Sketch (cross-sectionional cut and top-view); (b) SEM image.

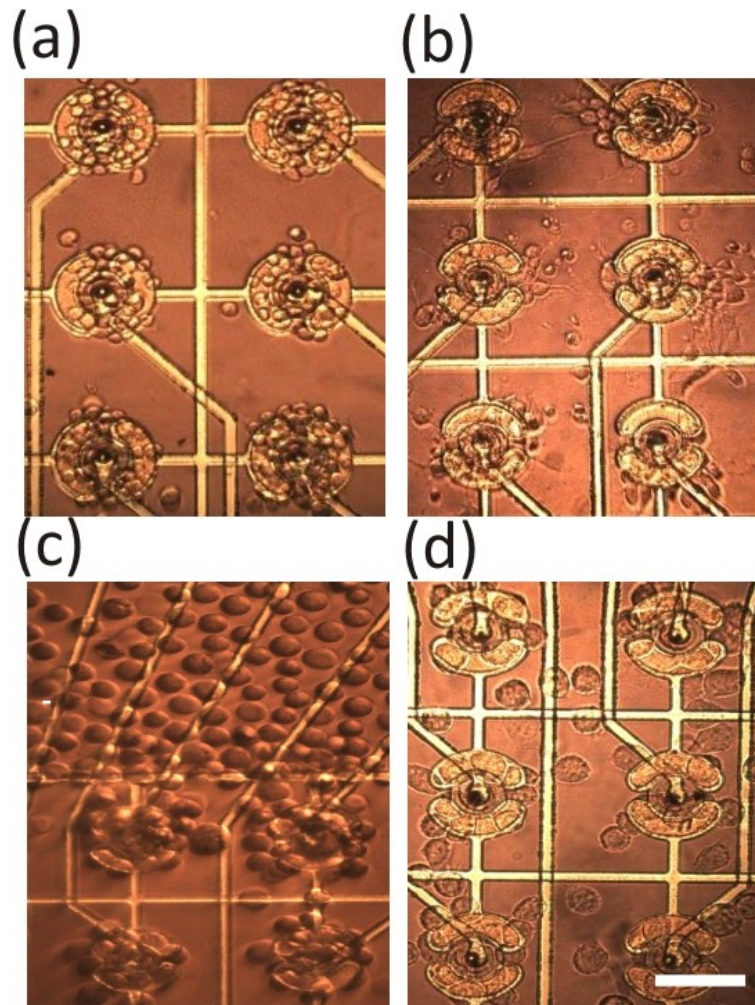


Figure 51: Attraction of different cell types with pDEP electrodes. (a) PNCs and (b) L929 tumor fibroblasts were positioned on the pDEP electrodes. Cells started to migrate from the electrode within 2 DIV.

3.3.3.2 Polymer patterning of MNC surface

As suggested in the tests using pDEP on the SNCs, polymer patterns were set onto the MNC's surface by S. Petersen (Chemical Institute of the University Darmstadt). With these polymers, one can spatially control the adhesion of cells. A hybrid copolymer, comprising the peptide cell-recognition motif RGD, attached to the protein-repellent polymer PDMAA, is used in a lithography process to graft a chemical microstructure onto the surface of the MNC (Petersen et al., 2009). **Figure 52** demonstrates the time-dependent accumulation of NHDF cells on the polymer films that have been attached to the surface of the MNC. The observed cell behavior is comparable with literature data (Wörz et al., 2007).

Experiments for the detection of intracellular potentials were done with these chips. Unfortunately, no such potentials were detected when polymers were deposited. However, a defined guiding of cells was shown with the polymers.

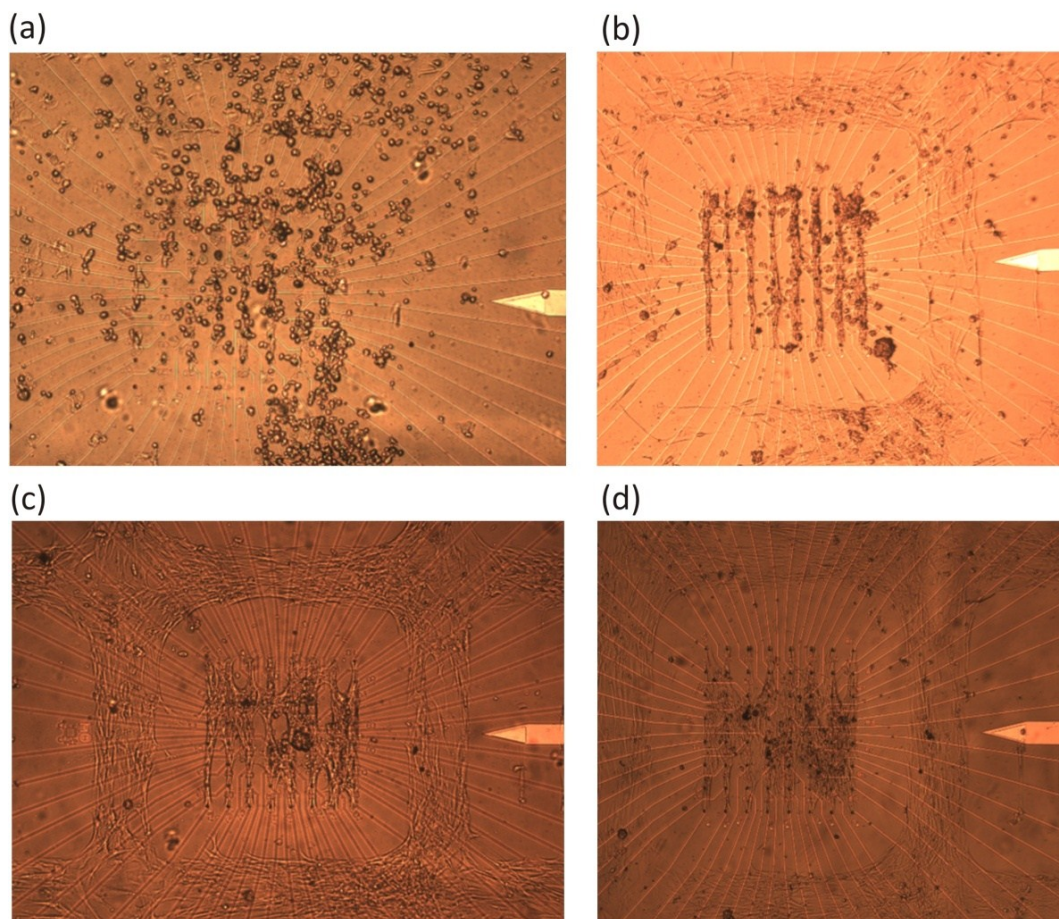


Figure 52: Time-dependent accumulation of living NHDF cells on cell-adhesive polymers. Cells organize a structured network that is guided by the polymer pattern. No pDEP was applied. (a) Cells sediment to the chip surface immediately after seeding; (b) after 1 DIV; (c) after 2 DIV; (d) after 3 DIV.

3.3.3.3 Electroporation of adherent cells using LOMINE

The principle of LOMINE is presented in **Figure 53**.

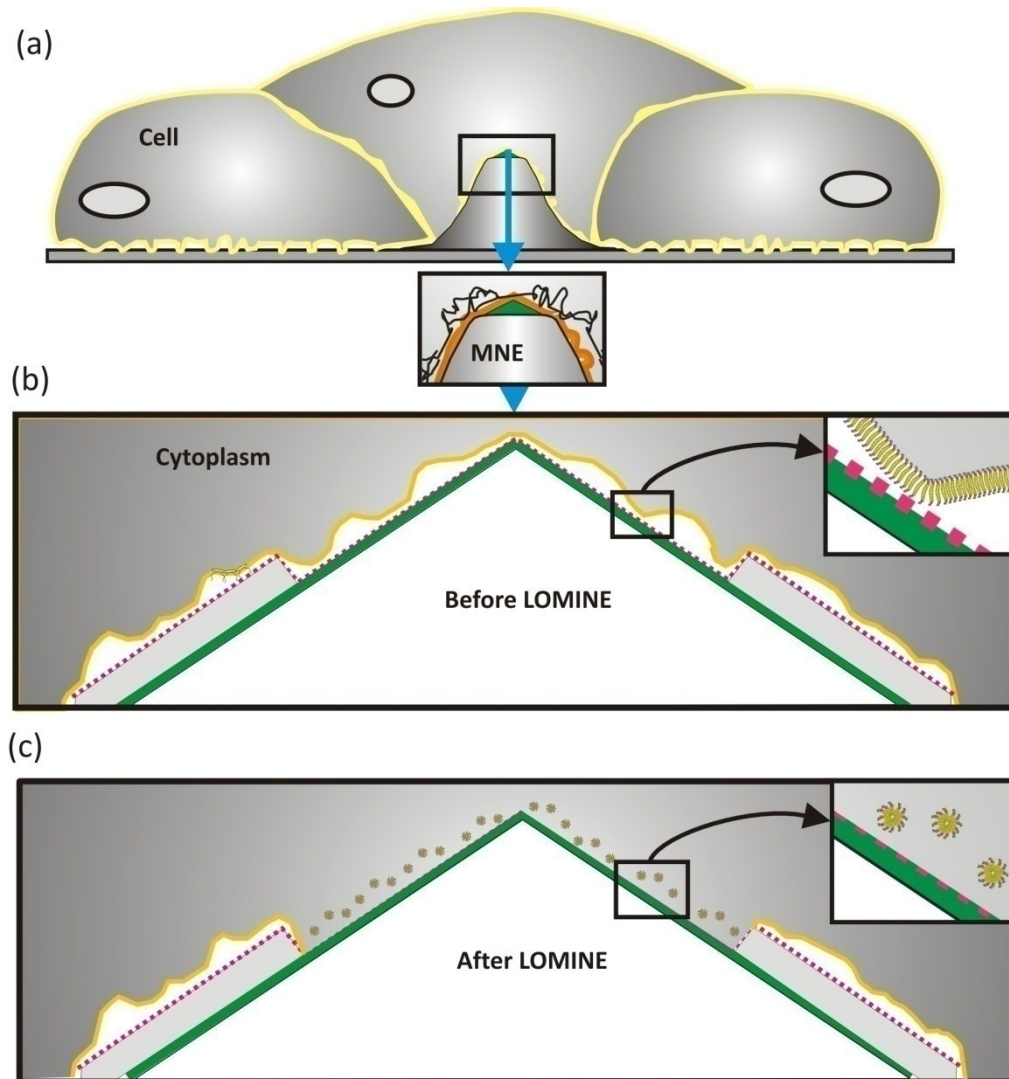


Figure 53: LOMINE principle of the PoreGenic® system. (a) Schematic cross-sectional view of a model cell growing over a silicon MNE. Insert shows the focal cell adhesion contacts and the MNE; (b) before electroporation: magnified, cross-sectional view of the MNE with adhered cell membrane consisting of phospholipid bilayer and extracellular matrix. Insert demonstrates focal cell contact point on metallization (green); (c) after electroporation: phospholipid bilayer is destroyed, micelles are building (Pliquett et al., 2007) and the MNE is in electrical contact with the cytoplasm. Now, the transmembrane potential V_m can be measured.

The first LOMINE experiments were promising; trypan blue showed an opening in the cell membrane for fibroblasts in the cell line L929 (**Figure 54**). The vital dye trypan blue stains dead cells dark-blue. The dye was added to the nourishing medium prior to the very high LEPs of symmetrical $4 V_{pp}$. This was done to prove that the MNEs are individually controllable. After one LEP, the cell in **Figure 54a** opened and began to leak cytoplasm. Subsequently, the trypan blue diffused into the electroporated cell, inducing a change in cell

color (**Figure 54b**). **Figure 55** presents the congruence of a reflected light microscopic image with a FIB-SEM. This figure clearly shows the advantages of the FIB-SEM technique in comparison to the conventional light microscopy. However, the FIB-SEM technique is prone to preparational artifacts.

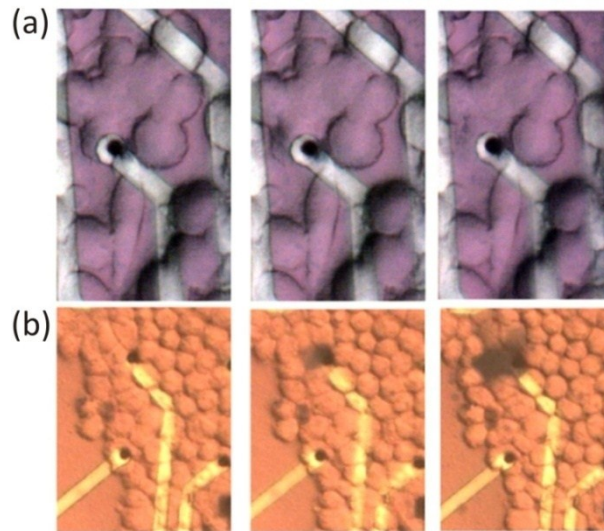


Figure 54: Electroporation of L929 fibroblasts. (a) Single cell electroporation causes opening of the cell membrane and leakage of cytoplasm. Images show cells before as well as 30 s and 360 s after LEP; **(b)** trypan blue diffuses into the cells due to a severe cell membrane rupture. Pitch: 50 μm , LEP pulse: symmetrical 4 V_{pp} added to the MNE potential before pulsing, pulse frequency = 20 Hz. White scale bar = 5 μm , black scale bar = 20 μm

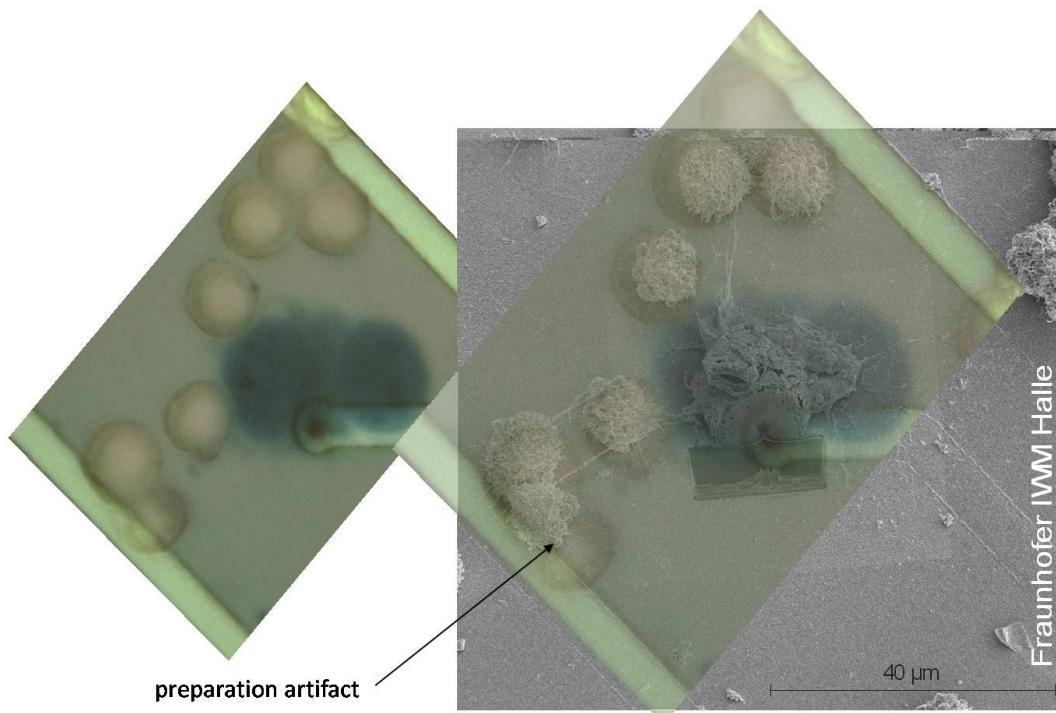


Figure 55: Congruence of a reflected light microscopical image and the corresponding FIB-SEM image. The electroporated and killed L929 fibroblast is stained blue by trypan. The FIB-SEM image combination (right) clarifies that the cell was leaking cytoplasm. In addition, this image shows a preparational artifact; the subsequent movement of a fixed cell.

3.3.3.4 Fluorescence microscopy

PNCs and fibroblasts were cultured on the tips of MNEs as shown in the FIB-SEM image in **Figure 56** and **Figure 57** (Koester et al., 2007b). In order to establish a more sensitive test method for the LEPs of PNCs, different experiments were attempted using the fluorescent RNA/DNA-binding propidium iodide (PI, 40 μ M in electroporation buffer, **Figure 56**) as well as the actin-binding rhodamine phalloidine (RP, 2 μ M in electroporation buffer, **Figure 57**). PI and RP do not pass through the intact cell membrane; however, they can pass through membranes of dead cells or artificial membrane pores produced by LEP. Pore size, diffusion and fluorescence signal directly depend on the LEP parameters (frequency, amplitude, MNE characteristics, etc.) and membrane characteristics. Dead, PI-penetrated cells already show strong fluorescent signals before LOMINE (**Figure 56, top left**). In contrast, the fluorescence of the living "target cells" above the MNE is produced only after LEP (see white arrow). In order to prove that the LEP used was tolerated by the living cells, vitality tests were administered to electroporated cells. MNC were treated with the same parameters and stored for 1 DIV in the incubator. On the following day, vitality staining with trypan blue was conducted again.

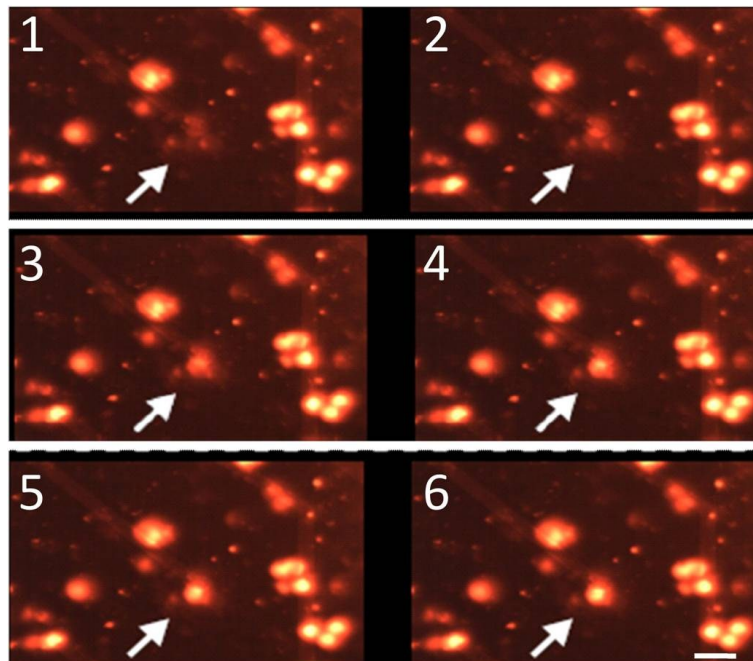


Figure 56: LOMINE sequence of PI staining of PNC. LEP pulse parameters: 2x symmetrical 2 V_{pp} and 1 x symmetrical 4 V_{pp} were added to the MNE potential before pulsing, pulse frequency = 100 kHz, pulse train length = 30 ms. White arrows indicate the electroporated single neuron. Scale bar = 10 μ m.

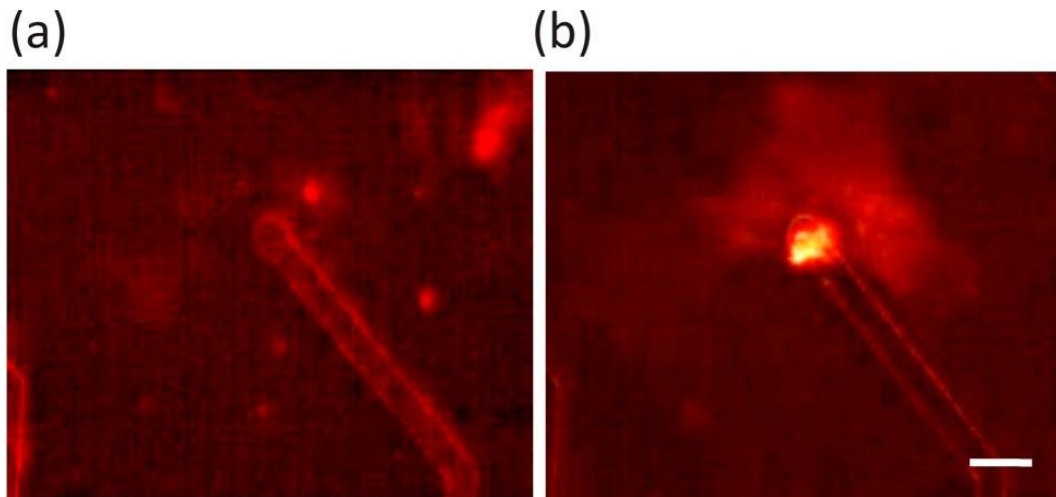


Figure 57: LOMINE of a NHDF. (a) Before; (b) 30 s after fluorescent staining with RP, 40x. LEP pulse parameters: $5 \times 3 V_{pp}$ were applied to the MNE potential before pulsing, pulse frequency = 100 kHz, pulse train length = 30 ms and additional $5 \times 3 V_{pp}$ were applied, pulse frequency = 10 kHz, pulse train length = 300 ms. The poor image quality is due to the low resolution of the USB-camera installed on the microscope and the limited magnification (40x-objective). Scale bar = 5 μm .

Figure 58 demonstrates that electroporated MNEs (white circles) did not show blue stained dead cells. This means that the LOMINE parameters used did not kill the cells. Some stained cells were visible on the chip, but this is a common and natural observation in cell cultures.

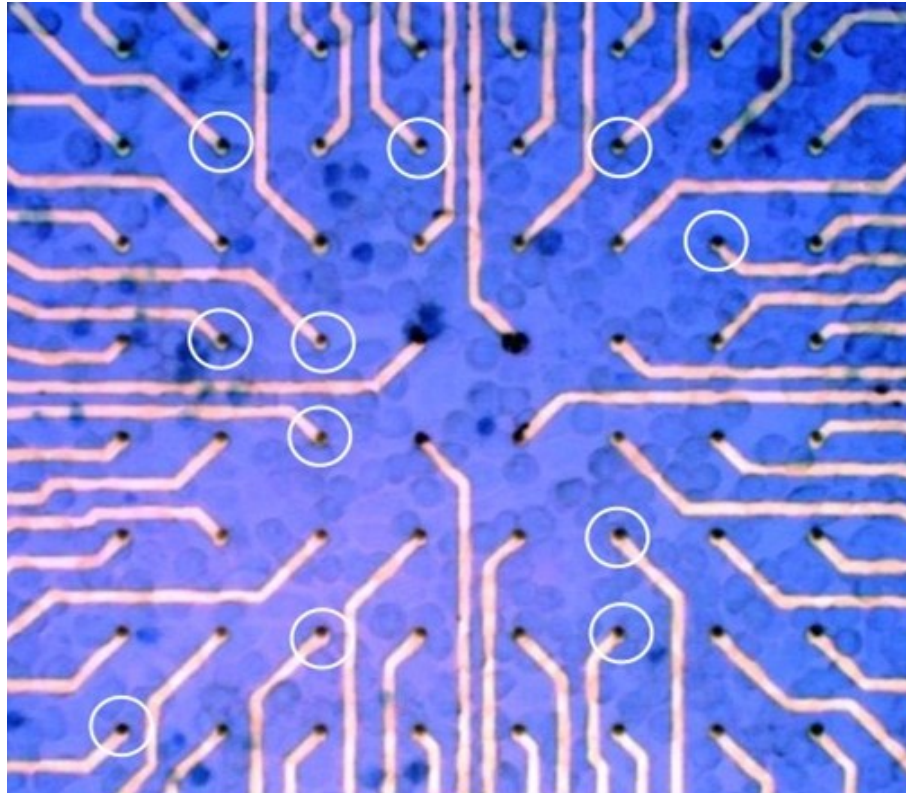


Figure 58: Vitality test after LOMINE. Vital staining of L929 fibroblasts with trypan blue 1 DIV after LEP with $1.5 V_{pp}$ were applied to the MNE potential before pulsing. No staining is observed at electroporated MNEs suggesting cell survival (white circles). However, this experiment did not allow for distinguishing between resealing of pores or non-electroporated cells.

3.3.3.5 Intracellular potential detection

Experiments show that the cells grow over the MNEs completely. The software programmed by C. Tautorat allows free adjustment of LEPs. A potential DC drift was seen when the power supply was switched on. **Figure 59** gives a schematic overview of the observed drift and possible LEP variations.

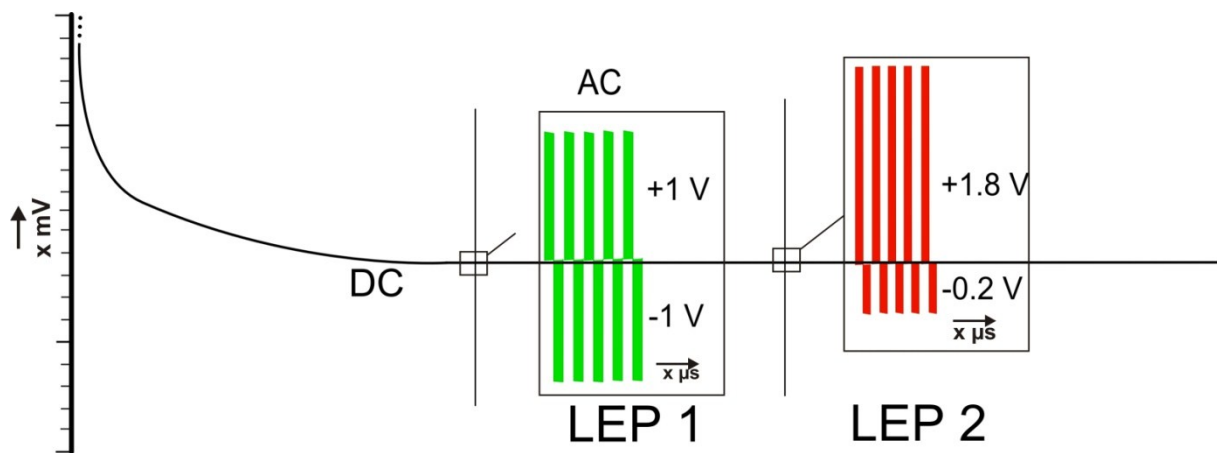


Figure 59: Scheme of the AC-pulsing after DC-signal approximation. The biphasic symmetrical LEP 1 (± 1 V) and the unsymmetrical LEP 2 (-1.8 V/ $+0.2$ V) were added to the measure DC-fraction. Scheme not to scale.

Possible LEP configurations are shown. After discharging the MNE potential, which depended on the MNE material, LEPs could be applied. Biphasic pulses were used, comprised of a negative pulse followed by a positive pulse, e.g. ± 1 V_{pp}. The membrane-opening characteristics were examined by means of different electroporation experiments. For this, the parameters of the LEP were varied, and the occurrence of electroporation was confirmed. Electroporation pulses with symmetrical voltage of $+1.5$ V_{pp} and a frequency of 100 kHz were applied to the MNEs (**Figure 60**). Cell-free MNEs (D1 and C8) reacted to these pulses with a voltage change of approximately +10 mV. Their potential approached the starting potential again after approximately 75 s. In contrast, electrodes grown over with cells reacted with a decrease in negative voltage (electrodes D5 and B5). These were the first hints of an interaction between the cells and the electroporation MNEs. This suggested that overgrown electrodes could be electrically recognized by gentle pre-pulsing. Pre-pulsing may therefore allow only electroporation of those MNEs that show higher potentials; that is, MNEs overgrown with cells.

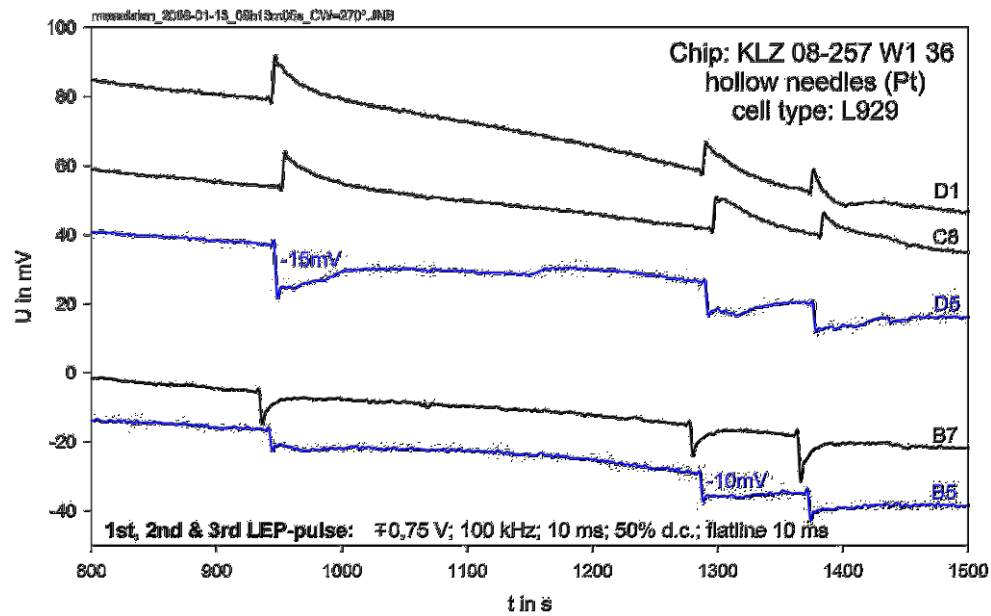


Figure 60: Comparison of different V_m potential measurements with L929 cells without intracellular contact. Cells overgrew MNES and reacted to special LEPs (see description in the figure). Cell-free MNES showed other reactions.

A typical voltage drop for overgrown MNEs was evident on electrode D6 after the first and second electroporation steps (**Figure 61**). The electroporation voltage was gradually increased from a symmetrical $\pm 0.75 V_{pp}$ to an unsymmetrical $-1/+0.75 V_{pp}$. After the voltage increase during the first electroporation-pulse phase to $-1 V$, the measured potential of MNE D6 strongly decreased. The voltage drop was approximately $-30 mV$.

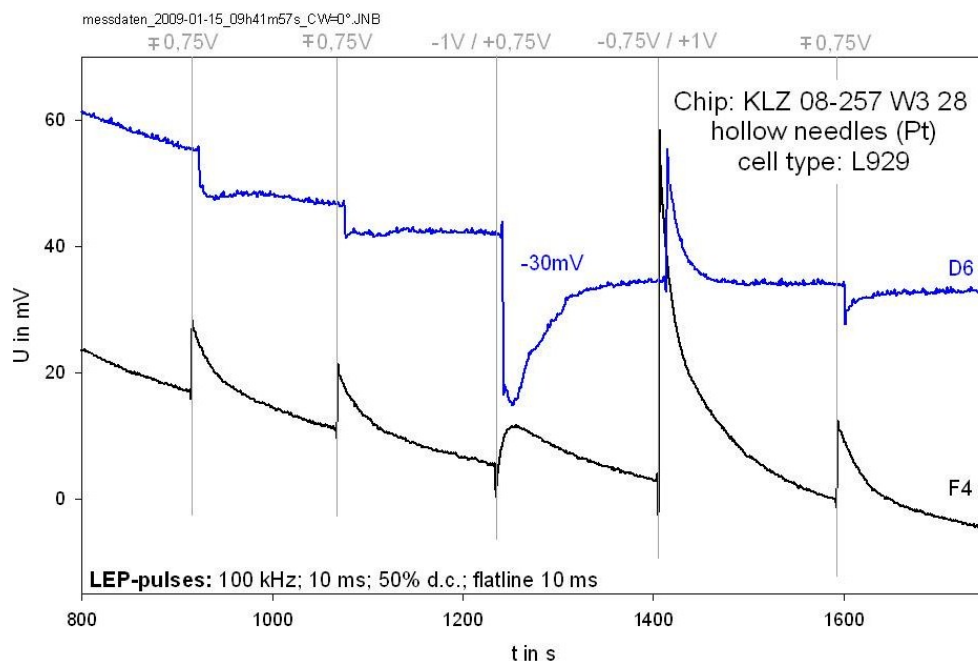


Figure 61: Reactions of L929 fibroblasts to special LEPs. Diagrams suggest possible V_m transmembrane potential measurements with MNE D6 (blue line).

This decrease was disproportionate to the increased voltage of -1 V. Comparisons with values from the literature show similar V_m potentials (-22 mV) for this cell type (Osipenko et al., 2000). However, an unambiguous proof for the intracellular measurement is still missing. In contrast to the cell-free MNE F4, the subsequent approach of the MNE D6 voltage to a normal value of approximately $+35$ mV is non-uniform. This observation might be explained by electrochemical reactions at the MNE tips. However, electrode D6 was slightly noisier than MNE F4. At this electrode, the recharging corresponded to a sigmoidal curve as expected for a homogeneous electro-chemical reaction. After this experiment, slightly higher voltage pulses were tested for intracellular measurements. **Figure 62** shows that a symmetrical voltage pulse of ± 0.9 V_{pp} may also lead to a successful measurement with MNE G4.

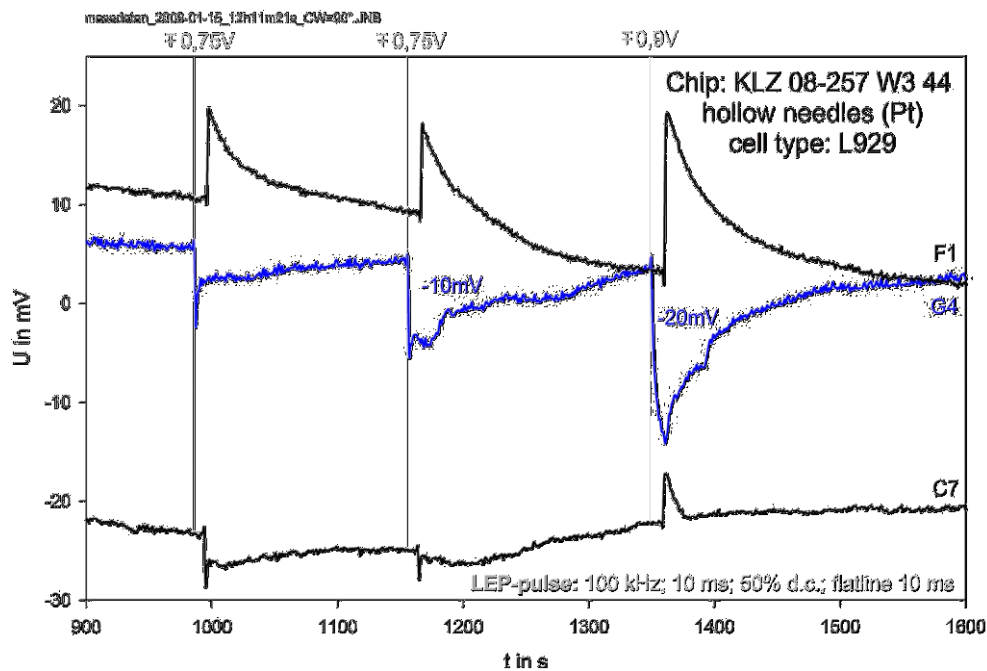


Figure 62: Reactions of L929 fibroblasts to special LEPs. Increase of the pulse voltage to ± 0.9 V_{pp} and the corresponding cell reaction (see MNE G4, blue line).

In this case, however, a voltage drop of -20 mV was observed. This corresponds to values from the literature, and depends on the physiological status of the individual cells (reproduction status, medium age etc.). As the measured voltage increased in stability, the likelihood that measured signals of biological and intracellular origin increased (**Figure 63**).

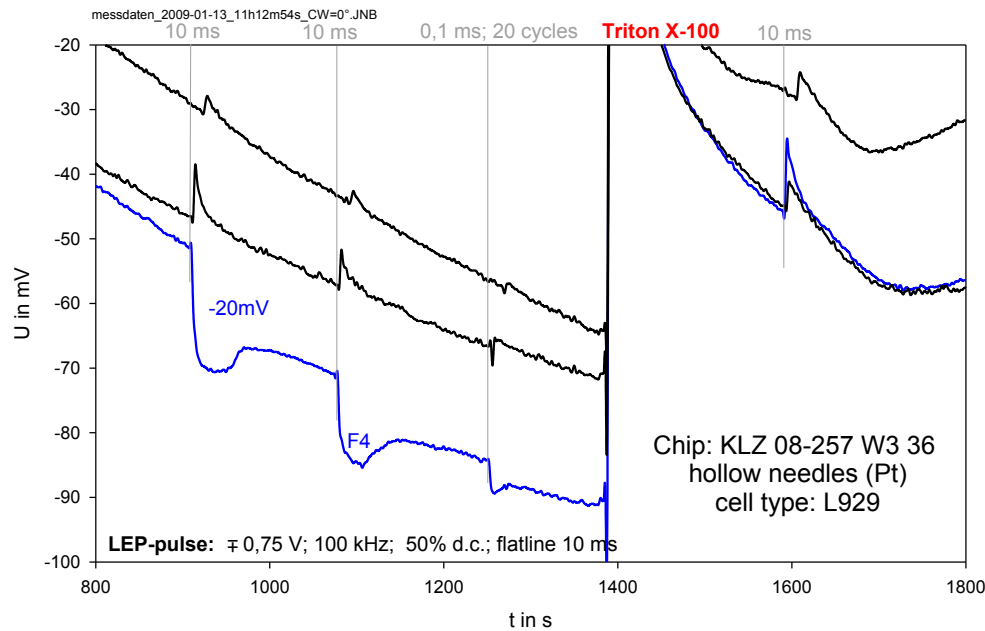


Figure 63: Reaction of a L929 fibroblast on LEPs. The experiment was terminated with Triton® X-100 to prove the biological origin of the evoked voltage drops.

The MNE F4 showed a voltage drop of approximately -20 mV for approximately 50 s. Interestingly, it was possible to evoke another strong voltage drop after adjusting the voltage levels to the starting parameters. This can probably be explained in the following way: after a successful opening of the membrane, the transmembrane potential V_m of the cell is measurable for a short time. However, the cell always tries to close possible membrane holes. This pore resealing can take up to minutes (Bier, 2002). Here, this seems to be the case, as the measured potential again ran into the more positive range. After further electroporation pulses, the membrane opened again and the same effect was measured.

If this interpretation was right, the voltage used did not kill the cells. In order to prove that no electro-chemical or electrical artifacts were detected, this experiment was terminated with Triton® X-100 to dissolve the cell membrane and extinguish the transmembrane potential. This is apparent from the significant amplitude change after adding Triton® X-100 followed by another electroporation incident (see **Figure 63** at 1400 s). In this case, the MNE F4 behaved as if it was not overgrown with a cell, since the cell membrane was dissolved by the surfactant. This indicates that the voltage drop of -20 mV for approximately 50 s was of biological origin.

The presented intracellular potential measurements were made without cell membrane sealing polymers (Baaken et al., 2007). We expect that these intracellular measurements will be more stable after applying seal-promoting chemical compounds in the future.

3.3.3.6 FIB-SEM examinations

LOMINE-treated MNCs were examined with the FIB-SEM technique. **Figure 64** shows FIB-SEMs of electroporated L929 mouse sarcoma fibroblasts. The magnified SEM suggests that the fibroblasts were opened and penetrated by the MNE. The digitally stained image supports this view, as well as the presented results in chapter 3.3.3.5. The combination of FIB-SEM images with the fluorescence experiments (**Figure 56** and **Figure 57**, p. 69) provides proof of a successful LOMINE.

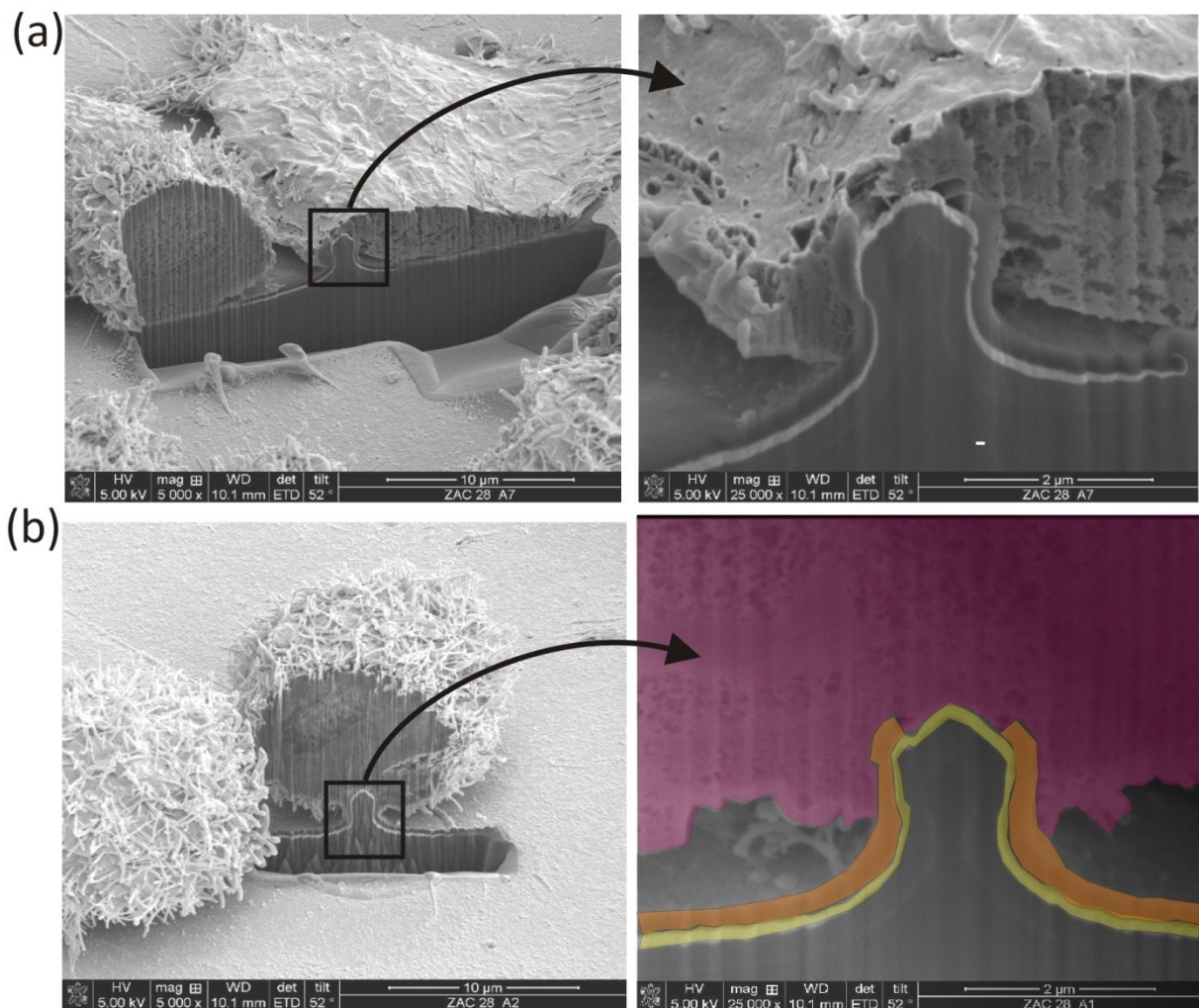


Figure 64: Electroporated L929 mouse sarcoma fibroblasts overgrow MNEs. A flat and a spherical cell persist in co-culture. (a) The FIB-SEMs show the membrane penetration by LOMINE. Cells do not show any disruption or cytoplasm dispersion; (b) electroporated and digitally stained L929 cell. Magenta = fibroblast, orange = needle passivation, yellow = MNE tip metallization.

3.3.3.7 Extracellular action potential detection

3.3.3.7.1 Hollow platinum MNE arrays

Another idea was to record APs of PCMs with the MNC. Due to the 3D-structure of the MNEs and their electrical properties, the author assumed that extracellular potential recording would be possible. When observed with a microscope, the entire heart cell tissue resembles a single contracting muscle cell. Therefore, the cardiac muscle is commonly called a functional syncytium, because PCMs are connected to one another (mechanically, chemically, and electrically). The syncytium consists anatomically of individual cells, but the entire cell mass responds as a unit, and all PCMs contract together. This is also true for smooth muscles. Three different types of needles were tested for the measurement of PCM signals. As an example, the PCM growth is shown on silver electro-plated solid silicon microneedles (**Figure 65**).

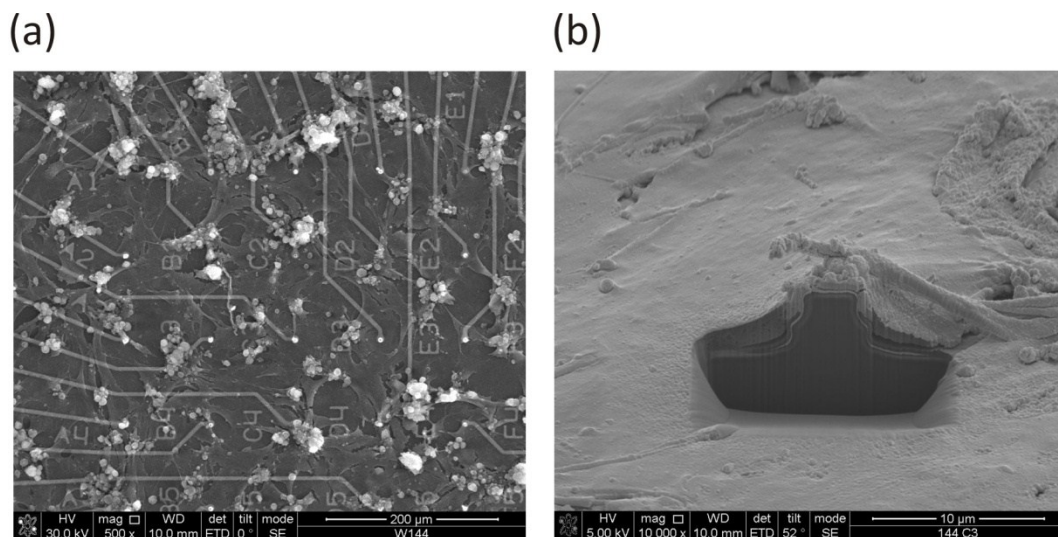


Figure 65: PCMs cultured on a MNC. (a) PCM clusters are growing on the MNC surface; (b) FIB-SEM of a flat single PCM overgrowing a silver electro-plated silicon microneedle.

When APs of PCMs are recorded with MEAs, the extracellular cardiac APs are sometimes called field potentials (FP) because the recorded signal only indirectly reflects the AP (Halbach et al., 2003). To simplify matters however, the author decided to continue to use the term AP. **Figure 66** shows the first experiments with PCMs of embryonic mice. No test substances were added and only the native cardioelectric activity was recorded. The measured signals are different from the intracellularly measured transmembrane AP (compare with **Figure 3, p. 7**). In addition, they show amplitudes up to only 3.2 mV and were very short, with lengths of approximately 1-2 ms. A possible reason was that platinum was

used for MNE-metallization. Metallic platinum electrodes cannot display the low frequency signal components of cardiac APs (signal period 300 ms); only fast changes of the signal can be detected. This is also the case with the commercially available devices using golden ring electrodes (Meyer et al., 2004b). Nevertheless, the detected signals showed amplitudes approximately 2 to 3 times higher than commercial systems (Meyer et al., 2004a).

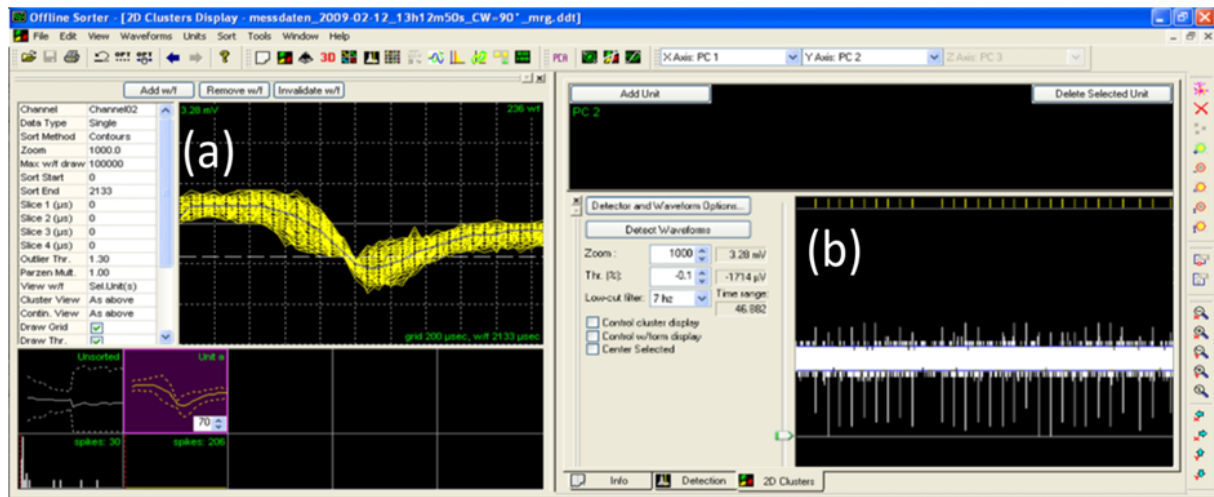


Figure 66: Extracellular signals of PCMs were detected by platinum MNEs. (a) The maximum measured signal amplitude was 3.2 mV_{pp}, AP length was 1-2 ms, high values compared with other measuring systems; (b) signal track of an MNE over time with compressed APs. Yellow: superimposed cardiac APs; recorded with software of Plexon Inc.

3.3.3.7.2 Silver electro-plated solid platinum MNE arrays

APs of PCMs were also recorded with silver electro-plated solid platinum MNEs and solid silver MNEs. Solid platinum MNEs are not hollow. Here, focus is on the first type of MNE.

The APs of eight PCMs are shown in different colors in **Figure 67**. Maximum and minimum voltages were measured at approximately 31 mV and 10 mV, respectively. An AP length of approximately 220 ms was determined. This figure shows that all PCMs start to fire and contract at nearly the same time, showing the characteristic of a functional syncytium. One must keep in mind that the measured MNEs are distributed across an area of 1 mm². Compared with the waveforms detected with hollow platinum MNE, the recorded signals are very different. This fact can be explained by the different electrode material (silver). Silver is less noble than platinum and therefore allows for a faster transportation of the charge carriers across the electrode-medium interface. Comparative observations in the literature show that the recorded signal form is quite similar to the waveform of intracellularly recorded cardiac APs with penetrating metal or glass microelectrodes (Omichi et al., 2000) (compare **Figure 3, p. 7** and **Figure 68 insert**).

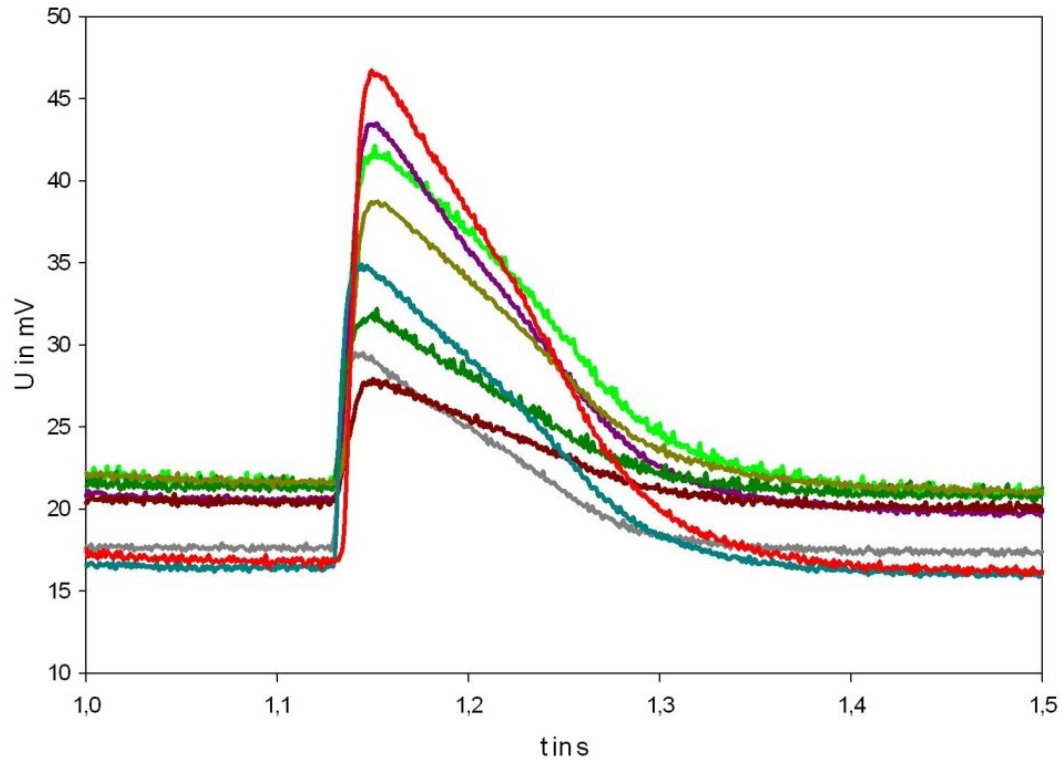


Figure 67: Extracellular recording of cardiac APs of eight PCM of rat embryos detected with eight silver-electroplated solid platinum MNEs. Extracellular AP length and amplitude maximum are approximately 220 ms and 31 mV, respectively. The measured signal as well as the signal form suggest very good electrode properties.

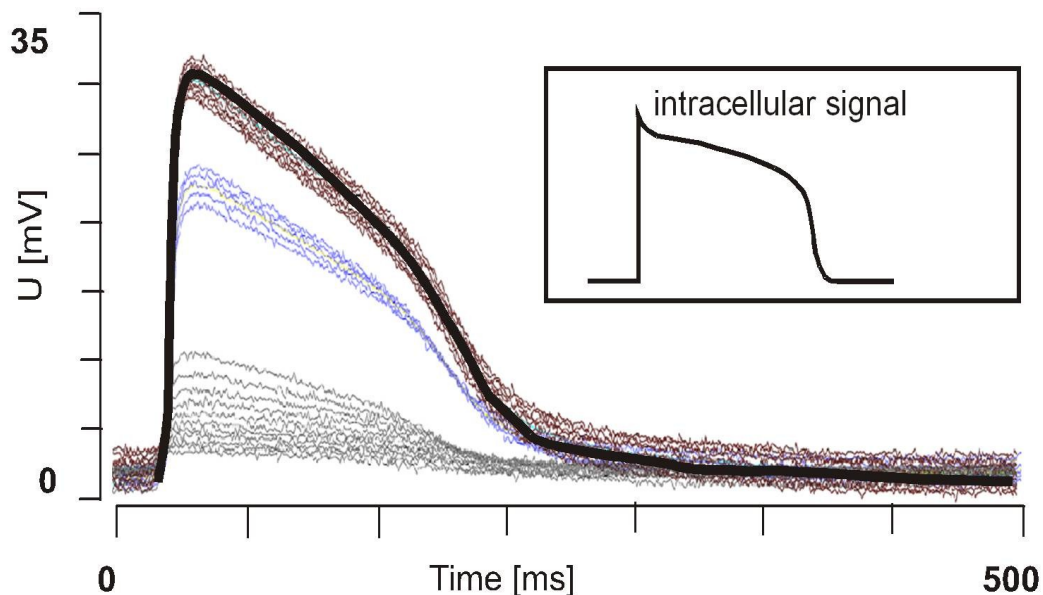


Figure 68: Extracellular recording of cardiac APs of three PCMs of rat embryos detected with three silver electro-plated solid platinum MNEs. AP length and amplitude maximum are approximately 220 ms and 31 mV, respectively. The measured signal as well as the signal form suggest very good electrode properties.

Nevertheless, because the PCMs form a functional syncytium, the author cannot precisely argue that the recorded APs are of single cell origin. The recorded AP trains are represented in **Figure 69** and **Figure 70**. Obviously, a potential drift is underlying the cardiac APs.

Additionally, a decline in the AP amplitudes can be observed in **Figure 68**, which may be explained by a poisoning of the electrodes.

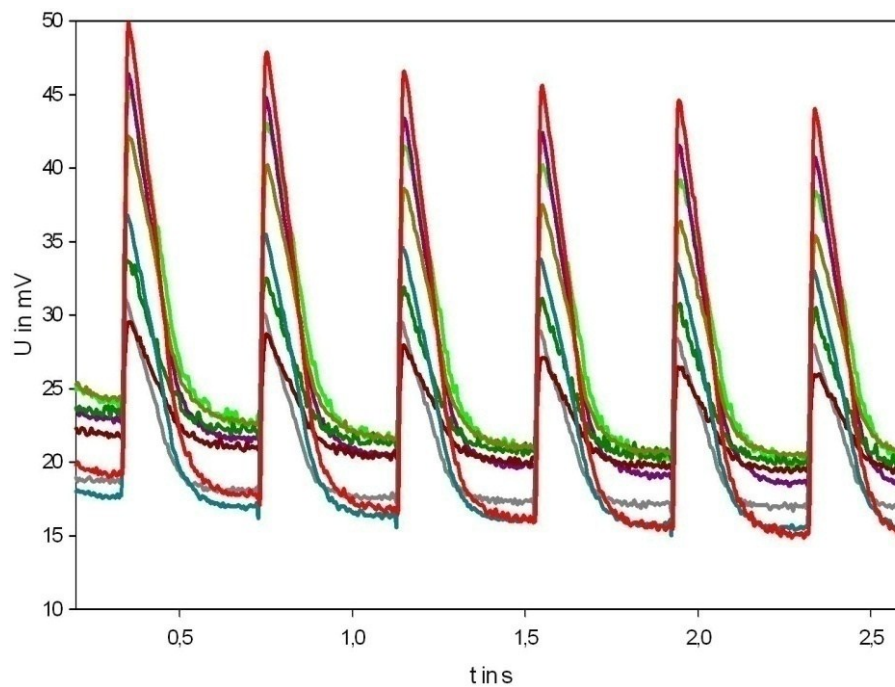


Figure 69: Signal track of eight PCMs over 5 s. A potential drift is clearly visible.

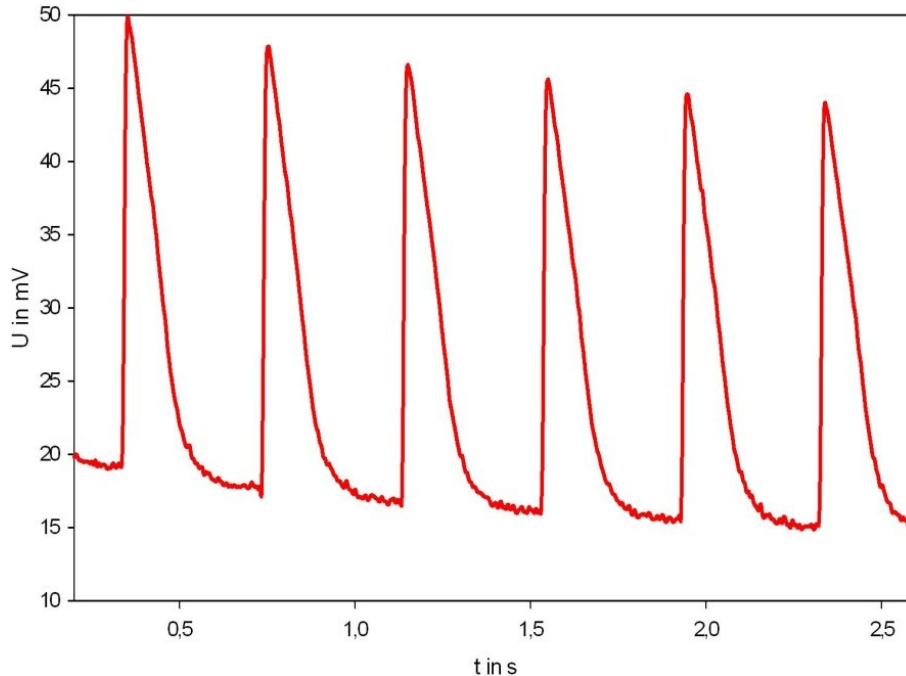


Figure 70: A cardiac AP recorded over 2.5 s.

3.3.3.7.3 MNC data in comparison to other methods

AP amplitudes of up to 3 mV were obtained with hollow platinum MNE. These values are comparable with those of planar GNC electrodes. Compared with our PoreGenic® system, the literature values are low. The potentials were stable throughout the recording time of at

least 2 h (data not shown). As a trade-off for higher amplitudes, the detection of the QT-phase, for example, is not possible (see *Torsade de Pointes*-Arrhythmias, chapter 1.4). A prolongation of the QT-phase (**Figure 71a**) can be caused by biochemically active substances such as TEA (Ochi and Nishiye, 1974). The prolongation is caused by the interaction of TEA with the hERG (Kv11.1 gene) I_{Kr} potassium ion channels.

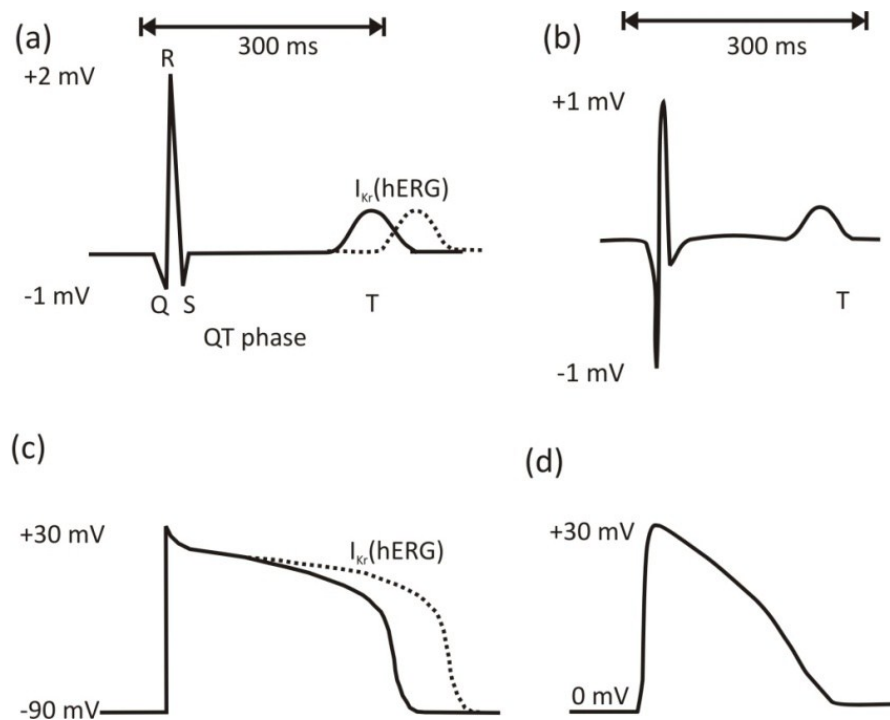


Figure 71: Different detection types of cardiac APs. (a) Extracorporeal electrocardiogram representing the QT-phase and the prolongation of the AP due to altered I_{Kr} (hERG) activity; (b) PCM AP extracellularly recorded with the QT-Screen of the MCS GmbH; (c) intracellularly detected cardiac AP of a PCM and the prolongation of the AP due to altered I_{Kr} (hERG) activity, compare with (a); (d) signal shape extracellularly recorded with the PoreGenic® system. All types except for (d) were redrawn after (Brown, 2004; Meyer et al., 2004b).

These currents can be affected by chemicals due to molecular binding (Fenichel et al., 2004; Sanguinetti and Tristani-Firouzi, 2006). Mandatory drug testing for hERG activity is done with automated systems (Kiss et al., 2003; Brown, 2004; Guthrie et al., 2005; Wible et al., 2005; Farre et al., 2009). Such systems are used in heart disease research (Krinke et al., 2009). Nevertheless, they are not suitable for the HTS needed for drug development (Brown, 2004). The cardiac AP detection displayed by the QT-Screen system (MCS GmbH) is shown in **Figure 71b**. For example, cardiac AP amplitudes of only approximately 1 mV_{pp} are measured with the QT-Screen system. However, this system works with single flat 2D-electrodes in a 96-well plate. **Figure 71b** also resembles the cardiac AP recorded with the hollow platinum MNEs, though the QT-phase could not be detected (compare **Figure 66, p. 76**). The image in

Figure 71c displays the intracellularly recorded wave of the cardiac AP. The prolongation of the QT-wave (**Figure 71a**) can be seen directly from the AP itself in **Figure 71c** (dashed line, please also compare with **Figure 68, p. 77** and **Figure 71d**).

Cardiac APs with amplitudes of up to 31 mV were recorded with the silver-electroplated solid platinum MNEs as well as solid silver MNEs, as demonstrated in **Figure 71d**. The detected shape resembles **Figure 71c**. These amplitude values were much higher than with commercially available systems using golden ring electrodes (Meyer et al., 2004b). A study using comparable dendritic spine-like gold-protrusion 3D-electodes, mentions potentials of *Aplysia* (a genus of sea hares) neurons. However, these gold 3D electrodes showed comparably low amplitudes of 0.165 to 0.770 mV_{pp} after stimulation (Hai et al., 2009).

It is known that channel properties of single PCMs can be examined with patch-on-chip systems (Kutchinsky et al., 2003; Guthrie et al., 2005; Farre et al., 2009). Even complementary metal oxide semiconductor (CMOS) based systems were recently developed for measuring cardiac APs (Pancrazio et al., 1998). With the presented PoreGenic® system, the measurement of the QT-phase might become needless because biochemical effects of substances on membrane channels can possibly be determined with this system. As Brown suggests, biochemical trials should use parameters derived from intracellular measurements.

4. Conclusions and Outlook

4.1 SNC

Three different biochips —SNC, GNC, and MNC— as well as three pre-amplifier systems were developed for the extra- and intracellular detection of cell potentials at the Chair of Biophysics at the University of Rostock, in cooperation with several project partners: Micronas GmbH (SNC), GeSiM mbH (GNC), and IMTEK (MNC). The biological applicability for all three types of biochip was examined by the author. In this thesis and in the attached manuscripts (appendix A), setup description, sterilizing methods, and experiments with the biochips concerning pDEP, SU-8 structures, substance tests, UMTS-exposure as well as transmembrane potentials were demonstrated with fibroblasts and APs of PNCs and PCMs.

The pDEP cell allocation approach showed ambivalent results, since allocated cells tended to migrate away from the pDEP electrodes after several hours. Nevertheless, the complete analysis showed that the average signal yield (54 units, $n = 3$) was better with pDEP compared to control SNCs (39 units, $n = 6$). These promising results allow the author to suggest using supporting photolithographical techniques to deposit cell-adhesive polymers onto the electrodes and to form connective lines between the electrodes to guide the cell growth and even to increase the signal yield. Additionally, cell repellent areas on the surface may avoid the adhesion of cells to undesired sites. A homemade approach (microspotting of electrode) without the use of photolithographical techniques failed for the SNCs. Cell allocation was successful for 1 DIV, however, the author expects that the neurons' electrical yield can be further increased using a combination of pDEP and photolithographical techniques to control subsequent soma migration. An application of cell-adhering polymers on the electrodes might decrease the motility of the cells. Intermediate cell-repellent silicon surfaces could be applied to hinder cell adherence and to increase the number of axons and dendrites above the recording electrodes. The pDEP approaches will be further pursued, focusing on the positioning of axons by pDEP.

A new idea may accelerate the labor-intensive pDEP-approach: a printed circuit board for the cell positioning by pDEP with ten SNCs was designed in cooperation with C. Tautorat (**Figure 72**). The supply of medium is guaranteed by the above-mentioned peristaltic pump. Unfortunately, the applied pDEP field strengths were not equal within the different chips. A redesign correcting this problem is projected.

Surprisingly, the cube-like SU-8 structures, which were supposed to promote orthogonal neuronal networks, actually reduced the network growth. Cells moved to the sidewalls of the SU-8 structures after a few DIV. Neuronal signals could not be detected.

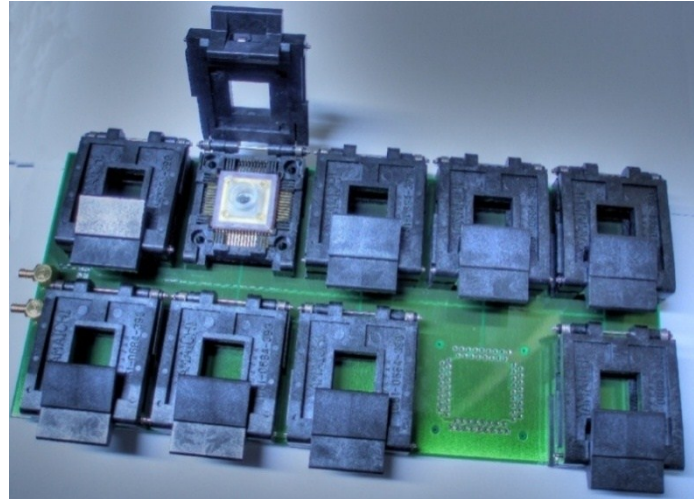


Figure 72: A preliminary printed circuit board for parallel pDEP with ten SNCs.

The control experiments with the SNCs showed their usability compared with other glass MEAs (Gross et al., 1995). Large amounts of chemicals were not necessary demonstrating the economic advantage of the SNC operation method. The embryos (15-20) of one NMRI mouse may provide cells for 80-100 SNCs or 160-200 GNCs. This is quite a lot compared with the customary 10-20 MEA chips (Gross et al., 1977). Though the SNC is technically ready for the electrical detection of neuronal signals, its long-term stability must be significantly improved. In this thesis, the SNC was predominantly used in EMF-exposure with a brass waveguide.

UMTS-exposure experiments were done only with SNCs showing low numbers of neuronal units, because pDEP was very labor-intensive and only three pDEP-SNCs could be successfully examined. Exposure to EMF was always combined with a warming of the cell suspension. This warming was measured, and the neuroelectric activity was registered and analyzed. The PSD showed that the PNCs' neuronal signal pattern reacts to the EMF in some frequency ranges. However, temperature control experiments resulted in the same observation. Due to this fact, the goal of measuring a specific EMF-effect was not accomplished. Unfortunately, the highest number of neuronal units on one single chip was found with the SNC after the UMTS project had ended. Surprisingly, in this case the donor

organism was a rat. Regrettably, nearly all other experiments were done with mice because the authors had relied on the communications of other groups.

4.2 GNC

Since the SNC's stability was unreliable, our group under Prof. Gimsa developed the GNC, which is more robust. The GNC's sensitivity is comparable to that of the SNC. However, in contrast to the SNC, it is autoclavable and reusable many times. The current version of GNC could not be used in UMTS-exposure due to the platinum shielding of the glass trough during the UMTS project. In a new generation of GNCs, the shielding is no longer needed, thanks to large ground electrodes. Based on this, the author suggests that the GNCs be used for future EMF studies.

In the GNC, substance tests were done, for example with VPA. The effects of VPA were described and analyzed. In addition to the MEA, a temperature sensor and an IDES are integrated into the GNC (**Manuscript 2, p. 104ff**).

4.3 MNC

The focus of this thesis was clearly upon the MNC for intracellular signal detection. In the future, this third type of biochip will combine pDEP electrodes, structured photolithographical polymer deposition for cell guiding, and 3D electrodes for the detection of intra- and extracellular cell potentials. For this thesis, a chip combining these structures was not available. Only the individual characteristics could be investigated with chip prototypes.

The author showed preliminary experimental data for intracellular detection with the L929 tumor fibroblast cell line. The electroporation of the cells was investigated with different stains as well as with the FIB method and SEM images. The measured transmembrane potentials V_m are comparable to literature values. However, the potentials decayed after a relatively short time. This may be due to a poisoning of the MNEs' surfaces, or to missing seal-promoting polymers that should have been deposited by one project partner. The photolithographical technique was used with the MNC to improve cell contact with the 3D microneedles. The cells remained at the defined polymer lines during the entire time of culture (30 DIV). These structures could be only preliminarily tested, because only a few MNCs containing these polymers were delivered by an alternative project partner (S. Petersen, University of Darmstadt).

New ideas will be implemented in the future. With new partners, our group plans to improve the MNC by integrating microfluidic channels into the MNEs and the MNC base (**Figure 73**). This new feature will allow us to introduce substances to the cell overgrowing the MNE. Recent discussions with chip manufacturing companies verified that these microfluidic channels with diameters of only 1 μm at the tips of the MNEs are feasible.

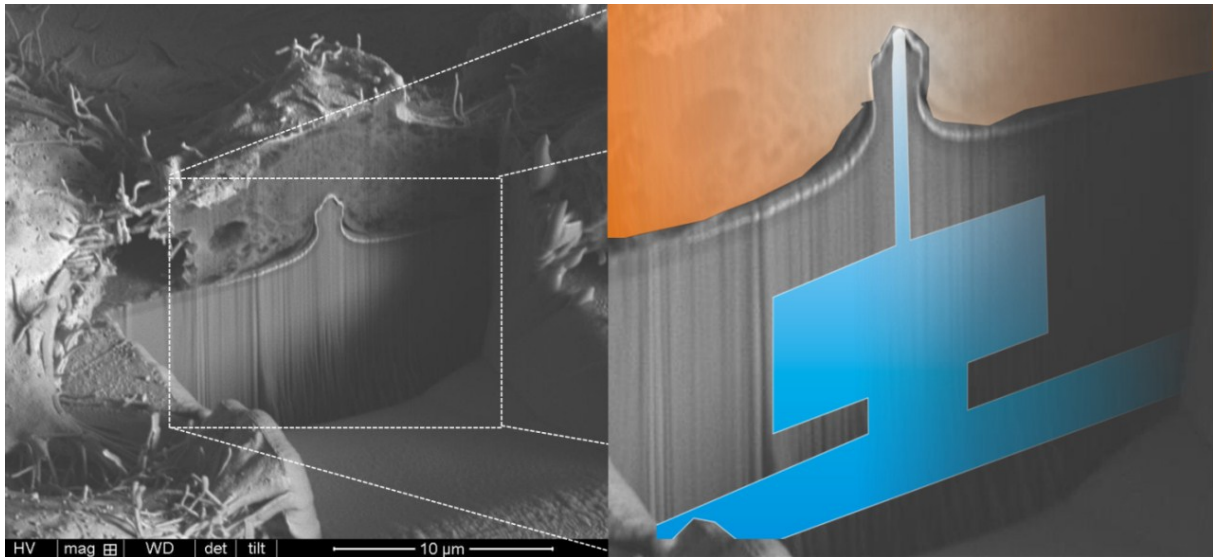


Figure 73: A schematic microfluidic channels is drawn in a FIB-SEM image. The channels will exhibit special dimensions for substance administration.

The long-term goal for the MNC is to measure substance effects on the intracellular potential (whole-cell mode) and on single membrane channels (cell-attached mode). The combined **Figure 74** demonstrates how these measured whole-cell mode signals may look like in future. A substance effect should be detectable when the substance has an impact on the transmembrane potential V_m . In addition, an automatic recognition system for the identification of deviations in potential reaction patterns will likely be implemented.

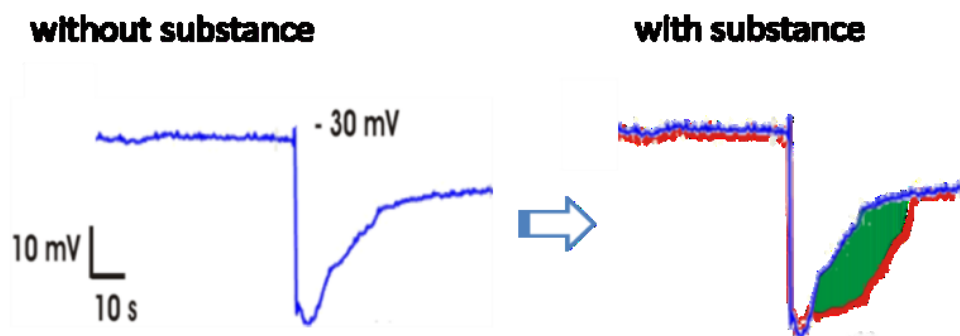


Figure 74: The possible scenario of a whole-cell detection of a substance-effect. Blue: real measured potential; red: possible potential shift due to the substance-effect.

In the future, current-voltage converter channels will be used to test the gigaseal quality. Substances introduced into the membrane can contribute to a reduction of the LEP voltages (Troiano et al., 1999) or facilitate the resealing process (Maskarinec et al., 2005). Multiple short pulses of small amplitude (Rols and Teissié, 1998) will achieve a smooth electroporation of the cells (Tautorat et al., 2008).

The next step will be to integrate cavities into the chip base around the MNEs to improve the sealing of the electroporated cells as described in the patents. The cell itself successfully seals its membrane: the cell grows over the MNE, the membrane spanning the cavities. After LOMINE, a cytoplasmic leak may appear and electrical contact may become short-circuited. With the protruding and recessed structures, small electrically insulated cavities are created. **Figure 75** shows a sketch of the structures, which may reduce the effects of possible cytoplasm leaking.

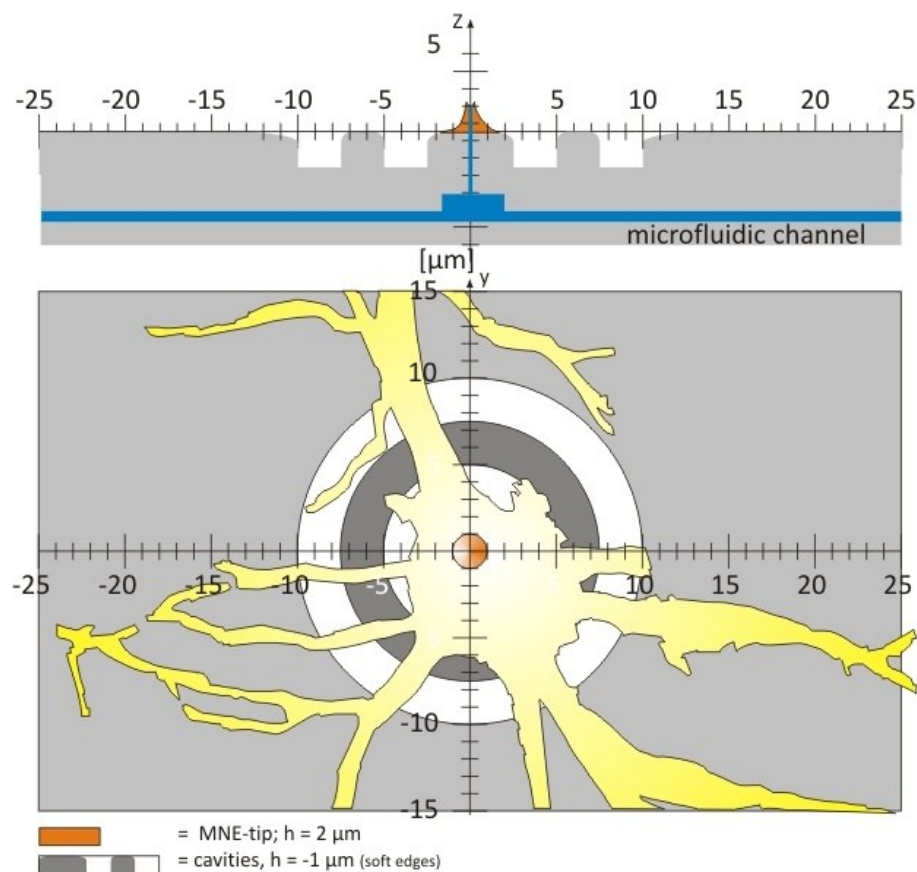


Figure 75: Cavities surrounding the MNEs will be integrated in the MNC base. The displayed neuron (yellow) overspans the cavities and increases the electric insulation properties after LOMINE. In addition, the microfluidic channels is shown (blue).

The author believes that the cavities will improve the sealing properties during LOMINE, resulting in improved potential measurements (**Figure 76**). In addition, cell-guiding

compounds can be deposited. Therefore, the cell-repellent properties of oligo(ethylene glycol)-terminated self-assembled monolayers (SAMs) can be reversed to cell-adhesive behaviors by the application of Br_2 , which is locally produced by an ultramicroelectrode of a scanning electrochemical microscope (SECM). After Br_2 -treatment, the SAMs show increased permeability and terminal hydrophobicity (Zhao et al., 2006; Zhao et al., 2008). In the future, this method could play a major role in improving the guidance of cells on the MNC. Additional procedures could be used to deposit gigaseal-promoting compounds at the MNEs. A future goal will be to optimize the stability of the electrode potentials and to compensate for the influence of electrode effects on the signals measured. This will make sure that intracellular potentials are reliably measured.

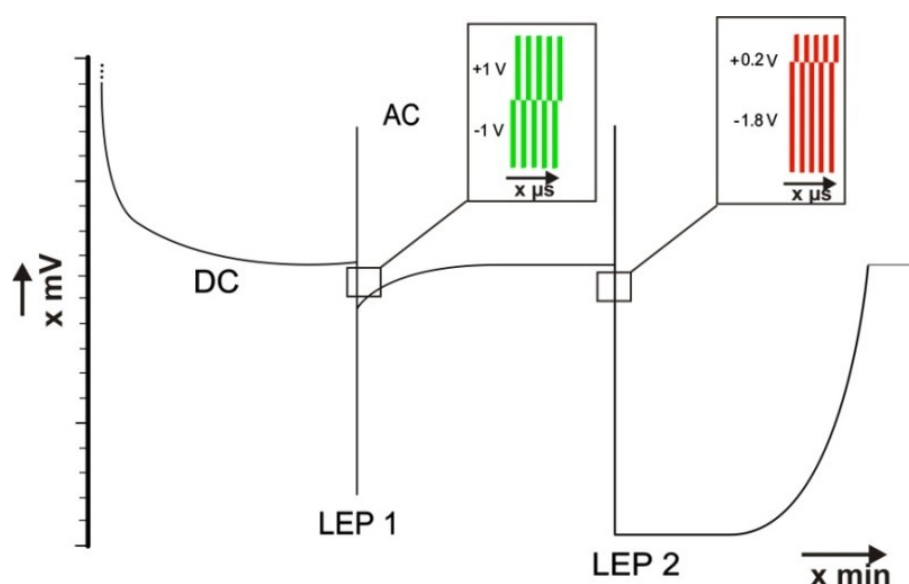


Figure 76: The possible scenario of a future whole-cell detection. After the optimized LEP 2 and using MNC-integrated cavities, a longer detection of V_m should be possible. In contrast to LEP 1, the optimized LEP 2 leads to an opening of the cell membrane and a stable transmembrane potential measurement.

In future, the PoreGenic® system might allow for the examination of gap junction-associated diseases such as neuropathies that destroy the myelin sheath, genetically-conditioned deafness, cataract formation (eye lens clouding), desmosome-associated diseases, for example the chronic skin blistering disease *Pemphigus vulgaris*, and the autoimmune blistering disease of the skin and mucous membranes (*Pemphigus foliaceus*) (**Figure 77**). These rarely appearing diseases (orphan diseases) could be examined with the PoreGenic® system. In these investigations, gap junction or desmosome-affecting drugs may be applied and the effects compared with other cells that are not administered these drugs. Due to the

structure of the MNE arrays, the cell-cell-communication between sick and healthy cells may be evaluated. Such organ-level diseases fall into the realm of pharmaceutical producers.

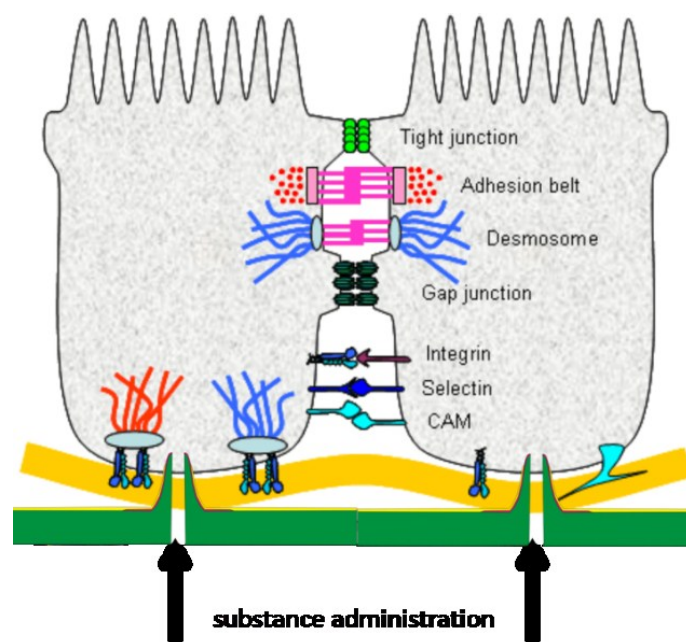


Figure 77: Model cells growing over two MNEs. The cells are connecting by tight junctions, adhesion belt, desmosomes and gap junctions responsible for different diseases.

As an example for future pharmaceutical studies, modern therapeutic antibodies that treat cancer cells can be named, e.g. Bevacizumab (trade name *Avastin*[®]; F. Hoffmann-La Roche AG). This humanized monoclonal antibody works in combination with 5-Fluorouracil/Folin acid and Irinotecan (*Camptosar*[®], Pfizer Inc.). 5-Fluorouracil is built into the DNA of the specific cell and blocks the functionality of the DNA. Irinotecan is able to induce apoptosis. This substance combination blocks VEGF of endothelial cells. Adherent endothelial cells of the bloodstream, for example those that connect malignant tumors with the blood vessels, die, therefore killing the tumor by depriving it of its blood supply. The endothelial cells should therefore be examined in an adherent state to study their natural characteristics. These observations can be done electrophysiologically, to clarify whether the endothelial cells can be locally killed. The future challenge will be to administer substances through microfluidic channels into single cells.

Furthermore, it is interesting to know whether certain tumor cells can be electroporated to encourage uptake of DNA/RNA. Certain gene sequences (e.g. for new channel proteins) would be introduced into the electroporated cell, perhaps prompting them to develop new well-defined characteristics. In the future state, channels can be investigated and genetically manipulated cells systematically examined for successful genetic transfer. The non-

electroporated cells, which overgrow the remaining MNEs can be examined as controls. One can investigate whether the manipulated cells have an effect on the non-manipulated cells.

Does the target cell influence the cell-partners by means of cell-cell communication?

Cells can grow in the MNCs over any time interval, exhibiting their natural physiological and morphological characteristics. Additionally, the scientist can examine the intercellular information exchanges across gap junctions of interlaced cells. This condition represents a substantial competitive advantage for the future success of the PoreGenic® system in comparison to commercial systems, e.g. the *IonWorks Quattro* patch clamp station (MDS Analytical Technologies, Sunnyvale, USA) for cells in suspensions. In the future, the PoreGenic® system will provide a new intracellular measuring technique for the analysis of drugs and other chemicals in different adherent cell types.

One can imagine that with pDEP, clustered PCM networks can be produced on the MNC. The clusters could be examined spatially, separated from one another. According to the author's observations, each of them may show its own beating frequency, e.g. 0.05- 4 Hz, since they are interlaced only by gap junctions forming a functional syncytium. The PCM clusters themselves are autarchic, and show no cellular connections to the other clusters. The author assumes that the analysis of these 64 individual PCM clusters on an array surface of 1 mm² is a unique approach. **Figure 78** shows, for example, the allocation of four PCM-clusters on the MNE array model and future polymer coatings for cell growth control. Using the stimulation function (data not shown) of the PoreGenic® system, each individual cluster can be stimulated by different pulses. Here, interesting studies, for example on defibrillation (electrical stimulation of the heart muscle) could be carried out with PCM clusters. Because of the widespread use of public access defibrillators (PADs), further studies would be necessary. Worldwide, thousands of emergency patients die due to improper defibrillation, in which the membranes of the heart muscle cells are temporarily or permanently opened so that interstitial liquid penetrates the cells. Defibrillation severely disturbs the ion distribution of the heart muscle cells, or even kills the cells, which may lead to chronic and even deadly arrhythmias. In Germany, PADs are set up in public spaces such as airports, subway and rail stations (Munich) and public offices. Additionally, a variety of skeletal muscle cells could be cultivated on the MNC. In these cases, it would be conceivable to combine intracellular investigations with stimulation experiments. Naturally, it will be possible to study the effect of gap junction-blockers on PCMs, such as 16-doxyl-stearic acid or heptanol (Qi et al., 2001).

These substance effects could be examined with adherent functional cell syncytia, e.g. cardiomyocytes. In these scenarios, the spreading of the drug through the gap junctions could be examined, which would become important for pharmaceutical studies about drug candidates spreading within the human body. Finally, fluorescence images are feasible during measurements with the PoreGenic® system.

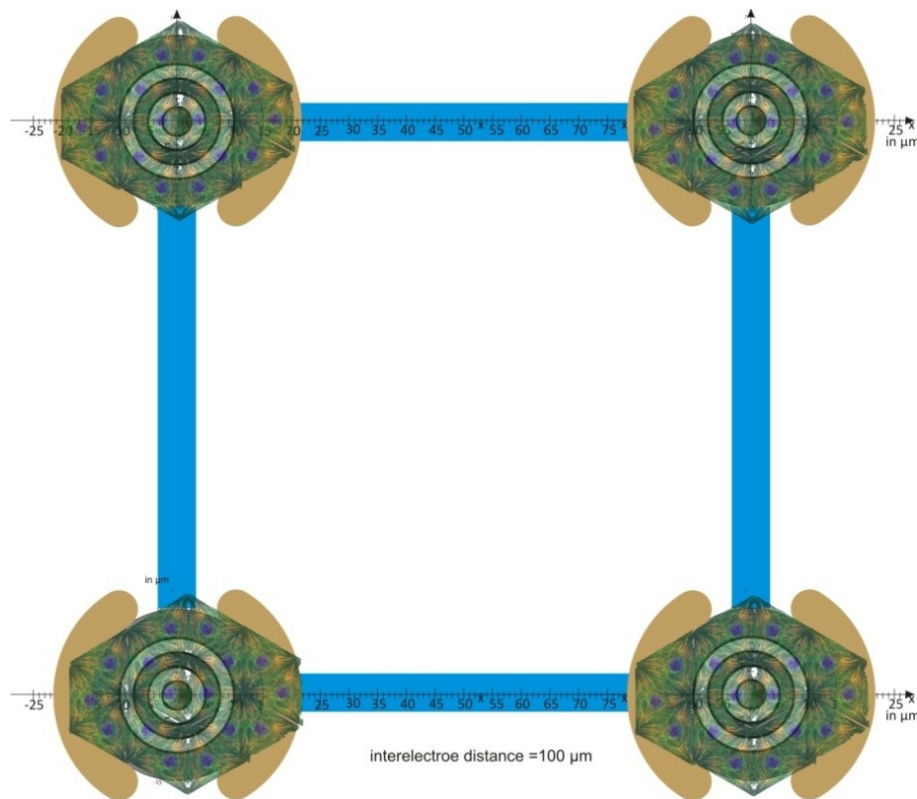


Figure 78: Model PCM growing over four MNEs. Four cell clusters may be obtained after pDEP. Blue: polymer lines are integrated for studies of e.g. neuronal communication analysis that require defined networks, white: cell repellent areas.

4.4 Recommendations for the application of biochips

In the conclusion, the three types of biochip presented can be applied very differently. The author suggests using the GNC in future extracellular work for the detection of neuronal signals. Additionally, frequency studies on PCM APs can be done with the GNC. The glass chips clearly show many advantages over the SNC: they are very rugged, autoclavable, acid sterilizable, and include IDEs and temperature sensors. The sensors of the SNC are very sensitive to oxidative processes, for example those that occur during sterilization. In summary, the GNC can be seen as an excellent successor to the SNC.

For extracellular recordings from PCMs, the author suggests using the MNCs due to the high amplitudes and the high-fidelity signal shapes, which reflect the transmembrane

waveforms. However, the significantly decreasing amplitudes likely due to electrode poisoning must be eliminated the future uses of MNCs. In addition, the MNC is the only type of chips introduced here suitable for future studies on cell membrane channels.

The author hopes and believes that the biochip systems presented are another step towards abolishing dubious animal experiments and helping to fulfill the 3Rs. In addition, the biochip systems depicted here could become valuable tools for pharmaceutical and chemical producers affected by the REACH guideline.

5. References

1. Acharya, S. 2005. The productivity tiger - time and cost benefits of clinical drug development in India. http://pharmalicensing.com/public/articles/view/1153412098_44bfac02291f1.
2. Adair, E. R. and Adams, B. W. 1980. Microwaves modify thermoregulatory behavior in squirrel monkey. *Bioelectromagnetics*, 1: 1-20.
3. Ahmed, G. U., Dong, P. H., Song, G., Ball, N. A., Xu, Y., Walsh, R. A., and Chiamvimonvat, N. 2000. Changes in Ca²⁺ Cycling Proteins Underlie Cardiac Action Potential Prolongation in a Pressure-Overloaded Guinea Pig Model With Cardiac Hypertrophy and Failure. *Circulation Research*, 86: 558-570.
4. Arun, T. J. K., Pushpendra, S., and Nadine, A. 2004. Dielectrophoresis of nanoparticles. *ELECTROPHORESIS*, 25: 3625-3632.
5. Baaken, G., Sondermann, M., Prucker, O., Behrend, J. C., and R  he, J. 2007. Planares Patch-Clamping f  r Hochdurchsatz-Untersuchungen an biologischen Membrankan  len. *Proceedings MikroSystemTechnik Kongress 2007*, 441-445.
6. Baum, A., Mevissen, M., Kamino, K., Mohr, U., and L  scher, W. 1995. A histopathological study on alterations in DMBA-induced mammary carcinogenesis in rat with 50 Hz, 100 μ T magnetic field exposure. *Carcinogenesis*, 16: 125-
7. Baumann, W., Ehret, R., Lehmann, M., Igel, G., Gahle, H.-J., Wolf, B., Sieben, U., Freund, I., and Brischwein, M. 1998a. DE 19827957A1. Verfahren und Vorrichtung zur Messung eines Zellpotentials. Patent.
8. Baumann, W., Ehret, R., Lehmann, M., Igel, G., Gahle, H.-J., Wolf, B., Sieben, U., Freund, I., and Brischwein, M. 1998b. DE 19841337C1. Verfahren und Vorrichtung zur intrazellul  ren Manipulation einer biologischen Zelle. Patent.
9. Baumann, W., Schreiber, E., Krause, G., Podssun, A., Homma, S., Schrott, R., Beikirch, H., Ehret, R., Keuer, A., Freund, I., and Lehmann, M. 2005. Zell Monitoring System mit multiparametrischen CMOS Biosensorchips. *Proceedings 7. Dresdner Sensor-Symposium - Neue Herausforderungen und Anwendungen in der Sensortechnik*, 95-98.
10. Baumann, W., Schreiber, E., Krause, G., Podssun, A., Homma, S., Schrott, R., Ehret, R., Freund, I., and Lehmann, M. 2004. Cell monitoring system with multiparametric CMOS micro-sensor chips. *Proceedings μ -TAS*, 2: 554-556.
11. Baumann, W., Schreiber, E., Krause, G., St  we, S., Podssun, A., Homma, S., Anlauf, H., Rosner, R., Freund, I., and Lehmann, M. 2002. Multiparametric neurosensor microchip. *Euroensors XVI.*, 1169-1172.
12. Baumann, W., Tautorat, C., Koester, P., Gimsa, J., Ehret, R., Freund, I., and Lehmann, M. 2008. Cell Monitoring Systems with CMOS Micro-Sensor-Chips. *NATO ADVANCED RESEARCH WORKSHOP, "Commercial and Pre-commercial Cell Detection Technologies for Defence against Bioterror - Technology, Market and Society"*, 77-79.

13. Bawin, S. M., Kaczmarek, L. K., and Adey, W. R. 1975. Effects of modulated VHF fields on the central nervous system. *Annals of the New York Academy of Sciences*, 274: 81-
14. Beall, C., Delzell, E., Cole, P., and Brill, I. 1996. Brain tumors among electronics industry workers. *Epidemiology*, 7: 130-
15. Bier, M. 2002. Resealing dynamics of a cell membrane after electroporation. *Physical Review*, E66: ID 062905.
16. Birch, S. 2002. Pharmaceutical R&D Outsourcing Strategies: An analysis of market drivers and resistors to 2010. *ISBN*, 1-84296-212-4.
17. Braeken, D., Jans, D., Rand, D., Huys, R., van Meerbergen, B., Loo, J., Borghs, G., Callewaert, G., and Bartic, C. 2008. Local electrical stimulation of cultured embryonic cardiomyocytes with sub-micrometer nail structures. *Conference Proceedings IEEE Eng Med Biol Soc.*, 4816-4819.
18. Brown, A. M. 2004. Drugs, hERG and sudden death. *Cell Calcium*, 35: 543-547.
19. Buehler, S. M., Koester, P. J., Tautorat, C., Altrichter, H., Baumann, W., and Gimsa, J. 2007. Bio-analytic silicon chips for the detection of developmental-neurotoxic effects of chemicals and drugs in the context of the European REACH program. *ALTEX - Alternatives to Animal Experimentation*, 24: 190-190.
20. Cole, K. S. and Curtis, H. J. 1939. Electric impedance of the squid giant axon during activity. *The Journal of General Physiology*, 22: 649-670.
21. Egert, U. and Haemmerle, H. 2002. Application of the microelectrode-array (MEA) technology in pharmaceutical drug research. *Sensoren im Fokus neuer Anwendungen*, w.e.b. Universitätsverlag: 51-54.
22. European Parliament and Council. 2006. Regulation (EC) No 1907/2006 of the European Parliament and of the Council of 18 December 2006 concerning the Registration, Evaluation, Authorisation and Restriction of Chemicals (REACH), establishing a European Chemicals Agency. *Official Journal of the European Union*, L396: 1-849.
23. Farre, C., Haythornthwaite, A., Stoelzle, S., Kreir, M., George, M., Brueggemann, A., and Fertig, N. 2009. Port-a-patch and patchliner: high fidelity electrophysiology for secondary screening and safety pharmacology. *Combinatorial Chemistry & High Throughput Screening*, 12: 24-37.
24. Fenichel, R. R., Malik, M., Antzelevich, C., Sanguinetti, M., Roden, D. M., Priori, S. G., Ruskin, J. N., Lipicky, R. J., and Cantilena, L. R. 2004. Drug-Induced Torsades de Pointes and Implications for Drug Development. *Journal of Cardiovascular Electrophysiology*, 15: 475-495.
25. Food and Drug Administration. 2005. FDA Guidance for Industry S7B Nonclinical Evaluation of the Potential for Delayed Ventricular Repolarization (QT Interval Prolongation) by Human Pharmaceuticals.

26. Fromherz, P., Offenhäuser, A., Vetter, T., and Weis, J. 1991. A neuron-silicon junction: a Retzius cell of the leech on an insulated-gate field-effect transistor. *Science*, 252: 1290-1293.
27. Fromherz, P. and Stett, A. 1995. Silicon-neuron junction: capacitive stimulation of an individual neuron on a silicon chip. *Physical Review Letters*, 75: 1670-1673.
28. Gale, K. and Iadarola, M. J. 1980. Seizure protection and increased nerve-terminal GABA: delayed effects of GABA transaminase inhibition. *Science*, 208: 288-291.
29. Garrido, R., Mattson, M. P., Hennig, B., and Toborek, M. 2001. Nicotine protects against arachidonic-acid-induced caspase activation, cytochrome c release and apoptosis of cultured spinal cord neurons. *Journal of Neurochemistry*, 76: 1395-1403.
30. Ghai, R. S., Bikson, M., and Durand, D. M. 2000. Effects of applied electric fields on low-calcium epileptiform activity in the CA1 region of rat hippocampal slices. *Journal of Neurophysiology*, 84: 274-280.
31. Gimsa, J. 1991. Dielectrophoresis and electrorotation of neurospora slime and murine myeloma cells. *Biophysical Journal*, 60: 749-760.
32. Gimsa, J. 2001. Characterization of particles and biological cells by AC-electrokinetics. 369-400.
33. Gimsa, J., Müller, T., Schnelle, T., and Fuhr, G. 1996. Dielectric Spectroscopy of Single Human Erythrocytes at Physiological Ionic Strength: Dispersion of the Cytoplasm. *Biophysical Journal*, 71: 495-506.
34. Gimsa, U., Iglic, A., Fiedler, A., Zwanzig, M., Kralj-Iglic, V., Jonas, L., and Gimsa, J. 2007. Actin is not required for nanotubular protrusions of primary astrocytes grown on metal nano-lawn. *Molecular Membrane Biology*, 24: 243-255.
35. Gintant, G. A., Limberis, J. T., McDermott, J. S., Wegner, C., and Cox, B. F. 2001. The canine Purkinje fiber: An in vitro model system for acquired long QT syndrome and drug-induced arrhythmogenesis. *Journal of Cardiovascular Pharmacology*, 37: 607-618.
36. Gluckman, B. J., Neel, E. J., Netoff, T. I., Ditto, W. L., Spano, M. L., and Schiff, S. J. 1996. Electric field suppression of epileptiform activity in hippocampal slices. *Journal of Neurophysiology*, 76: 4202-4205.
37. Goldman, D. E. 1943. Potential, impedance, and rectification in membranes. *Journal of General Physiology*, 27: 37-60.
38. Graham, C., Cook, M. R., Cohen, H. D., and Gerkovich, M. M. 1994. Dose response study of human exposure to 60 Hz electric and magnetic fields. *Bioelectromagnetics*, 15: 447-463.
39. Gramowski, A., Jügelt, K., Weiss, D., and Gross, G. W. 2004. Substance identification by quantitative characterisation of oscillatory activity in murine spinal cord networks on microelectrode arrays. *European Journal of Neuroscience*, 19: 2815-2825.

40. Gramowski, A., Konstantin, J., Simone, S., Roland, S., Gerard P., M., Andrea, W.-D., Jan, L., Olaf, S., and Dieter G., W. 2006. Functional screening of traditional antidepressants with primary cortical neuronal networks grown on multielectrode neurochips. *European Journal of Neuroscience*, 24: 455-465.
41. Gross, G. W. 1979. Simultaneous single unit recording in vitro with a photoetched laser deinsulated gold multimicroelectrode surface. *IEEE Transactions on Biomedical Engineering*, 26: 273-279.
42. Gross, G. W., Rhoades, B. K., Azzazy, H. M., and Wu, M. C. 1995. The use of neuronal networks on multielectrode arrays as biosensors. *Biosensors and Bioelectronics*, 10: 553-567.
43. Gross, G. W., Rieske, E., Kreutzberg, G. W., and Mayer, A. 1977. A new fixed-array multielectrode system designed for long-term monitoring of extracellular single unit neuronal activity in vitro. *Neuroscience Letters*, 6: 101-105.
44. Gross, G. W., Williams, A. N., and Lucas, J. H. 1982. Recording of spontaneous activity with photoetched microelectrode surfaces from mouse spinal neurons in culture. *Journal of Neuroscience Methods*, 5: 13-22.
45. Guthrie, H., Livingston, F. S., Gubler, U., and Garippa, R. 2005. A place for high-throughput electrophysiology in cardiac safety: screening hERG cell lines and novel compounds with the ion works HTTM system. *Journal of Biomolecular Screening*, 10: 832-840.
46. Gutierrez, R. C., Hung, J., Zhang, Y., Kertesz, A. C., Espina, F. J., and Colicos, M. A. 2009. Altered synchrony and connectivity in neuronal networks expressing an autism-related mutation of neuroligin 3. *Neuroscience*, 162: 208-221.
47. Hai, A., Dormann, A., Shappir, J., Yitzchaik, S., Bartic, C., Borghs, G., Langedijk, J. P. M., and Spira, M. E. 2009. Spine-shaped gold protrusions improve the adherence and electrical coupling of neurons with the surface of micro-electronic devices. *Journal of the Royal Society Interface*, 52: 533-539.
48. Halbach, M. D., Egert, U., Hescheler, J., and Banach, K. 2003. Estimation of Action Potential Changes from Field Potential Recordings in Multicellular Mouse Cardiac Myocyte Cultures. *Cellular Physiology and Biochemistry*, 13: 271-284.
49. Hamill, O. P., Marty, A., Neher, E., Sakmann, B., and Sigworth, F. J. 1981. Improved patch-clamp techniques for high-resolution current recording from cells and cellfree membrane patches. *Pfluegers Archiv*, 391: 85-100.
50. Hansen, V. and Streckert, J. 1998. Feldtheoretische Simulation der Hohlleitungs-Experimente zum Einfluß hochfrequenter elektromagnetischer Felder auf humane periphere Lymphozyten. *Forschungs-Gemeinschaft Funk Edition Wissenschaft*, 14: 14-23.

51. Heida, T., Rutten, W. L. C., and Marani, E. 2001. Dielectrophoretic Trapping of Dissociated Fetal Cortical Rat Neurons. *IEEE Transactions on Biomedical Engineering*, 48: 921-930.
52. Heilmann, A., Altmann, F., Cismak, A., Baumann, W., and Lehmann, M. 2007. Investigation of Cell-Sensor Hybrid Structures by Focused Ion Beam (FIB) Technology. *mrs proceedings, ID 0983-LL03-03*,
53. Held, J., Gaspar, P., Ruther, P., Cismak, A., Heilmann, A., and Paul, O. 2007. Systematic Characterization of DRIE-Based Fabrication Process of Silicon Microneedles. *MRS Fall 2007 Meeting, Boston, Nov. , 2007, 1052-DD07-07*,
54. Held, J. 2009. Microneedle Electrode Arrays for Cellular Recording Applications. *PhD thesis*, Albert-Ludwigs-University Freiburg-
55. Held, J., Gaspar, J., Koester, P. J., Tautorat, C., Cismak, A., Baumann, W., Trautmann, A., Ruther, P., and Paul, O. 2008a. Microneedle Arrays for Intracellular Recording Applications. *Dig. Tech. Papers IEEE MEMS Conference, Tucson, USA, 2008, 268-271*.
56. Held, J., Gaspar, J., Koester, P. J., Tautorat, C., Hagner, M., Cismak, A., Heilmann, A., Baumann, W., Ruther, P., and Paul, O. 2009. Hollow Microneedle Electrode Arrays for Intracellular Recording Applications. *Dig. Tech. Papers IEEE MEMS Conference, Sorrento, Italy, 2009, 220-223*.
57. Held, J., Gaspar, J., Ruther, P., and Paul, O. 2008b. Microneedle Arrays Electrode With Dielectrophoretic Electrodes For Intracellular Recording Applications. *Conference Proceedings of the 6th International Meeting on Substrate-Integrated Micro Electrode Arrays*, 295-296.
58. Hodgkin, A. L. and Huxley, A. F. 1936. Action Potentials Recorded from Inside a Nerve Fibre. *Nature*, 144: 710-711.
59. Hodgkin, A. L. and Katz, B. 1949. The effect of sodium ions on the electrical activity of the giant axon of the squid. *Journal of Physiology*, 108: 37-77.
60. Huys, R., Braeken, D., Van Meerbergen, B., Winters, K., Eberle, W., Loo, J., Tsvetanova, D., Chen, C., Severi, S., Yitzchaik, S., Spira, M., Shappir, J., Callewaert, G., Borghs, G., and Bartic, C. 2008. Novel concepts for improved communication between nerve cells and silicon electronic devices. *Solid-State Electronics*, 52: 533-539.
61. Ilchmann, F., Ressler, J., Meyer, J., Grothe, H., and Wolf, B. 2006. Recording chamber for glass sensor chips with MEA and integrated oxygen-, pH- and temperature sensors. *International MEA Meeting NMI Reutlingen*, 222-223.
62. Jones, T. B. 1995. Electromechanics of Particles. *Cambridge University Press*, Cambridge, New York, Melbourne, ISBN 978-0521431965.
63. Jongsam, H. J. and Schoonlingen, C. C. 1970. Electronic spread of current in monolayers of cultured heart cells. *Pfluegers Archiv*, 314: 144-145.

64. Kinosita, K. Jr. and Tsong, T. Y. 1977. Voltage-induced pore formation and hemolysis of human erythrocytes. *Biochimica et Biophysica Acta*, 471: 227-242.
65. Kiss, L., Bennett, P. B., Uebele, V. N., Koblan, K. S., Kane, S. A., and Neagle, B. S. K. 2003. High throughput ion-channel pharmacology: planar-array-based voltage clamp. *Assay and Drug Development Technologies*, 1: 127-135.
66. Koester, P. J., Buehler, S. M., Reimer, T., Stubbe, M., Tautorat, C., Baumann, W., and Gimsa, J. 2009a. Modular glass chip system measuring the electric activity and adhesion of neuronal cells – application and drug testing with sodium valproic acid. *Lab-on-a-chip*, in preparation-
67. Koester, P. J., Buehler, S. M., Sakowski, J., Tautorat, C., Altrichter, H., Baumann, W., and Gimsa, J. 2007a. Modular glass chip system for the acquisition of the electric activity and physiological parameters of differentiated stem cells. *ALTEX - Alternatives to Animal Experimentation*, 24: 208-209.
68. Koester, P. J., Sakowski, J., Baumann, W., Glock, H.-W., and Gimsa, J. 2007b. A new exposure system for the in vitro detection of GHz field effects on neuronal networks. *Bioelectrochemistry*, 70: 104-114.
69. Koester, P. J., Tautorat, C., Held, J., Ruther, P., Paul, O., Beikirch, H., Gimsa, J., and Baumann, W. 2009b. Towards automated patch clamp of adherent cells: cardiomyocyte action potentials recorded with 3D microelectrode array chips. *Biosensors and Bioelectronics*, submitted.
70. Koester, P. J., Tautorat, C., Podssun, A., Gimsa, J., Jonas, L., and Baumann, W. 2008a. A new Principle for intracellular Potential Measurements of adherently growing Cells. *Conference Proceedings of the 6th International Meeting on Substrate-Integrated Micro Electrode Arrays*, 271-274.
71. Koester, P. J., Tautorat, C., Podssun, A., Gimsa, J., Jonas, L., and Baumann, W. 2008b. Dielectrophoretic positioning of cells for the measurement of intracellular potentials using kidney-shaped electrodes. *Conference Proceedings of the 6th International Meeting on Substrate-Integrated Microelectrode Arrays, Reutlingen, 2008*, 322-323.
72. Koester, P. J., Tautorat, C., Sakowski, J., Baumann, W., and Gimsa, J. 2008c. Dielectrophoretic Neuron Positioning on MEAs in Semiconductor Chips for the Extracellular Detection of the Neuronal Network Activity. *Conference Proceedings of the 6th International Meeting on Substrate-Integrated Micro Electrode Arrays*, 319-320.
73. Kolozsi, E., Mackenzie, R. N., Rouillet, F. I., Decatanzaro, D., and Foster, J. A. 2009. Prenatal exposure to valproic acid leads to reduced expression of synaptic adhesion molecule neuroligin 3 in mice. *Neuroscience*, 163: 1201-1210.
74. Krause, G., Lehmann, S., Lehmann, M., Freund, I., Schreiber, E., and Baumann, W. 2006. Measurement of electrical activity of long-term mammalian neuronal networks on semiconductor neurosensor chips and comparison with conventional microelectrode arrays. *Biosensors and Bioelectronics*, 21: 1272-1282.

75. Krinke, D., Jahnke, H. G. P. O., and Robitzki, A. A. 2009. A microelectrode-based sensor for label-free in vitro detection of ischemic effects on cardiomyocytes. *Biosensors and Bioelectronics*, 24: 2798-2803.
76. Krnjevic, K. and Schwartz, S. 1967. The action of gamma-Aminobutyric acid on cortical neurones. *Experimental Brain Research*, 3: 320-336.
77. Kutchinsky, J., Friis, S., Asmild, M., Taborski, R., Pedersen, S., Vestergaard, R. K., Jacobson, R. B., Krzywkowski, K., Schröder, R. L., Ljungstrøm, T., Hélix, N., Sørensen, C. B., Bech, M., and Willumsen, N. J. 2003. Characterization of potassium channel modulators with QPatch automated patch-clamp technology: system characteristics and performance. *Assay and Drug Development Technologies*, 1: 685-693.
78. Lehmann, M., Baumann, W., Brischwein, M., Gahle, H.-J., Freund, I., Ehret, R., Drechsler, S., Palzer, H., Kleintges, M., Sieben, U., and Wolf, B. 2001. Simultaneous measurement of cellular respiration and acidification with a single CMOS ISFET. *Biosensors and Bioelectronics*, 16: 195-203.
79. Löscher, W. 1981. Effect of Inhibitors of GABA Aminotransferase on the Metabolism of GABA in Brain Tissue and Synaptosomal Fractions. *Journal Of Neurochemistry*, 36: 1521-1527.
80. Löscher, W., Rohlf, A., and Rundfeldt, C. 1995. Reduction in firing rate of substantia nigra pars reticulata neurons by valproate: influence of different types of anesthesia in rats. *Brain Research*, 702: 133-144.
81. Maskarinec, S. A., Wu, G., and Lee, K. Y. C. 2005. Membrane Sealing by Polymers. *Annals of the New York Academy of Sciences*, 1066: 310-320.
82. Maswiwat, K. 2008. Electromanipulation of Ellipsoidal Cells in Fluidic Micro-Electrode Systems. *PhD thesis*, University of Rostock.
83. Mehnert, L. 2005. Charakterisierung der neuroaktiven Wirkungen GABAA-Rezeptor-aktiver Substanzen mittels neuronaler Netzwerke auf Mikroelektroden-Arrays.
84. Meyer, T., Boven, K. H., Gunther, E., and Fejtl, M. 2004a. Micro-electrode arrays in cardiac safety pharmacology: a novel tool to study QT interval prolongation. *Drug Safety*, 27: 763-772.
85. Meyer, T., Leisgen, C., Gonser, B., and Gunther, E. 2004b. QT-screen: high-throughput cardiac safety pharmacology by extracellular electrophysiology on primary cardiac myocytes. *Assay Drug Development Technology*, 2: 507-514.
86. Ndoumbé Mbonjo Mbonjo, H., Streckert, J., Bitz, A., Hansen, V., Glasmachers, A., Gencol, S., and Rozic, D. 2004. Generic UMTS test signal for RF bioelectromagnetic studies. *Bioelectromagnetics*, 25: 415-425.
87. Neher, E. and Sakmann, B. 1992. Die Erforschung von Zellsignalen mit der Patch-Clamp-Technik. *Spektrum der Wissenschaft*, May: 48-55.

88. Neher, E. and Sakmann, B. 1976. Single-channel currents recorded from membrane of denervated frog muscle fibers. *Nature*, 260: 799-802.
89. Netzer, R., Ebner, A., Bischoff, U., and Pongs, O. 2001. Screening lead compounds for QT interval prolongation. *Drug Discovery Today*, 6: 78-84.
90. Neumann, E., Sowers, A. E., and Jordan, C. A. 1989. Electroporation and electrofusion in cell biology. *Springer, New York*, ISBN 978-0306430435.
91. Nicholls, J. G., Martin, A. R., and Wallace, B. G. 1995. Membrankanäle und Signalentstehung. *Vom Neuron zum Gehirn*, Gustav Fischer Verlag, Stuttgart, ISBN 978-3437205170: 3-17.
92. Numberger, M. and Draguhn, A. 1996. Patch-Clamp-Technik. *Spektrum Akademischer Verlag*, ISBN 3827400236.
93. Ochi, R. and Nishiye, H. 1974. Effect of intracellular tetraethylammonium ion on action potential in the guinea-pig's myocardium. *Pfluegers Archiv*, 348: 305-316.
94. Olofsson, J., Nolkantz, K., Ryttsén, F., Lambie, B. A., Weber, S. G., and Orwar, O. 2003. Single-cell electroporation. *Current Opinion in Biotechnology*, 14: 29-34.
95. Omichi, C., Lee, M.-H., Ohara, T., Naik, A. M., Wang, N. C., Karagueuzian, H. S., and Chen, P.-S. 2000. Comparing cardiac action potentials recorded with metal and glass microelectrodes. *American Journal of Physiology - Heart and Circulatory Physiology*, 279: 3113-3117.
96. Osborn, A. and Gentleman, A. 2003. Secret French move to block animal-testing ban, *The Guardian*, <http://www.guardian.co.uk/world/2003/aug/19/eu.businessofresearch>.
97. Osipenko, O. N., Tate, R. J., and Gurney, A. M. 2000. Potential Role for Kv3.1b Channels as Oxygen Sensors. *Circulation Research*, 86: 534-540.
98. Otto, F., Görtz, P., Fleischer, W., and Siebler, M. 2003. Cryopreserved rat cortical cells develop functional neuronal networks on microelectrode arrays. *Journal of Neuroscience Methods*, 128: 173-181.
99. Pancrazio, J. J., Bey, J., Loloee, A., SubbaRao, M., Chao, H. C., Howard, L., Milton Gosney, W., Borkholder, D. A., Kovacs, T. A., Manos, P., Cuttino, D. S., and Stenger, A. 1998. Description and demonstration of a CMOS amplifier-based-system with measurement and stimulation capability for bioelectrical signal transduction. *Biosensors and Bioelectronics*, 13: 971-979.
100. Parak, W. J., George, M., Kudera, M., Graub, H. E., and Behrends, J. C. 2001. Effects of semiconductor substrate and glia-free culture on the development of voltage-dependent currents in rat striatal neurones. *European Biophysical Journal*, 29: 607-620.
101. Petersen, S., Loschonsky, S., Prucker, O., Rühle, J., and Biesalski, M. 2009. Cell micro-arrays from surface-attached peptide-polymer monolayers. *Physica status solidi. A, Applications and materials science*, 206: 468-473.

102. Pine, J. 1980. Recording action potentials from cultured neurons with extracellular microcircuit electrodes. *Journal of Neuroscience Methods*, 2: 19-30.
103. Pliquett, U., Joshi, R. P., Sridhara, V., and Schoenbach, K. H. 2007. High electrical field effects on cell membranes. *Bioelectrochemistry*, 70: 275-282.
104. Pohl, H. A. 1951. The Motion and Precipitation of Suspensoids in Divergent Electric Fields. *Journal of Applied Physics*, 22: 869-871.
105. Pohl, H. A. and Crane, J. S. 1971. Dielectrophoresis of Cells. *Biophysical Journal*, 11: 711-727.
106. Pottel, R., Göpel, K.-D., Henze, R., Kaatz, U., and Uhlendorf, V. 1984. The dielectric permittivity spectrum of aqueous colloidal phospholipid solutions between 1 kHz and 60 GHz. *Biophysical Chemistry*, 19: 233-244.
107. Prasad, S., Yang, M., Zhang, X., Ozkan, C. S., and Ozkan, M. 2003. Electric Field Assisted Patterning of Neuronal Networks for the Study of Brain Functions. *Biomedical Microdevices*, 5: 125-137.
108. Qi, X., Varma, P., Newman, D., and Dorian, P. 2001. Gap Junction Blockers Decrease Defibrillation Thresholds Without Changes in Ventricular Refractoriness in Isolated Rabbit Hearts. *Circulation*, 104: 1544-1549.
109. Reyes, D. R., Iossifidi, D., Auroux, P.-A., and Manz, A. 2002. Micro Total Analysis Systems. 1. Introduction, Theory, and Technology. *Analytical Chemistry*, 74: 2623-2636.
110. Rohlfs, A., Rundfeldt, C., Koch, R., and Loscher, W. 1996. A comparison of the effects of valproate and its major active metabolite E-2-en-valproate on single unit activity of substantia nigra pars reticulata neurons in rats. *Journal of Pharmacology And Experimental Therapeutics*, 277: 1305-1314.
111. Rols, M.-P. and Teissié, J. 1998. Electroporation of cells to macromolecules. *Biophysical Journal*, 75: 1423-
112. Russel, W. M. S. and Burch, R. L. 1959. The principles of humane experimental technique.
113. Sale, A. J. H. and Hamilton, W. A. 1968. Effects of high electric fields on microorganisms III. Lysis of erythrocytes and protoplasts. *Biochimica et Biophysica Acta*, 163: 37-43.
114. Sanguinetti, M. C. and Tristani-Firouzi, M. 2006. hERG potassium channels and cardiac arrhythmia. *Nature*, 440: 463-469.
115. Schmid, G., Überbacher, R., and Samaras, T. 2007. Radio frequency-induced temperature elevations in the human head considering small anatomical structures. *Radiation Protection Dosimetry*, 124: 15-20.
116. Schrott, R. 2009. Integration eines Neuro-Sensors in ein Messsystem sowie Untersuchungen zur Unit-Separation. 1-191.

117. Schrott, R., Bausch, G., Kirchner, K.-P., Tautorat, C., Baumann, W., Weiss, D., and Beikirch, H. 2006. Evaluation System for Neural Data Acquisition and Analysis. *Conference Proceedings of the 5th International Meeting on Substrate-Integrated Micro Electrode Arrays*, 77-78.
118. Schrott, R., Tautorat, C., Podssun, A., Koester, P. J., Kirchner, K.-P., Bausch, G., Beikirch, H., Baumann, W., and Freund, I. 2007. CMOS Sensorsystem zur Untersuchung elektrisch aktiver Zellen. *Proceedings MikroSystemTechnik Kongress 2007*, 445-447.
119. Shu, P. L., Tsung, L. C., Jia-Jia, J. C., and Shun-Fen, T. 2004. Design of Microscopy-based Microcontact Printing Stamp and Alignment Device for Patterned Neuronal Growth. *Journal of Medical and Biological Engineering*, 24: 45-50.
120. Silbernagel, S. and Despopoulos, A. 2003. Taschenbuch der Physiologie. *Thieme, Stuttgart, 6th edition*, ISBN 978-3135677064.
121. Simeonova, M. and Gimsa, J. 2006. The influence of the molecular structure of lipid membranes on the electric field distribution and energy absorption. *Bioelectromagnetics*, 27: 652-666.
122. Singer, S., Nicolson, J., and Garth, L. 1972. The Fluid Mosaic Model of the Structure of Cell Membranes. *Science*, 175: 720-731.
123. Stenger, D., Gross, G. W., Keefer, E., Shaffer, K. M., Andreadis, J. D., Ma, W., and Pancrazio, J. J. 2001. Detection of physiologically active compounds using cell-based biosensors. *Trends in Biotechnology*, 19: 304-310.
124. Stett, A., Burckhardt, C., Weber, U., van Stiphout, P., and Knott, T. 2003a. CYTOCENTERING: A novel technique enabling automated cell-by-cell patch clamping with the CYTOPATCH chip. *Receptors and Channels*, 9: 59-66.
125. Stett, A., Egert, U., Guenther, E., Hofmann, F., Meyer, T., Nisch, W., and Haemmerle, H. 2003b. Biological application of microelectrode arrays in drug discovery and basic research. *Analytical and Bioanalytical Chemistry*, 377: 486-495.
126. Stevens, R. G. 1987. Electric Power Use And Breast Cancer: A Hypothesis. *American Journal of Epidemiology*, 125: 556-561.
127. Sudsiri, J., Wachner, D., and Gimsa, J. 2007. On the temperature dependence of the dielectric membrane properties of human red blood cells. *Bioelectrochemistry*, 70: 134-140.
128. Sukhotina, I., Streckert, J. R., Bitz, A. K., Hansen, V. W., and Lerchl, A. 2006. 1800 MHz electromagnetic field effects on melatonin release from isolated pineal glands. *Journal of Pineal Research*, 40: 86-91.
129. Taglialatela, M., Vandongen, A. M., Drewe, J. A., Joho, R. H., Brown, A. M., and Kirsch, G. E. 1991. Patterns of internal and external tetraethylammonium block in four homologous K⁺ channels. *Molecular Pharmacology*, 40: 299-307.

130. Tattersall, J. E. H., Scott, I. R., Wood, S. J., Nettell, J. J., Bevir, M. K., Wang, Z., Somasiri, N. P., and Chen, X. 2001. Effects of low intensity radiofrequency electromagnetic fields on electrical activity in rat hippocampal slices. *Brain Research*, 904: 43-53.
131. Tautorat, C. 2005. Entwurf und Realisierung einer Testumgebung für einen neuronalen Silizium-Hybrid-Netzwerksensor, Diploma thesis.
132. Tautorat, C., Koester, P. J., Podssun, A., Beikirch, H., Gimsa, J., Jonas, L., and Baumann, W. 2008. Local Micro-Invasive Needle Electroporation - A Technical Challenge. *Conference Proceedings of the 6th International Meeting on Substrate-Integrated Micro Electrode Arrays*, 340-341.
133. Thalau, H.-P. 2002. Embryonalentwicklung unter Einfluss hoch- und niederfrequenter elektromagnetischer Felder. *Edition Wissenschaft*, 17: 2-80.
134. Thomas Jr., C. A., Springer, P. A., Loeb, G. E., Berwald-Netter, Y., and Okun, L. M. 1972. A miniature microelectrode array to monitor the bioelectric activity of cultured cells. *Experimental Cell Research*, 74: 61-66.
135. Trautmann, A., Ruther, P., Baumann, W., and Lehmann, M. 2004. Fabrication of Out-of-Plane Electrodes for Intracellular Potential Measurements on Living Adherent Cells. *Conference Proceedings of the 4th International Meeting on Substrate-Integrated Micro Electrode Arrays*, 79-80.
136. Troiano, G. C., Tung, L., Sharma, V., and Stebe, K. J. 1999. The Reduction in Electroporation Voltages by the Addition of a Surfactant to Planar Lipid Layers. *Biophysical Journal*, 76: 3150-3157.
137. van Stiphout, P., Knott, T., Danker, T., and Stett, A. 2005. 3D Microfluidic Chip for Automated Patch-Clamping. *Proceedings of the MST-Congress 2005*, 435-438.
138. Waldegrave, W. 1986. Council Directive 86/609/EEC of 24 November 1986 on the approximation of laws, regulations and administrative provisions of the Member States regarding the protection of animals used for experimental and other scientific purposes. *Official Journal of the European Union*, 358: 1-7.
139. Wang, X. and Li, M. 2003. Automated electrophysiology: high throughput of art. *Assay and Drug Development Technologies*, 1: 695-708.
140. Weaver, J. C. 1993. Electroporation: A general phenomenon for manipulating cells and tissues. *Journal of Cellular Biochemistry*, 51: 426-435.
141. Wible, B. A., Hawryluk, P., Ficker, E., Kuryshew, Y. A., Kirsch, G., and Brown, A. M. 2005. HERG-Lite: a novel comprehensive high-throughput screen for drug-induced hERG. *Journal of Pharmacological and Toxicological Methods*, 52: 136-145.
142. Wikipedia. 2009. Scheme of the transmembrane action potential; http://en.wikipedia.org/wiki/Action_potential.
143. World Health Organization. 2006. http://who.int/peh-emf/research/rf_research_agenda_2006.pdf.

144. Wörz, A., Berchtold, B., Kandler, S., Prucker, O., Egert, U., Aertsen, A., and Rühe, J. 2007. Tailormade surfaces for a guided adhesion and outgrowth of cells. *Proceedings MikroSystemTechnik Kongress 2007*, 979-983.
145. Zhao, C., Witte, I., and Wittstock, G. 2006. Switching on Cell Adhesion with Microelectrodes. *Angewandte Chemie*, 118: 5595-5597.
146. Zhao, C., Zawisza, I., Nullmeier, M., Burchardt, M., Träuble, M., Witte, I., and Wittstock, G. 2008. Microelectrochemical Modulation of Micropatterned Cellular Environments. *Langmuir*, 24: 7605-7613.
147. Zhe, Y., Guangxin, X., Liangbin, P., Lihua, H., Zhongyao, Y., Wanli, X., and Jing, C. 2004. Negative Dielectrophoretic Force Assisted Construction of Ordered Neuronal Networks on Cell Positioning Bioelectronic Chips. *Biomedical Microdevices*, 6: 311-324.
148. Ziegler, C. 2000. Cell-based biosensors. *Fresenius Journal of Analytical Chemistry*, 366: 552-559.
149. Zimmermann, U. 1996. The effect of high intensity electric field pulses on eukaryotic cell membranes: Fundamentals and applications. In: *Electromanipulation*, ISBN 978-0849344763: 1-106.
150. Zimmermann, U. and Scheurich, P. 1981. High frequency fusion of plant protoplasts by electric fields. *Planta*, 151: 26-32.

Appendices

6. Appendix A - Publications

6.1 Manuscript 1 – UMTS EMF setup with the SNC

Bioelectrochemistry, 2007, vol. 70, pp. 104-114



Available online at www.sciencedirect.com



Bioelectrochemistry 70 (2007) 104–114

Bioelectrochemistry

www.elsevier.com/locate/bioelechem

A new exposure system for the *in vitro* detection of GHz field effects on neuronal networks

Philipp Koester^a, Jan Sakowski^a, Werner Baumann^a, Hans-Walter Glock^b, Jan Gimsa^{a,*}

^a University of Rostock, Institute of Biology, Chair of Biophysics, Gertrudenstr. 11A, D-18057 Rostock, Germany
^b Faculty of Computer Science and Electric Engineering, Chair of Theoretical Electrotechnics, Albert-Einstein-Str. 2, D-18051 Rostock, Germany

Received 15 June 2005
Available online 18 April 2006

Abstract

The possible effects of high-frequency electromagnetic fields (EMF) on biological systems are a subject of public concern and scientific discussion. It is generally accepted that the absorption of part of the field energy may cause a temperature rise in biological tissue. Nevertheless, our setup aims to detect possible athermal effects on the electric activity of neuronal *in vitro* networks. Such networks were formed by primary neurons derived from the murine frontal cortex and cultivated on micro-sensor chips. The action potentials of the neurons were detected in real time by an integrated, electrically passive microelectrode array. For EMF exposure, the chips were introduced into a rectangular wave-guide that could be operated in the propagating or standing wave modes. The drive signals were either continuous waves (1.9–2.2 GHz) or a generic mobile phone signal (UMTS-standard) of up to approximately 8 W. An on-chip sensor allowed the temperature progression to be recorded. In addition, ISFETs and Clark-like electrodes were integrated for the on-chip detection of pH and O₂, respectively.

© 2006 Elsevier B.V. All rights reserved.

Keywords: Multi-electrode array; Micro-sensor chip; Biochip; EMF; UMTS; Wave-guide

6.2 Manuscript 2 – Modular glass chip system

Lab on a Chip, 2010, vol. 10, pp. 1579-1586

PAPER

www.rsc.org/loc | Lab on a Chip

Modular glass chip system measuring the electric activity and adhesion of neuronal cells—application and drug testing with sodium valproic acid

Philipp Julian Koester,^{†a} Sebastian Moritz Buehler,^{†a} Marco Stubbe,^a Carsten Tautorat,^a Mathias Niendorf,^b Werner Baumann^a and Jan Gimsa^{*a}

Received 11th November 2009, Accepted 23rd February 2010

First published as an Advance Article on the web 31st March 2010

DOI: 10.1039/b923687b

We developed a modular neurochip system by combining a small ($16 \times 16 \text{ mm}^2$) glass neurochip (GNC) with a homemade head stage and commercial data acquisition hardware and software. The system is designed for the detection of the electric activity of cultivated nerve or muscle cells by a 52-microelectrode array (MEA). In parallel, cell adhesion can be registered from the electric impedance of an interdigitated electrode structure (IDES). The GNC was tested with various cell lines and primary cells. It is fully autoclavable and re-useable. Murine embryonic primary cells were used as a model system to correlate the electric activity and adhesion of neuronal networks in a drug test with sodium valproic acid. The test showed the advantage of the parallel IDES and MEA measurements, *i.e.* the parallel detection of cytotoxic and neurotoxic effects. Toxic exposure of the cells during neuronal network formation allows for the characterization of developmental neurotoxic effects even at drug concentrations below the EC_{50} -value for acute neurotoxic effects. At high drug concentrations, the degree of cytotoxic damage can still be assessed from the IDES data in the event that no electric activity develops. The GNC provides optimal cell culture conditions for up to months in combination with full microscopic observability. The 4" glass wafer technology allows for a high precision of the GNC structures and an economic production of our new system that can be applied in general and developmental toxicity tests as well as in the search for neuro-active compounds.

6.3 Manuscript 3 – Introduction to the intracellular potential measurements with the MNC and the PoreGenic® system

Proceedings of the *6th International Meeting on Substrate-Integrated Microelectrode Arrays*, Reutlingen, 2008, pp. 271 - 274

Technology

A new Principle for intracellular Potential Measurements of adherently growing Cells

Philipp Julian Koester¹, Carsten Tautorat¹, Angela Podssun¹, Jan Gimsa¹, Ludwig Jonas², and Werner Baumann^{1*}

¹ University of Rostock, Chair of Biophysics, Rostock, Germany

² University of Rostock, Electron Microscopy Center, Medical Faculty, Rostock, Germany

* Corresponding author. E-mail: werner.baumann@uni-rostock.de

The investigation of cellular reactions in living cell cultures gets increasingly into focus of drug development and environmental monitoring. Existing classical methods for intracellular measurements are time-consuming and complex. Existing Patch-on-chip systems are limited to the investigation of suspended single cells. Nevertheless, most cells in the human body are adherently growing. To address this problem, we are developing a new chip system with 64 micro-structured needle electrodes arranged within a measuring area of 1 mm². We believe that the intracellular investigation of electro-chemical properties and processes in adherently growing cells will become possible with our new analytical chip.

6.4 Manuscript 4 – First intracellular recordings with 3D microelectrode arrays after local electroporation

Biosensors & Bioelectronics, <http://dx.doi.org/10.1016/j.bios.2010.08.003>

Biosensors and Bioelectronics 26 (2010) 1731–1735



Contents lists available at ScienceDirect

Biosensors and Bioelectronics

journal homepage: www.elsevier.com/locate/bios



Short communication

Recording electric potentials from single adherent cells with 3D microelectrode arrays after local electroporation

Philipp Julian Koester^{a,*}, Carsten Tautorat^a, Helmut Beikirch^b, Jan Gimsa^a, Werner Baumann^a

^a University of Rostock, Chair of Biophysics, Gertrudenstrasse 11a, 18057 Rostock, Germany

^b University of Rostock, Institute of Electronic Appliances and Circuits, Albert-Einstein-Strasse 2, 18059 Rostock, Germany

ARTICLE INFO

Article history:

Received 14 April 2010
Received in revised form 30 July 2010
Accepted 2 August 2010
Available online 7 August 2010

Keywords:

Electrophysiology
Patch-on-chip
Patch clamp
Whole-cell
Transmembrane potential
Tumor cell
Single cell electroporation

ABSTRACT

This short communication reports on the innovative method of the local micro-invasive needle electroporation (LOMINE) of single adherent cells. The investigation of cellular reactions in living cell cultures represents a fundamental method, e.g. for drug development and environmental monitoring. Existing classical methods for intracellular measurements using, e.g. patch clamp techniques are time-consuming and complex. Present patch-on-chip systems are limited to the investigation of single cells in suspension. Nevertheless, the most part of the cells of the human body is adherently growing. Therefore, we develop a new chip system for the growth of adherent cells with 64 micro-structured needle electrodes as well as 128 dielectrophoretic electrodes, located within a measuring area of 1 mm². With this analytical chip, the intracellular investigation of electro-chemical changes and processes in adherently growing cells will become possible in the near future. Here, we present first intracellular measurements with this chip system.

© 2010 Elsevier B.V. All rights reserved.

6.5 Manuscript 5 – Dielectrophoresis with the SNC

Proceedings of the *6th International Meeting on Substrate-Integrated Microelectrode Arrays*,
Reutlingen, 2008, pp. 319 - 320

Technology

Dielectrophoretic Neuron Positioning on MEAs in Semiconductor Chips for the Extracellular Detection of the Neuronal Network Activity

Philipp Julian Koester, Carsten Tautorat, Jan Sakowski, Werner Baumann, and Jan Gimsa*

University of Rostock, Chair of Biophysics, Rostock, Germany
* Corresponding author. E-mail: jan.gimsa@uni-rostock.de

Biological cells are more or less homogeneously distributed when seeded on a sensor chip. Different methods can be applied when artificial substrates are used to stimulate cell growth in a predetermined way. Such methods are applied to single cells, cell aggregates or cell networks. One can use photolithography or, more easily, dielectrophoresis to allocate cells to specific adhesive sites or to electrically conducting structures. Here, we present silicon chips containing an array of plane microelectrodes for the measurement of extracellular potentials from neurons. The same electrodes are used for dielectrophoretic cell allocation.

6.6 Manuscript 6 – Dielectrophoresis with the MNC

Proceedings of the 6th International Meeting on Substrate-Integrated Microelectrode Arrays, Reutlingen, 2008, pp. 317 - 318

Technology

Dielectrophoretic Positioning of Cells for the Measurement of intracellular Potentials using Kidney-Shaped Electrodes

Philipp Julian Koester¹, Carsten Tautorat¹, Angela Podssun¹, Jan Gimsa¹, Ludwig Jonas², and Werner Baumann^{1*}

¹ University of Rostock, Chair of Biophysics, Rostock, Germany

² University of Rostock, Electron Microscopy Center, Medical Faculty, Rostock, Germany

* Corresponding author. E-mail: werner.baumann@uni-rostock.de

The combination of cell culture with new technical measuring principles leads to a number of problems, e.g. the positioning of specific cells at sites of interest, such as micro-electrodes. Additionally, a high number of cells hinder the measurement of single cell signals. Both problems can be tackled combining active dielectrophoretic positioning of cells at desired chip locations and by long-term fixation of cells by biopolymer coatings.

7. Appendix B - Author's scientific activity

7.1 Oral presentations

1. Koester, P.J. and S. Buehler

MOGS - Mini-Glaschips mit optischen Metabolitensensoren für stammzellbasierte neuronale Netzwerke. Contest presentation, Venturesail idea contest, August 12, 2007 (2nd place winner), Rostock

2. Koester, P.J., C. Tautorat, J. Gimsa, and W. Baumann

Electroporation in bioanalytical sensor chips – A new tool for the analysis of intracellular potentials in adherent cells. 12th Symposium on maritime electrical engineering, electronics and information engineering, October 08-10, 2007, Rostock

3. Koester, P.J., C. Tautorat, A. Podssun, J. Gimsa, and W. Baumann

Analytikchip zur Erfassung intrazellulärer Potentiale adhären wachsender Zellen nach lokaler Elektroporation: Einleitung - Biologische Aspekte. Microsystems technology congress, October 15-17, 2007, Dresden

4. Koester, P.J., C. Tautorat, A. Podssun, J. Gimsa, and W. Baumann

A new tool for the analysis of intracellular potentials in adherent cells. IPP Seminar of the DAAD (German Academic Exchange Service) at the University of Rostock, November 2nd, 2007

5. Koester, P.J., C. Tautorat, J. Held, J. Gaspar, P. Ruther, O. Paul, A. Cismak, A. Heilmann, J. Gimsa, and W. Baumann.

Local microinvasive needle electroporation (LOMINE) of single cells attached on silicon chips. 13th International Biotechnology Symposium (IBS) and Exhibition, October 12-17, 2008, Dalian, China

6. Koester, P.J., C. Tautorat, A. Podssun, J. Gimsa, L. Jonas, and W. Baumann:

A New Principle For Intracellular Potential Measurements Of Adherently Growing Cells. 6th International Meeting on Substrate-Integrated Micro Electrode Arrays, July 8-11 2008, Reutlingen

7. Koester, P.J., and C. Tautorat

PoreGenic® – Wirkstofftests und Grundlagenforschung an adhären vernetzen Zellen. Contest presentation, University of Rostock's idea contest, July 8, 2009 (2nd place winner)

8. Koester, P.J., and C. Tautorat
PoreGenic® – Wirkstofftests und Grundlagenforschung an adhärenz vernetzten Zellen.
Contest presentation, BMBF (Bundesministerium für Forschung und Bildung)
„GO-Bio“ call, October 7, 2009, Potsdam (One of six winners out of 54 applicants)
9. Koester, P.J., Tautorat, C., Held, J., Ruther, P., Paul, O., Beikirch, H., Gimsa, J. and W. Baumann
Recording electric potentials from single adherent cells with 3D microelectrode arrays after local electroporation. Biosensors 2010, 20th Anniversary World Congress on Biosensors, 26-28 May 2010, Glasgow, UK
10. Koester, P.J., Tautorat, C., Held, J., Gaspar, J., Ruther, P., Paul, O., Beikirch, H., Gimsa, J. and W. Baumann
Whole-Cell Mode Detection with the 3D-MEA-Chip PoreGenic®. 5-8 October 2010, Jahrestagung der Deutschen Gesellschaft für Biomedizinische Technik (DGBMT) im VDE (BMT 2010), Rostock-Warnemünde

7.2 Publications

1. Koester, P.J., J. Sakowski, W.H. Baumann, H.-W. Glock, and J. Gimsa, (2007): A new exposure system for the in-vitro detection of GHz field effects on neuronal networks.
Bioelectrochemistry 70, 104-114
2. Koester, P.J., S. Buehler, M. Stubbe, C. Tautorat, M. Niendorf, W. Baumann, and J. Gimsa, (2009a): Modular glass chip system measuring the electric activity and adhesion of neuronal cells – application and drug testing with sodium valproic acid.
Lab on a chip, 2010, 1579-1586
3. Koester, P.J., C. Tautorat, J. Gimsa, and W. Baumann, (2009b): Recording electric potentials from single adherent cells with 3D microelectrode arrays after local electroporation
Biosensors & Bioelectronics, <http://dx.doi.org/10.1016/j.bios.2010.08.003>

7.3 Conference contributions

2006

1. Baumann, W., R. Ehret, E. Thedinga, A. Kob, S. Drechsler, A. Podssun, P. Koester, C. Tautorat, R. Schrott, H. Beikirch, I. Freund, and M. Lehmann: Cell monitoring system with multiparametric CMOS biosensor chips. In: *Proceedings of the 5th International Meeting on Substrate-Integrated Micro Electrode Arrays*, Reutlingen, 2006, Conference Proceedings ISBN 3-938345-02-0, 161-162.

2007

1. Koester, P.J., S.M. Buehler, J. Sakowski, C. Tautorat, H. Altrichter, W. Baumann, and J. Gimsa: Modular glass chip system for the acquisition of the electric activity and physiological parameters of differentiated stem cells. In: *Proceedings of the 14th World Congress on Alternatives to Animal Testing*, Linz, Austria, September 28-30, 2007, *ALTEX*: 24 (3), 208-209, ISSN:0946-7785.
2. Koester, P.J., C. Tautorat, A. Podssun, J. Gimsa, and W. Baumann: Analytikchip zur Erfassung intrazellulärer Potentiale adhärent wachsender Zellen nach lokaler Elektroporation: Einleitung – Biologische Aspekte. In: *Proceedings of the MEMS Congress*, October 2007, Dresden, VDE Verlag GmbH, Berlin, Offenbach, 433-436, ISBN 978-3-8007-3061-2.
3. Koester, P.J., C. Tautorat, J. Gimsa, and W. Baumann: Electroporation in bioanalytical sensor chips – A new tool for the analysis of intracellular potentials in adherent cells. In: *Proceedings of the 12th Symposium on Maritime Electrical Engineering, Electronics and IT*, October 2007, Rostock, 99-105.
4. Tautorat, C., P.J. Koester, A. Podssun, J. Gimsa, and W. Baumann: Analytikchip zur Erfassung intrazellulärer Potentiale adhärent wachsender Zellen nach lokaler Elektroporation: Einleitung - Elektrotechnische Aspekte. In: *Proceedings of the MEMS Congress*, October 2007, Dresden VDE Verlag GmbH, Berlin-Offenbach, 975-978, ISBN 978-3-8007-3061-2.
5. Buehler, S.M., P. J. Koester, C. Tautorat, H. Altrichter, W. Baumann, and J. Gimsa: Bio-analytic silicon chips for the detection of developmental-neurotoxic effects of chemicals and drugs in the context of the European REACH program. In: *Proceedings of the 14th World Congress on Alternatives to Animal Testing*, Linz, Austria, September 28-30, 2007, *ALTEX*: 24 (3), 190, ISSN: 0946-7785.

6. Schrott, R., C. Tautorat, A. Podssun, P. J. Koester, K.-P. Kirchner, G. Bausch, H. Beikirch, W. Baumann, and I. Freund: CMOS Sensorsystem zur Untersuchung elektrisch aktiver Zellen. In: *Proceedings of the MEMS Congress*, October 2007, Dresden, VDE Verlag GmbH, Berlin, Offenbach, 445-449, ISBN 978-3-8007-3061-2.
7. Schrott, R., C. Tautorat, K.-P. Kirchner, P. J. Koester, G. Bausch, , W. Baumann, I. Freund and H. Beikirch: Hardwareentwurf für ein Messsystem zur Untersuchung elektrisch aktiver Zellen. In: *Proceedings of the 12th Symposium on Maritime Electrical Engineering, Electronics and IT*, October 2007, Rostock, 93-97.

2008

1. Koester, P.J., S. Buehler, C. Tautorat, J. Sakowski, R. Schrott, W. Baumann, and J. Gimsa: A New Glass Chip System Acquiring Electric Activity And Physiological Parameters Of Differentiated Stem Cells (II2-O-005). In: *Proceedings of the 13th International Biotechnology Symposium (IBS) and Exhibition*, October 2008, Dalian, China, *Journal of Biotechnology* 136S, 126-127, ISSN 0168-1656.
2. Koester, P.J., C. Tautorat, J. Sakowski, W. Baumann, and J. Gimsa: Dielectrophoretic neuron trapping on semiconductor chips for the extracellular detection of the neuronal network activity. In: *Proceedings of the 13th International Biotechnology Symposium (IBS) and Exhibition*, October 2008, Dalian, China, *Journal of Biotechnology* 136S, 120-121, ISSN 0168-1656.
3. Koester, P.J., C. Tautorat, J. Held, J. Gaspar, P. Ruther, O. Paul, A. Cismak, A. Heilmann, J. Gimsa, and W. Baumann: Local microinvasive needle electroporation (LOMINE) of single cells attached on silicon chips. In: *Proceedings of the 13th International Biotechnology Symposium (IBS) and Exhibition*, October 2008, Dalian, China, *Journal of Biotechnology* 136S, 462, ISSN 0168-1656.
4. Koester, P.J., S. Buehler, C. Tautorat, J. Sakowski, R. Schrott, W. Baumann, and J. Gimsa: A New Glass Chip System Acquiring Electric Activity And Physiological Parameters Of Differentiated Stem Cells. In: *Proceedings of the 6th International Meeting on Substrate-Integrated Micro Electrode Arrays*, July 2008, Reutlingen, 315-316, ISBN 3-938345-05-0.
5. Koester, P.J., C. Tautorat, A. Podssun, J. Gimsa, L. Jonas, and W. Baumann: A New Principle For Intracellular Potential Measurements Of Adherently Growing Cells.

In: *Proceedings of the 6th International Meeting on Substrate-Integrated Micro Electrode Arrays*, July 2008, Reutlingen, 271-274, ISBN 3-938345-05-5.

6. Koester, P.J., C. Tautorat, J. Sakowski, W. Baumann, and J. Gimsa: Dielectrophoretic Neuron Positioning On MEAs in Semiconductor Chips For The Extracellular Detection Of The Neuronal Network Activity. In: *Proceedings of the 6th International Meeting on Substrate-Integrated Micro Electrode Arrays*, July 2008, Reutlingen, 319-320, ISBN 3-938345-05-5.
7. Koester, P.J., C. Tautorat, A. Podssun, J. Gimsa, L. Jonas, and W. Baumann: Dielectrophoretic Positioning Of Cells For The Measurement Of Intracellular Potentials Using Kidney-Shaped Electrodes. In: *Proceedings of the 6th International Meeting on Substrate-Integrated Micro Electrode Arrays*, July 2008, Reutlingen, 317-318, ISBN 3-938345-05-5.
8. Tautorat, C., P.J. Koester, A. Podssun, H. Beikirch, J. Gimsa, L. Jonas, and W. Baumann: Local Microinvasive Needle Electroporation – A Technical Challenge. In: *Proceedings of the 6th International Meeting on Substrate-Integrated Micro Electrode Arrays*, July 2008, Reutlingen, 340-341, ISBN 3-938345-05-5.
9. Tautorat, C., P.J. Koester, J. Held, J. Gaspar, P. Ruther, O. Paul, A. Cismak, A. Heilmann, J. Gimsa, H. Beikirch, L. Jonas, and W. Baumann: Intracellular Potential Measurements of Adherently Growing Cells using Microneedle Arrays. In: *μ -TAS Proceedings*, October 2008, San Diego, USA, 1777-1780, ISBN 978-0-9798064-1-4/1556-5904.
10. Held, J., J. Gaspar, P.J. Koester, C. Tautorat, A. Cismak, A. Heilmann, W. Baumann, A. Trautmann, P. Ruther, and O. Paul: Microneedle arrays for intracellular recording applications. In: *Proceedings of MEMS 2008*, January 2008 , Tucson, USA, 268-271, ISBN: 978-1-4244-1793-3.

2009

1. Held, J., J. Gaspar, P. J. Koester, C. Tautorat, M., Hagner, A. Cismak, A. Heilmann, W. Baumann, P. Ruther, and O. Paul: Hollow Microneedle Electrode Arrays for Intracellular Recording Applications. In: *Proceedings of the Digital Technical Papers IEEE MEMS Conference*, 2009, 220-223, ISBN: 978-1-4244-2977-6.

2. Held, J., J. Gaspar, P.J. Koester, C. Tautorat, M. Hagner, A. Cismak, A. Heilmann, W. Baumann, P. Ruther, and O. Paul: Integration of Microfluidic Features with Microneedle Electrode Arrays for Intracellular Recording Applications. In: *Proceedings of the MST Congress*, Dresden, VDE Verlag GmbH, Berlin, Offenbach, 476-479, ISBN 978-3-8007-3183-1.
3. Sriperumbudur, K. K., P. J. Koester, M. Stubbe, C. Tautorat, J. Held, W. Baumann, and J. Gimsa: Local Electroporation of Single Adherent Cells by Microstructured Needle Electrodes, COMSOL Conference, 2009, Bangalore, India, cds.comsol.com/access/dl/papers/7359/Sriperumbudur.pdf.

2010

1. Koester, P.J., C. Tautorat, J. Held, J. Gaspar, P. Ruther, O. Paul, H. Beikirch, J. Gimsa, and W. Baumann: *Whole-Cell Mode Detection with the 3D-MEA-Chip PoreGenic®*. In: Proceedings of Annual Conference of the German Society of biomedical engineering (BMT 2010), 5-8 October 2010, Rostock-Warnemünde, Biomed Tech 2010; 55 (Suppl. 1), 6-9, Walter de Gruyter, Berlin, New York. DOI 10.1515/BMT.2010.493, ISSN 0939-4990
2. Reimer, T., W. Baumann, P.J. Köster and J. Gimsa: *Gap Junction-induced signal transmission in cortical neuronal networks cultured on glass neurochips*. In: Proceedings of Annual Conference of the German Society of biomedical engineering (BMT 2010), 5-8 October 2010, Rostock-Warnemünde, Biomed Tech 2010; 55 (Suppl. 1), Walter de Gruyter, Berlin, New York. DOI 10.1515/BMT.2010.588, ISSN 0939-4990
3. Koester, P.J., C. Tautorat, J. Held, P. Ruther, J. Gaspar, O. Paul, H. Beikirch, J. Gimsa, and W. Baumann: *GO-Bio 3: PoreGenic® - 1. Whole-Cell Patch Clamp Recordings with a 3D-MEA chip*. In: *Proceedings of the 7th International Meeting on Substrate-Integrated Micro Electrode Arrays*, July 2008, Reutlingen, 291-292, ISBN-13 978-3-938345-08-5.
4. Koester, P.J., C. Tautorat, J. Held, P. Ruther, J. Gaspar, O. Paul, H. Beikirch, J. Gimsa, and W. Baumann: *GO-Bio 3: PoreGenic® - 2. Cardiomyocyte Action Potential Recordings with a 3D-MEA Chip*. In: *Proceedings of the 7th International Meeting on Substrate-Integrated Micro Electrode Arrays*, July 2008, Reutlingen, 293-294, ISBN-13 978-3-938345-08-5.
5. Koester, P.J., C. Tautorat, T. Reimer, M. Zwanzig, W. Baumann and J. Gimsa: *Gold Shark Teeth Structures on MEAs - Electroplating of Nano-Structures on Metallic*

- Microelectrodes*. In: *Proceedings of the 7th International Meeting on Substrate-Integrated Micro Electrode Arrays*, July 2008, Reutlingen, 289-290, ISBN-13 978-3-938345-08-5.
6. Sriperumbudur, K. K., P. J. Koester, W. Baumann and J. Gimsa: *Effect of electrode dimensions on nerve fiber signal recordings*. In: *Proceedings of the 7th International Meeting on Substrate-Integrated Micro Electrode Arrays*, July 2008, Reutlingen, 255-256, ISBN-13 978-3-938345-08-5.
7. Reimer, T., W. Baumann, P.J. Köster and J. Gimsa: *Burst– induced Inhibition in Cortical Neuronal Networks in vitro*. In: *Proceedings of the 7th International Meeting on Substrate-Integrated Micro Electrode Arrays*, July 2008, Reutlingen, 66-67, ISBN-13 978-3-938345-08-5.

7.4 Book contributions

1. Gimsa, U., A. Scheunemann, D. Wachner, J. Sakowski, P. Köster, and J. Gimsa (2006): Effekte hochfrequenter elektromagnetischer Felder auf zellulärer Ebene – eine Literaturstudie, 89 pages, Shaker Verlag. Aachen. ISBN-10:3-8322-5251-7.
2. Baumann, W., C. Tautorat, A. Podssun, P. Köster, J. Gimsa, R. Ehret, I. Freund, and M. Lehmann (2008): Cell Monitoring Systems with CMOS MicroSensor-Chips. In: NATO ADVANCED RESEARCH WORKSHOP, "Commercial and Pre-commercial Cell Detection Technologies for Defence against Bioterror ", IOS Press, 77-79, ISBN 978-1-58603-858-8.

7.5 Digitally published posters

1. ID-Nr. EP10644: A new exposure system for the in vitro detection of GHz field effects on neuronal networks.

➔ www.eposters.net/

2. ID-Nr. EP10641: Modular glass chip system for the acquisition of the electric activity and physiological parameters of differentiated stem cells

➔ www.eposters.net/,
<http://stemcells.net/>
www.HTScreening.net/
www.Lab-on-a-Chip.com/
www.Metabolomics.net/, and
www.NanoTechnology.net/

3. ID-Nr. EP10645: Bio-analytic silicon chips for the detection of developmental-neurotoxic effects of chemicals and drugs in the context of the European REACH program.

➔ www.eposters.net/
<http://stemcells.net/>
www.HTScreening.net/
www.Lab-on-a-Chip.com/
www.Metabolomics.net/ and
www.NanoTechnology.net/

8. Appendix C

8.1 Summary of the author's original work

The author herein declares that the following ideas, work-, and data interpretation procedures were developed or initiated by him. The following list contains the main aspects and may be incomplete.

- invention and biocompatibility test of biochip assemblage procedures for all three types of biochips (SNC, GNC and MNC)
- development of sterilization procedures (PAA, knick'n'clean® flora sticks)
- electrode testing experiments (hardware development by C. Tautorat)
- the idea to use pDEP for cell allocation with the SNC and the MNC
- the idea to implement pDEP electrodes into the MNC and the development of pDEP-MNC layouts
- the development of the experimental pDEP setups (pDEP-board developed by C. Tautorat)
- experiments on pDEP cell positioning with PNCs and L929 cells
- development of the fluorescent experiments with the MNC
- adaptation of the MNC trough for a 100x immersion objective, development of new trough layout for small series production
- development of the cell culture protocols for PNCs and PCMs
- mouse, rat and cell line preparations and culture procedures (PNCs, PCMs and fibroblasts)
- UMTS and temperature setup and experiments with PNCs (in cooperation with Dr. J. Sakowski)
- all concepts of biochemical experiments described in the attached publications and publication manuscripts (see appendices) with the except of the IDES experiments and part of the VPA experiments
- all electrophysiological measurements on SNC, GNC (VPA experiments in cooperation with S. Bühler and T. Reimer) and MNC (in cooperation with C. Tautorat) and data interpretations

- responsible for various grant applications (2006 and 2007 venturesail scientific competition, 2009 University of Rostock Innovation competition, GO-Bio call 2010)

9. Appendix D - Tables

9.1 List of Figures

Figure 1: Distribution of clinical development cost	3
Figure 2: Neuronal information signals.....	5
Figure 3: Comparison of the cardiac AP and the surface electrocardiogram.....	7
Figure 4: Schematic exemplary patch clamp configurations.....	9
Figure 5: Schematic layout of the PoreGenic® system (C. Tautorat).....	16
Figure 6: Robust and washable aluminum-housing for the PoreGenic® setup	17
Figure 7: Schematics of MNC fabrication processes.....	18
Figure 8: Kidney-shaped pDEP-electrodes.....	19
Figure 9: The preparation of the mouse brain	22
Figure 10: Three explanted hearts of postnatal rats (P3).....	24
Figure 11: Setup scheme for pDEP cell allocation	25
Figure 12: Electrode mapping for pDEP cell allocation	26
Figure 13: Power adjustments of the UMTS generator.....	28
Figure 14: Setup scheme of EMF exposure.....	29
Figure 15: Acrylic cap forPNC protection during EMF exposure.....	30
Figure 16: The effect of autoclaving on the SNC quality.	33
Figure 17: Averaged fidelity of 58 electrodes of a SNC is decreasing due autoclaving cycles.....	34
Figure 18: Comparison of autoclaving and knick'n'clean stick on the signal yield	35
Figure 19: Neuronal activity yield over approximately 2 years	36
Figure 20: Modeled sinusoidal output signal and measured voltage at the electrode	37
Figure 21: Signal transmission test. 58 electrodes show good sinusoidally shaped signal transmissions	38
Figure 22: Neuronal network cultured on a SNC.....	38
Figure 23: Fluorescent image of PNC network growing on an SNC and cell nuclei	39
Figure 24: Electrophysiological control recording of PNCs.....	40
Figure 25: Recorded signals of the same SNC after application of 2 µl bicuculline (2 mM)	40
Figure 26: Recorded signals after application of Triton-X100.....	41
Figure 27: Electric detection of primary postnatal rat pup neurons	41
Figure 28: Data recording with a competing MEA type.....	42
Figure 29: Correlation of neuronal growth on a SNC and the recorded electrical signal patterns.....	43
Figure 30: pDEP with PNCs on a SNC.....	43
Figure 31: Cell growth after pDEP.....	44
Figure 32: Cell growth after pDEP.....	44
Figure 33: Comparison of a pDEP-SNC and a control SNC.....	45
Figure 34: Comparison of control SNCs with pDEP- SNCs.....	46
Figure 35: A single SNC electrode is coated with a glas micropipette.....	47
Figure 36: SNCs with spotting patterns on specific electrodes and uncoated areas.....	47
Figure 37: Comparison of neuronal motility after PDL/laminin-spotting of electrodes on chip XME7_1	48
Figure 38: SU-8 structures on the SNC	49
Figure 39: Neuronal growth between the SU-8 structures.....	49
Figure 40: Signal waveform with the UMTS signal	51
Figure 41: PSDs of the spike rates	52
Figure 42: Temperature profile according to the PSD of the heating experiments.....	53
Figure 43: Comparison of the sum of the PSD of the spike rates with the PSD of the temperature profile.	54
Figure 44: Neuronal growth and electrical control registration on a GNC after 21 DIV.	57
Figure 45: Effect of VPA on the uniformity of AP frequency at 12 DIV.....	58
Figure 46: Effect of VPA on the uniformity of AP frequency at 21 DIV.....	59
Figure 47: PCM growth and electrophysiological registration on the GNC after 14 DIV	61
Figure 48: Cardiac AP detection with three different GNCs	62
Figure 49: Dimensions of the MNC.....	63
Figure 50: Dimensions of two pDEP electrode framing one MNE	64
Figure 51: Attraction of different cell types with pDEP electrodes.....	64
Figure 52: Time-dependent accumulation of living NHDF cells on cell-adhesive polymers.....	65
Figure 53: LOMINE principle of the PoreGenic® system.....	66

Figure 54: Electroporation of L929 fibroblasts.....	67
Figure 55: Congruence of a light microscopical image and the corresponding FIB-SEM image.	67
Figure 56: LOMINE sequence of PI staining of PNC.....	68
Figure 57: LOMINE of a NHDF	69
Figure 58: Vitality test after LOMINE	69
Figure 59: Scheme of the AC-pulsing after DC-signal approximation	70
Figure 60: Comparison of different V_m potential measurements with L929 cells without intracellular contact....	71
Figure 61: Reactions of L929 fibroblasts to special LEPs	71
Figure 62: Reactions of L929 fibroblasts to special LEPs	72
Figure 63: Reaction of a L929 fibroblast on LEPs	73
Figure 64: Electroporated L929 mouse sarcoma fibroblasts overgrow MNEs	74
Figure 65: PCMs cultured on a MNC.	75
Figure 66: Extracellular signals of PCMs were detected by platinum MNEs.....	76
Figure 67: Extracellular recording of cardiac APs of eight PCM of rat embryos detected with eight silver-electro-plated solid platinum MNEs	77
Figure 68: Extracellular recording of cardiac APs of three PCMs of rat embryos detected with three silver electro-plated solid platinum MNEs.	77
Figure 69: Signal track of eight PCMs over 5 s. A potential drift is clearly visible.	78
Figure 70: A cardiac AP recorded over 2.5 s.	78
Figure 71: Different detection types of cardiac APs.	79
Figure 72: A preliminary printed circuit board for parallel pDEP with ten SNCs.	82
Figure 73: A schematic microfluidic channels is drawn in a FIB-SEM.....	84
Figure 74: The possible scenario of a whole-cell detection of a substance-effect.....	84
Figure 75: Cavities surrounding the MNEs will be integrated in the MNC base	85
Figure 76: The possible scenario of a future whole-cell detection	86
Figure 77: Model cells growing over two MNEs.....	87
Figure 78: Model PCM growing over four MNEs.....	89

9.2 List of tables

Table 1: Frequency fractions of the UMTS signal.....	28
Table 2: Experiments with different biochip types.	32
Table 3: Overview of the sterilization experiments.	36
Table 4: Electrode characteristics.....	56

9.3 List of internet links

<i>Acharya, S. 2005. The productivity tiger - time and cost benefits of clinical drug development in India.</i>	http://pharmalicensing.com/public/articles/view/1153412098_44bfac02291f1 ,
<i>Chair of Biophysics, University of Rostock</i>	www.biologie.uni-rostock.de/biophysik/
<i>Food and Drug Administration. 2005. FDA Guidance for Industry S7B Nonclinical Evaluation of the Potential for Delayed Ventricular Repolarization (QT Interval Prolongation) by Human Pharmaceuticals.</i>	http://www.fda.gov/RegulatoryInformation/Guidances/ucm129121.htm :
<i>German mobile phone program</i>	www.emf-forschungsprogramm.de/
<i>Osborn, A. and A. Gentleman. 2003. Secret French move to block animal-testing ban, The Guardian.</i>	http://www.guardian.co.uk/world/2003/aug/19/eu.businessofresearch
<i>REACH</i>	http://www.reach-info.de/
<i>Wikipedia. 2009a. Scheme of the transmembrane action potential;</i>	http://en.wikipedia.org/wiki/Action_potential
<i>Wikipedia. 2009b. The cardiac Action Potential.</i>	http://en.wikipedia.org/wiki/Cardiac_action_potential#Phase_0
<i>World Health Organization. 2006: 2006 Research Agenda</i>	http://who.int/peh-emf/research/rf_research_agenda_2006.pdf

9.4 List of abbreviations

μ -TAS	micro total analysis systems	MNE	microstructured needle electrode
AC	alternating current	nDEP	negative dep
ADP	Adenosine diphosphate	NHDF	normal human skin (dermal) fibroblast
AP	action potential	NMA	neuro-measuring adapter
ATP	Adenosine triphosphate	NMRI	Naval Medical Research Institute
CLCC	ceramic leadless chip carrier	PAA	peracetic acid
CMOS	complementary metal oxide semiconductor	PAD	public access defibrillator
CMS®	cell monitoring systems	PBS	phosphate-buffered saline
CPFET	cell potential field effect transistor	PCA	principal component analysis
D10	DMEM enriched with 10 % horse serum	PCM	primary cardiomyocyte
D10/10	D10 enriched with 10% fetal calf serum	pDEP	positive dielectrophoresis
DAPI	4',6-diamidin-2'-phenylindoldihydrochlorid	pDEP-SNCs	dielectrophoresis was applied with such SNCs
DECT	digital enhanced cordless telephone	PDL	poly-D-lysine
DIV	days in vitro, describing the days in culture	PDMAA	poly(dimethylacrylamide)
DMEM	Dulbecco's modified Eagle's medium	PET	polyethylene
DNA	deoxyribonucleic acid	PI	propidium iodide
DRIE	deep reactive ion etching	PNC	primary neuronal cell
EMF	high-frequency electro-magnetic field	POM	poly-oxymethylen
EU	European Union	PSD	power spectral density
FCS	fetal calf serum	REACH	registration, evaluation, authorization and restriction of chemicals
FDA	Food and Drug Administration	RNA	ribonucleic acid
FDD	frequency division duplex	RP	rhodamine phalloidine
FFT	fast Fourier transformation	SAR	specific absorption rate
Fh-IWM	Fraunhofer Institute for Mechanics of Materials	SECM	scanning electrochemical microscope
FIB	focused-ion-beam technique	SEM	scanning electron microscope
FP	field potential	SNC	silicon neurochip
GABA _a	γ -aminobutyric acid	TD	temperature diode
GDA	glutamate decarboxylase	TEA	tetraethylammonium
GFT	glass fiber thermo sensor	UMTS	Universal Mobile Telecommunications System
Gigaseal	insulation resistance between cell and electrode	Units	electrical active neuron or enzyme activity dimension
GNC	glass neurochip	VEGF	vascular endothelial growth factor
GSM	Global System for Mobile Communications	VPA	sodium valproate
HCS	high-content drug screening		
hERG	human Ether-à-go-go Related Gene potassium ion channel		
HS	horse serum		
HTS	high-throughput drug screening		
IDES	interdigitating electrode structure		
in vitro	latin: within the glass		
in vivo	latin: within the living		
ISFET	ion-sensitive field effective transistor		
LEP	local electroporation		
LOMINE	local microinvasive needle electroporation		
MCS	Multichannel Systems GmbH, Reutlingen		
MEA	microelectrode array		
MNC	microneedle chip		

